What limits the yield of levoglucosan during fast pyrolysis of cellulose?

by

Juan Proano-Aviles

A dissertation submitted to the graduate faculty

in partial fulfillment of the requirements for the degree of

DOCTOR OF PHILOSOPHY

Co-majors: Mechanical Engineering and Biorenewable Resources and Technology

Program of Study Committee:
Robert C. Brown, Major Professor
Xianglan Bai
James Michael
Dave Raman
Brent Shanks

Iowa State University

Ames, Iowa

2017

DEDICATION

I have learned that the path of the graduate student is a humbling one, and it is one of the most challenging I have encountered. I started this journey inspired and supported by each one of my compatriots so this work is dedicated to them, the Ecuadorian people.

TABLE OF CONTENTS

Page

LIST OF TABLES

LIST OF FIGURES

ACKNOWLEDGMENTS

ABSTRACT

The pyrolysis of cellulose to form levoglucosan is investigated in this study. Although the stoichiometric yield of levoglucosan from the pyrolysis of cellulose is expected to be 100%, only about 60 wt.% yields are reported in the literature.[1–3] Several possible reasons for this limitation are investigated through experiments in micropyrolyzers and computational studies on the depolymerization of cellulose. Heat and mass transfer limitations in an experimental apparatus is one possible limitation on the yield of levoglucosan. Repolymerization of condensed phase reaction intermediates could prevent the formation and release of volatile levoglucosan. Thermohydrolysis of pyrolyzing cellulose to form non-volatile and thermally unstable glucose has also been proposed as a mechanism that reduces levoglucosan yields. Secondary reactions in the gas phase were also investigated to explain limitations on levoglucosan yields. Population balance models were developed to test ideas on how cellulose depolymerized to form levoglucosan at less than stoichiometric yields. These models were supported with chemical kinetic data obtained from transient pyrolysis experiments.

Under carefully controlled experimental conditions, no evidence was found for heat and mass transfer effects limiting levoglucosan yields to 60 wt.% nor do secondary reactions in the condensed- or gas-phases appear to offer a satisfactory explanation. Based on modeling results, it appears levoglucosan-forming reaction rates that decrease as oligosaccharide chain length decreases is the most plausible explanation for limitations on levoglucosan yield from cellulose.

CHAPTER 1

INTRODUCTION

Cellulose $(C_6H_{10}O_5)_n$ is the most abundant natural polymer and finds uses in the production of paper, cardboard, cellophane, rayon, natural fibers, as well as dietary fiber and food filler.[4–6] Cellulose rich biomass resources appear as a viable candidate to produce power, fuels, and chemicals in a sustainable manner with a lower environmental impact when compared to fossil derived products.

In the search of energy security and alternative ways to produce clean energy, biomass resources and technologies have gained an important role due to its advantage to produce high energy dense liquid fuels that can compete, blend in, and potentially replace an important fraction of today's petroleum derived versions. The phrase "grow your own fuels" can become a reality in a future society, where agricultural and forestry residues and dedicated crops can be processed to produce power, chemicals, and energy carriers to satisfy the ever-growing human needs.[7–9]

Pyrolysis of biomass is a promising technology because of the large variety of chemical species that can be produced from the thermal degradation of biomass, and the potential to produce "green" products that can compete and surpass those derived from petroleum.[8,10,11]

Levoglucosan $(C_6H_{10}O_5)$ is the most abundant product from cellulose pyrolysis. It is an anhydrosugar, which means it is a molecule formed by the intramolecular elimination of a water molecule from a sugar molecule, simultaneously forming a heterocyclic ring.[12]

Levoglucosan is further classified as a glycosane anhydrosugar, because its formation included the anomeric hydroxyl group.

Almost 100 years ago, a patent for production of levoglucosan from cellulose, starch, or sawdust in a vacuum was filed in Switzerland,[13] constituting the oldest patent registered for the production of this anhydrosugar. The objective of this patent was the production of anhydrosugars as the precursor of glucose that finally would be fermented. This constitutes the first registered commercial effort to transform plant carbohydrates into alcohols through levoglucosan.

Today, levoglucosan's main industrial uses include food additive and pharmaceutical,[14–16] but there are pathways to directly convert it into ethanol for fuel production by biochemical means of modified microorganisms or hydrolyzing it to glucose followed by more traditional fermentation.[17] The main non-industrial use of levoglucosan is as a tracer compound to monitor biomass burning, especially in forest fires.[18,19]

Brief inspection of the molecular formulas for levoglucosan and cellulose indicate that the maximum theoretical yield of the anhydrosugar from the carbohydrate is 100 wt.%.[20] However, the full potential of production has not been accomplished, neither in benchtop scale reactors nor larger operations. This dissertation theoretically and experimentally explores the reasons why yields of levoglucosan from cellulose are much less than stoichiometric expectations. Since the highest yields are reported for fast pyrolysis cases, the scope of this research program is limited to this operational condition.

Some aspects of the pyrolysis reaction studied in this dissertation are the possibility that the anhydrosugar does not completely escape the reactor after its formation from cellulose, either by suffering degradation reactions in the condensed phase due to an inability to volatilize, or in degradation reactions in the gas phase due to extended residence times and high reactor temperature.

Levoglucosan could possibly take part in recombining reactions and repolymerizing to form larger anhydrosugars in the condensed phase. A novel Controlled Pyrolysis Duration Quench reactor (CPD-Quench) allowed the evolution of products during cellulose pyrolysis to be studied. Some of the experimental results from this study provide evidence of polymerization reactions.

Recently, participation of reaction-produced water in thermohydrolysis have been proposed as a possible explanation for the limited levoglucosan production from cellulose pyrolysis. Experiments were performed with the CPD-Quench reactor to investigate this hypothesis.

Finally, kinetic study of cellulose pyrolysis utilizing the results from controlled duration experiments and evolved gas analysis and provided important insight into the process. Various models of cellulose pyrolysis that help explain the experimental evidence are explored.

CHAPTER 2

BACKGROUND

Cellulose and Levoglucosan

Cellulose $(C_6H_{10}O_5)_n$ is a polymer of glucose (anhydroglucose units),[21–24] with

cellobiose as the repeating unit.[1,25–28] Figure 1 shows a simplified structure of cellulose.

The degree of polymerization usually refers to the number of repeating glucose units (n),

therefore the cellobiose unit will repeat n/2 times. Due to the particularity of cellobiose

being the repeating unit, the β 1,4-glycosidic bonds in cellulose alternate in position and

function. One glycosidic bond connects two monomers to form cellobiose, and the other

one connects two cellobiose units together in the polymer chain; however, energetically

they should require the same energy for dissociation during pyrolysis.[29]
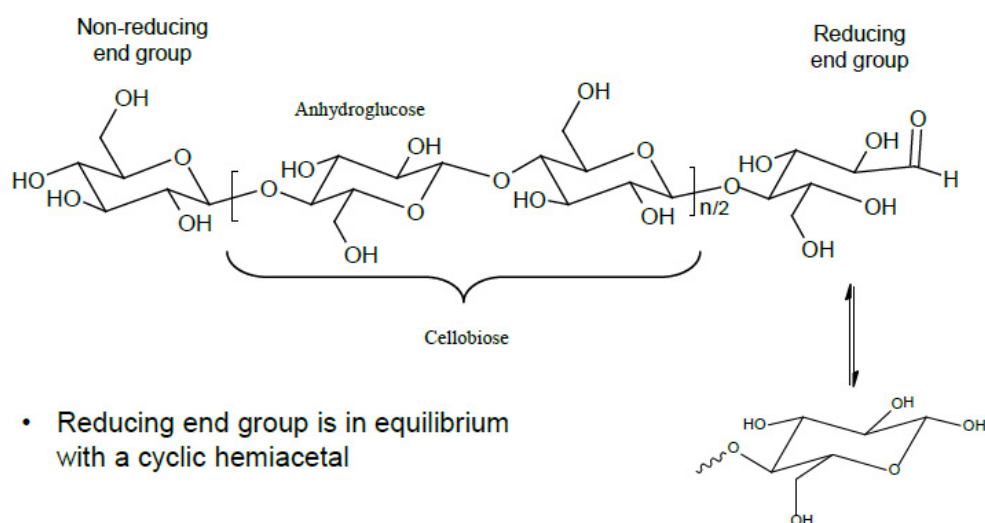
Figure 1. Simplified structure of cellulose. The schematic shows the presence of the reducing-end group (RE) and the non-reducing-end group (NR).[26]

It is also important to notice the presence of reducing-end groups (RE) and non-reducing-end groups (NR) in the structure of cellulose. NR are more stable because those are in a cyclic or ring form whereas the RE can interchange between an acyclic (acetaldehyde) form and the cyclic hemiacetal (ring form).[30] The acetaldehyde form is prone to fragmentation during thermal degradation;[31,32] however, the hemiacetal form is more abundant.[30] These end groups are important during the pyrolysis of cellulose.[33–35]
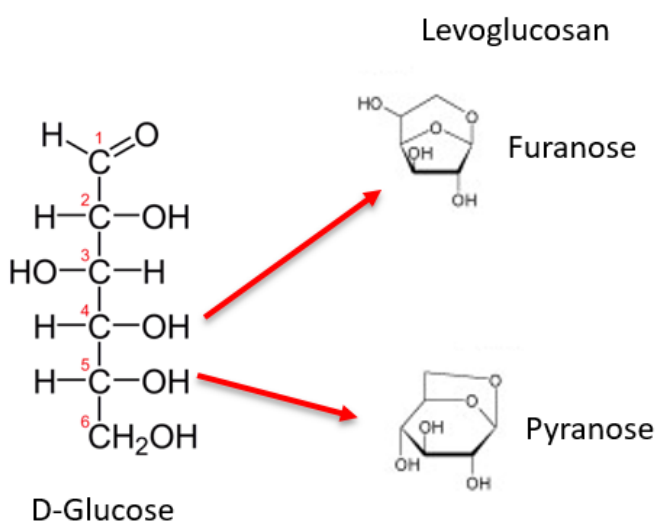
Figure 2. *Hydroxyl groups on D-glucose that lead to the formation of a furanose or pyranose ring, dehydration step not shown. Adapted.*[12,31,36,37]

The anhydrosugar levoglucosan ($C_6H_{10}O_5$) is the most abundant product from fast pyrolysis of pure cellulose.[1,38,39] It has a reported boiling point of 385 °C;[40] therefore pyrolysis reaction temperatures should be above this value to promote evaporation of the anhydrosugar and prevent degradation reactions in the condensed phase.[41–43] Levoglucosan can adopt two main forms: pyranose and furanose, thee form depending upon how the ring is structured during pyrolysis. Similar to the change of glucose from the

acyclic to the cyclic form, ring closing can occur between the oxygen on the aldehyde group attached to C_1 and the hydroxyl group attached to C_4, to form a furanose ring, or with C_5, to form a pyranose ring. The pyranose levoglucosan yield is higher.[1]

Condensed Phase Degradation of Levoglucosan

Various researchers have studied levoglucosan in the liquid state during pyrolysis, proposing that the fate of this anhydrosugar depends on the competition between evaporation and repolymerization.[21,42–44] As early as 1983, Shafizadeh[43] proposed a reaction pathway for cellulose pyrolysis that included a liquid intermediate called "active cellulose," which contained levoglucosan and its isomer. He indicated that decomposition reaction would take place if this intermediate was not opportunely removed.

To study what happens to this liquid intermediate, which mainly contains anhydrosugars,[38,45–47] Hosoya et al.[44] used a batch reactor consisting of a closed ampoule containing different amounts of levoglucosan. The amount of levoglucosan in the reactor changed the relative participation of vapor and liquid/solid products during pyrolysis. They found that large amounts of levoglucosan would lead to large yields of char. In this case, a small fraction of levoglucosan evaporated and increased the pressure inside of the ampoule. This increase in pressure prevented the evaporation of the remainder levoglucosan that underwent the recombination pathway to form char. This high loading experimental condition represents a case where mass transfer is limited, and the liquid intermediate is forced to remain in the reacting zone to degrade to char, as described by Shafizadeh.[21,43]

Recently, Bai et al.[48] used experimental data to study the competition between evaporation and repolymerization of levoglucosan in a slow-heating-rate thermogravimetric analyzer. Moreover, they utilized the experimental data to propose a mathematical model to represent the competing pathways that levoglucosan can follow during pyrolysis. Their experiments had low and high mass transfer conditions, controlled by placing perforated lids on sample holders for some of the experiments. The results were similar to those of Hosoya et al.[44] When the lid was used, evaporation was slowed, allowing more char to form during pyrolysis. Furthermore, the use of different carrier gasses changed the amount of char obtained. Cases with helium, which has a higher diffusion coefficient than nitrogen,[49] favored mass transfer and led to lower char yields under otherwise similar pyrolysis conditions.

The model by Bai et al.[42] had good agreement with experimental data when it was used to predict char yields during slow pyrolysis; however, they reported that when extrapolated to fast pyrolysis conditions, the model predicted high levels of polymerization, and these contradict the micropyrolysis experimental observations.

Competition between evaporation and repolymerization of levoglucosan

The model proposed by Bai et al.[42] enabled them to study the behavior of levoglucosan during pyrolysis experiments. Their model proposes a competition between evaporation and oligomerization.

The model assumes there is no thermal gradient within the sample, which is valid for the case analyzed in this work given the small size, 100 μg. Another assumption is that the

liquid formed during the process will adopt a hemispherical shape; this is acceptable because surface tension will force the liquid body to adopt a shape with the minimum possible surface area. Additionally, other factors such as wettability of the stainless-steel surface and presence of volatiles between the cup surface and liquid surface are not accounted for simplification of the case.

The model consists of the system of equations given as Equations 5 to 9. The sub-indexes poly and evap refer to polymerization and evaporation, respectively.

$$M_T = M_o + \int_0^t \left[\frac{dM_L}{dt}\right]_{evap} dt \qquad\qquad \textit{Equation 1}$$

$$\frac{dM_L}{dt} = \left[\frac{dM_L}{dt}\right]_{poly} + \left[\frac{dM_L}{dt}\right]_{evap} \qquad\qquad \textit{Equation 2}$$

$$\left[\frac{dM_L}{dt}\right]_{poly} = \left[-A_p exp\left(-\frac{1000E_{ap}}{RT}\right)\right]S \qquad\qquad \textit{Equation 3}$$

$$\left[\frac{dM_L}{dt}\right]_{evap} = -\left[A_e exp\left(-\frac{1000E_{ae}}{RT}\right)\right]M_L \qquad\qquad \textit{Equation 4}$$

$$S = \sqrt[3]{2\pi\left(\frac{3M_T}{\rho}\right)^2} \qquad\qquad \textit{Equation 5}$$

Where:

M_T = Total mass of reaction mixture, composed of liquid levoglucosan (M_L) and oligosaccharides (M_{olig})

M_o = Initial mass of sample (kg)

A_p = Polymerization pre-exponential factor (s^{-1})

A_e = Evaporation pre-exponential factor (kg m^{-2} s^{-1})

E_{ap}= Polymerization activation energy (kJ mol^{-1})

E_{ae}= Evaporation activation energy (kJ mol^{-1})

R= Universal ideal gas constant (kJ kmol^{-1} K^{-1})

S= Sample surface area exposed for evaporation (m^2)

T= Sample temperature (K)

The temperature profile in the pyrolyzer can be represented as the response to a step input, instantaneous insertion in the hot furnace, to a first order thermal system. The temperature evolution of the sample can be expressed as shown in Equation 10. The thermal measurements revealed the thermal characteristic time (τ_{th}) to be 0.2 s for the exposed bead thermocouple and 0.6 for the stainless-steel sample cup.[50]

$$T = T_o exp\left(-\frac{t}{\tau_{th}}\right) + T_f\left[1 - exp\left(-\frac{t}{\tau_{th}}\right)\right] \qquad \textit{Equation 6}$$

Numerical solution to the system of equations 5-10 using the trapezoidal integration method was implemented in Excel.[51]

Evidence of Gas Phase Degradation of Levoglucosan

Degradation of levoglucosan produces compounds such as levoglucosenone, acetaldehyde, glyoxal, 2-furfural, 5-hydroxymethyl furfural, and non-condensable gasses, among others.[44,52–56] Hosoya et al.[41] proposed that levoglucosan in the gas phase can be stabilized by hydrogen-donor components, but if degradation further proceeds, mainly carbon monoxide and carbon dioxide are produced.[44]

In reactors with long gas residence times, such as the free-fall reactor used by Johnston et al. [57], levoglucosan formed from cellulose pyrolysis might be consumed in secondary gas phase reactions. This free fall reactor has 18 ports distributed lengthwise that allow sampling produced gasses for analysis by a Time-of-flight Mass Spectrometer (TOF-MS). Depending on the operating conditions, the residence time of the gas phase products is between 1-5 s, as estimated using a computational fluid dynamics simulation approach. In Figure 3, the relative intensity corresponding to levoglucosan obtained while pyrolyzing cellulose follows an increasing trend for the cases with the reactor at 400 and 500 °C; however, when the reactor wall was at 600 °C, the levoglucosan intensity decreased with increasing reactor length, suggesting its gas phase thermal degradation.
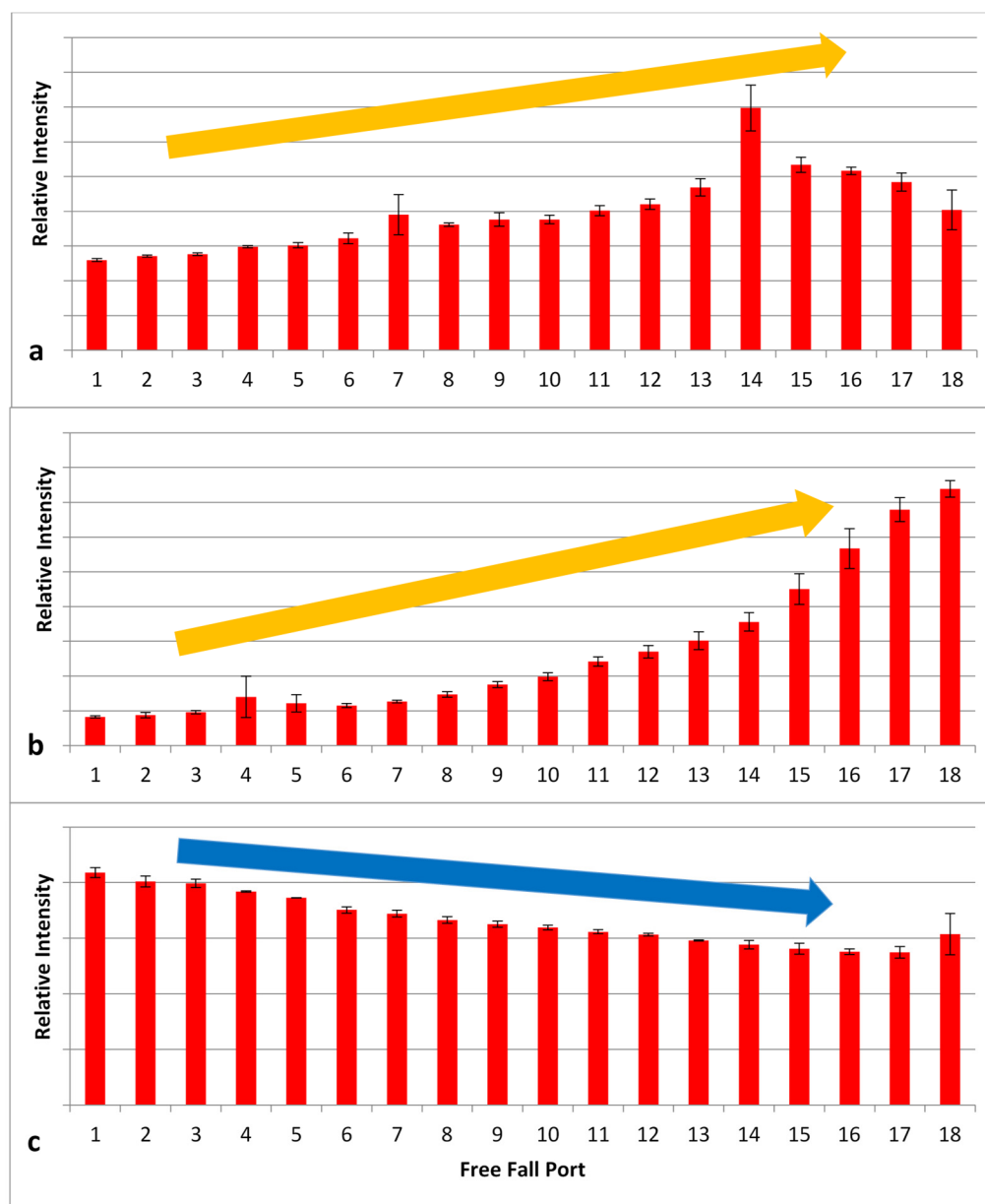
Figure 3. Relative levoglucosan intensity determined by TOF-MS during free-fall experiments at 400 (a), 500 (b), and 600 °C (c) with 5 SLPM nitrogen sweep gas show ongoing and complete cellulose pyrolysis. The error bars indicate one standard deviation from the mean in each direction.[57]

Agglomeration, Coalescence and Char Formation

Experiments in coal pyrolysis indicate that tar production (condensable liquids) is favored by small particle size, high carrier gas, high heating rates, low pressures or vacuum, and use barriers to prevent material coalescence or agglomeration.[58,59] In the typical micropyrolyzer used today to study fast pyrolysis of biomass, a majority of these conditions is achieved.

Zhou et al.[60] mixed calcium hydroxide with extracted lignin to prevent its agglomeration during fast pyrolysis in a fluidized bed. As a result, bio-oil yield increased and the char obtained was a fine powder, in contrast to the large agglomerates that form and eventually defluidize the bed when attempting to pyrolyze untreated lignin.[61]

Co-pyrolysis of cellulose and technical lignin has been found to reduce repolymerization of levoglucosan.[41,62,63] Saka's group showed that co-pyrolysis of aromatic compounds such as guaiacol, 4-methylguaiacol, and veratrole, which are typical products of lignin pyrolysis, with cellulose reduced repolymerization of levoglucosan.[41] Also, high boiling point aromatics, 1,2-benzanthoraquinone and 9-phenylacridine, co-pyrolyzed with cellulose lead to a complete inhibition of char production.[64] Even though they did not quantify the anhydrosugar production, they claimed that levoglucosan was the major component of the detected volatile cellulose pyrolysis products from these co-pyrolysis experiences. They indicated that the polarity of the substituent groups on the aromatic compounds allowed them to interact with the hydrophilic surface of the molten intermediate of cellulose pyrolysis, and stabilized the levoglucosan produced during pyrolysis.

Cellulose Pyrolysis Mechanisms

Cellulose fast pyrolysis, with heating rates higher than 100 $^{\circ}Cs^{-1}$, yield a variety of products. Compilation of the reported identified products from this reaction includes around 100 compounds, but there are a few that make up more than 80 wt.% of the total. Among the most abundant are levoglucosan, 2-furaldehyde, 5-hydroxymethylfurfural, acetaldehyde, formic acid, carbon monoxide, carbon dioxide, and char.[1,38,46,65]
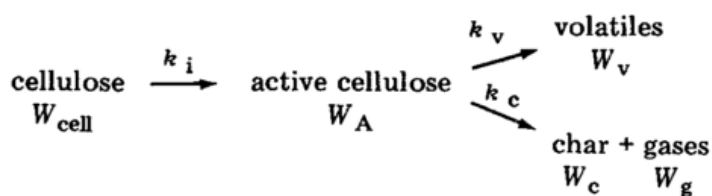
Figure 4. Schematic of the reaction mechanism proposed by Bradbury et. al for cellulose pyrolysis.[38] A simple example of the models that include an active intermediate to explain cellulose pyrolysis.

For many years, the cellulose pyrolysis mechanisms postulated the formation of an unidentified intermediate product followed by competing processes to convert it into volatile products like levoglucosan and degradation products such as char, water, and non-condensable gases.[21,38,43,66,67] Figure 4 displays an example of such model. The nature of the intermediate is still a matter of debate. Some authors emphasize the "active" character of the intermediate,[34,35,68,69] others proposed that the intermediate is simply oligosaccharides or anhydrooligosaccharides from the depolymerization of cellulose.[70–75]

Recently Vinu et al.[71] proposed multiple steps to explain the pyrolysis of cellulose. Figure 5 summarizes the mechanism. They include pathways for production of

anhydrooligosaccharides, levoglucosan, and glucose. One of these mechanisms, named

thermohydrolysis, produces glucose selectively from the reducing-end group of the

molecule by the action of water, postulated to arise from dehydration reactions elsewhere

in the cellulose chain. Glucose, being non-volatile, would eventually polymerize and

dehydrate to char and water, explaining levoglucosan yields that are less than 100% from

cellulose pyrolysis.
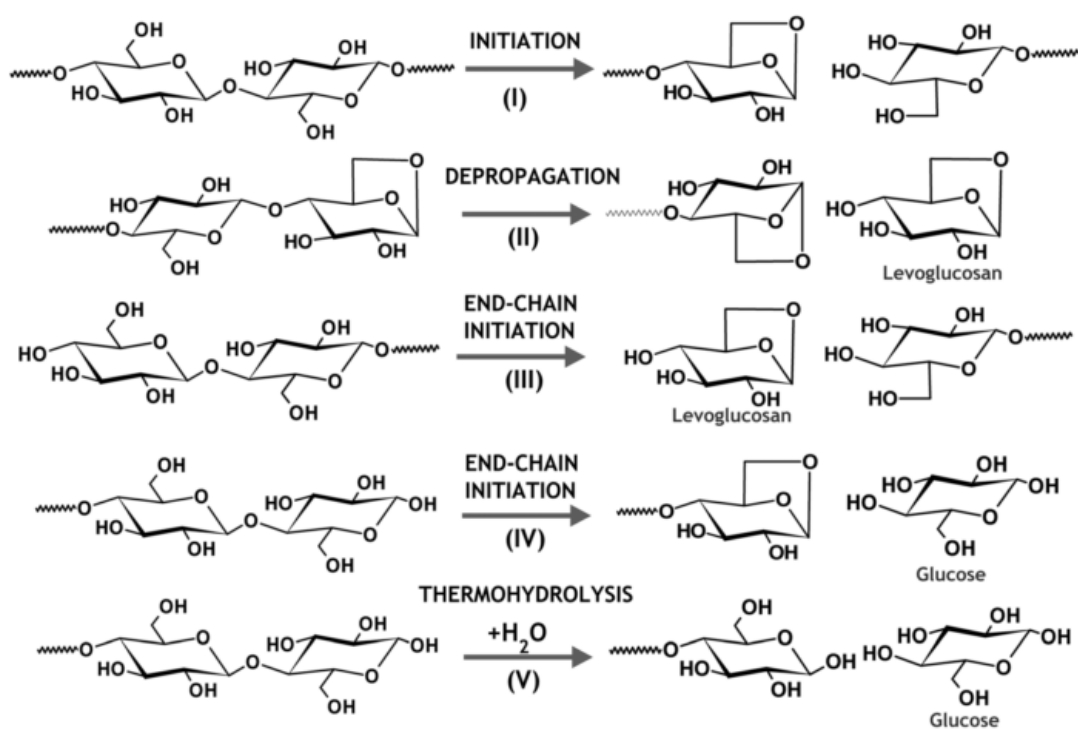
Figure 5*. Mechanisms of formation of levoglucosan and glucose through chain reactions involving glycosidic bond cleavage and hydrolysis.*[71]

Ball et al.[65] suggested that thermohydrolysis would only act on the amorphous

regions of native cellulose, having little to no effect on the crystalline regions. They also

indicate that water can interfere with product cyclization to levoglucosan.[76]

Although these glucose-forming reactions offer a potential explanation for levoglucosan yields that are no more than 60 wt.% from pyrolysis of pure cellulose, none of the reported experimental work has evidenced the production of glucose as an intermediate product as would be expected.[21,77] Thus, it is premature to assign them as a definitive explanation for the observed yields of levoglucosan from cellulose pyrolysis.

Challenges to Determine Kinetic Data from Pyrolysis

The scientific literature contains many studies on the kinetics of biomass and cellulose pyrolysis.[3,78–80] However, reaction orders and kinetic parameters for elementary reactions of pyrolysis are not widely available yet[3,81–83]

Given the complexity of the reaction, many studies assumed the process could be approximated by a global, single step, first order, and Arrhenius type reaction.[82,84–86] Even with this approach, discrepancies exist between the different values for activation energy.[3,82] The origin of these discrepancies relates to the conditions of the experiments. Di Blasi[67] pointed out one crucial limitation to the use of this kind of kinetic data. She indicated that this sort of simplification was not able to capture the complex nature of the reactions in cellulose pyrolysis; however, the simple models can be combined with physical phenomena to understand the process.

The values of kinetic parameters relates to the apparatus and experimental conditions that originated them.[82,87,88] Some kinetic parameters can predict reaction rates outside the reaction conditions from which they were developed, but generally they fail in this respect, indicating that they do not represent elementary reactions. Commonly, there is

inter-dependence between chemical and physical phenomena during pyrolysis. For this reason, we need to either extensively understand their interplay or minimize the effects of the physical phenomena to obtain relevant chemical kinetic information.[89,90]

Many early studies relied on thermogravimetric analysis (TGA) and differential scanning calorimetry (DSC) to get kinetic data from chemical reactions. These two techniques can be used separately, although they usually work together. Either way, intrinsically these methods are not a good representation of fast pyrolysis due to their low heating rates (<3 °Cs^{-1}).[91] Recently, devices based on micro-electro-mechanical systems (MEMS) have allowed DSC studies with heating rates characteristic of fast pyrolysis (>1000 °Cs^{-1});[92] so far this type of instruments have been successful in studying synthetic polymers, [93] but the methodology to study cellulose and biomass are still in development.[94] Experimental apparatus based on fluidized beds, TGA instruments, electrically heated elements, and laser heating have been developed to allow measurement of chemical kinetics during pyrolysis. [3,39,77,78,84,95–104]. However, these studies generally report various differences in heat and mass transfer effects as reasons for variations in kinetic parameters reported in the literature.[82,105]

In some coal pyrolysis experiments, mass transfer interfered with measuring the kinetics of reactions.[58,59,106] Mass transfer limitations were identified as internal and external. Internal mass transfer refers to the transport of the gaseous products from the interior of the coal matrix to its external surface, and the external mass transfer limitations represents the restrictions to move the gas from the surface to the bulk surrounding gas.

Finally, the transport of these products already in the bulk phase can affect kinetic measurements as well.

Another issue that may lead to incorrect kinetic data interpretation is the presence of distributed kinetics. When multiple types of bonds are being broken during pyrolysis, the reaction kinetics reaction may be represented by a set of parallel, first order reactions that have a distribution of activation energies.[58,107] A complex reacting system being studied as a single first order reaction will apparently have an activation energy superficially lower than the activation energy represented by the set of parallel reactions. This is not a problem for reactive systems which proceed via a small number of chemical reactions.[58]

In the next sections, heat and mass transfer effects are discussed to better understand their impact on the measurement of kinetics constants during pyrolysis of solid fuels. Moreover, the extensive literature on coal pyrolysis provides some insight into biomass. Also, a review of different methods to study the kinetics of solid-gas reactions, reactions in the condensed phase, and gaseous phase reactions is presented.

Mass Transfer Limitations

Internal

Internal mass transfer of products is important in pyrolysis of large particles, and negligible for small ones.[108,109] The exception occurs when the time scales of mass transfer and the reaction are comparable. The approach to study internal mass transfer depends on the characteristic of the particle matrix under pyrolysis. If the structure of the biomass is maintained, the internal mass transfer can be studied as flow through a porous media. If the

matrix melts to form a liquid body (plastic behavior) or a metaplast (liquid and solid portions) the motion of gas through a viscous substance is studied.[58,110] For certain coals, it has been evidenced that formation of liquid during pyrolysis is enhanced when using high heating rates.[58]

When the matrix of coal or biomass is maintained during pyrolysis, the char structure is similar to the initial structure. In this case, the porous media approximation is utilized to study intra-particle mass transfer, as indicated in coal pyrolysis and heterogeneous reactions literature.[58,59,110] To simplify the study of the complex porous geometry, the matrix is characterized by the porosity (ϕ_p), tortuosity ($\tilde{\tau}$), constriction factor (σ_c), and the diffusivity of the products in the carrier gas (D_{AB}). The obtained factor in Equation 1 is called the effective or Knudsen diffusivity (D_e).[109] The tortuosity considers the complexity of the main porous paths, the constriction factor accounts for the changes in cross-sectional area of the porous paths, and the porosity includes the total available pore fraction inside the matrix. Full biomass particles are more likely to maintain its structure after pyrolysis, contrary to what happens with its model compounds cellulose and lignin when individually pyrolyzed.

$$D_e = \frac{D_{AB}\phi_p\sigma_c}{\tilde{\tau}} \qquad \text{Equation 7}$$

To verify internal mass transfer limitation, the Wagner-Weisz-Wheeler modulus (M_W) should be calculated, Equation 2. This number compares the observed kinetic rate (k_{obs}) with the rate of transport of gases through the porous media represented by the ratio of the effective diffusivity (D_e) to the square power of the characteristic length of the

particle or film (L_C^2). A number larger than 4 indicates presence of strong pore diffusion.

Values around 0.15 indicate desirable kinetic limited experiments.[108,109]

$$M_W = \frac{k_{obs}L_C^2}{D_e} \qquad \text{Equation 8}$$

On the other hand, when the porous structure is lost or modified during pyrolysis to

form a liquid, the transport mechanism is more complex. After the particle melts, the

existing pores collapse due to surface tension. Later, volatiles form and nucleate inside of

the melt, followed by their coalescence to form larger bubbles. Images of char particles

after coal pyrolysis are shown in Figure 6. The bubbles travel to the surface to be released

as a burst from the liquid. This transport of gas can be summarized as nucleation, growth,

and burst. Additionally, it is usual to observe swelling of the particles due to the bubble

growth, and this phenomenon is largely dependent on operational conditions and substrate

characteristic. The viscosity of the melt is the dominant property in bubble nucleation,

growth, and coalescence, and has an impact in product diffusivity.[59,106,111]
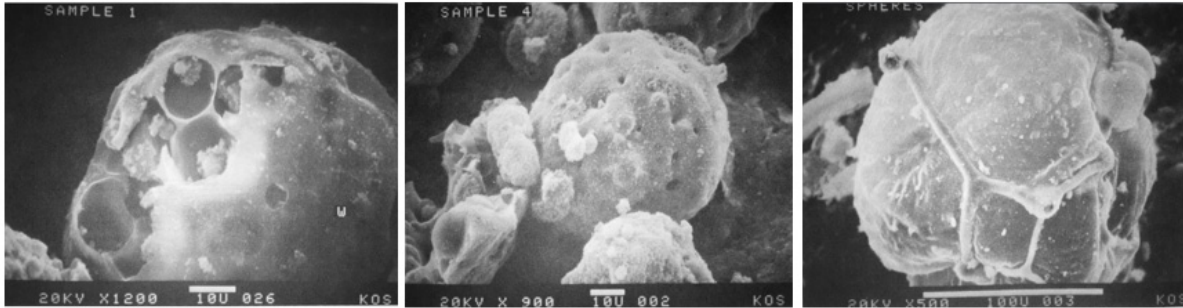
Figure 6. Electron micrographs of char from bituminous coal pyrolysis. Left: Burst of gas, leaving bubbles cell structure behind, no large coalescence. Middle: Volatiles escaped from the melt-phase through small orifices created by the high pressure of volatiles. Right: Bubbles coalesced and swelled the particle.[58]

Cellulose, lignin, and bituminous coal all present liquid intermediate products during pyrolysis,[59,106,112,113] but the latter has the best-studied examples. Rheological measurements are necessary to determine the presence of fluid intermediate and its properties (mainly viscosity) to help study the transport of gas through the liquid intermediate. Even though high heating rate pyrolysis favors the formation of a liquid intermediate, viscosity has been measured only for slow pyrolysis experiments. Moreover, getting viscosity data is challenging in fast pyrolysis, and its significance is limited to the used experimental conditions.

In coal pyrolysis, two processes compete during the melt phase. The first breaks bonds to give way to a liquid state. The second one is the formation of high molecular products that provoke a seemingly re-solidification of the matrix to form char through secondary reactions. Here, the effective evaporation of products takes an important role to lessen the extent of these repolymerization reactions.[114]

Additionally, the formation of the liquid intermediate during pyrolysis can include the coalescence of particles to form a larger molten cake, or the agglomeration of particles to create a body that resembles a bunch of grapes. Both processes cause problems in reactors such as fluidized beds when pyrolyzing coal[59] or technical lignin[61].

Depending on the behavior of the substrate, the mass transfer at the particle or agglomerated/coalesced body level can affect the measurement of chemical kinetics. A comparison of relevant processes' time constants is necessary to verify any possible interference on getting chemical kinetic data.

Some strategies to overcome internal mass transfer are the use of smaller particles,

the use of anti-agglomeration inert agents that prevent the contact between neighboring

particles, and the use of appropriate temperature history to manage the production of the

liquid intermediate.

External

External mass transfer refers to the transport of substances between the surface of

the particle and the bulk surrounding gas. Essentially it is the transport of substances

through a thin boundary layer on the surface of the particle by the action of diffusion. For

determined temperature and pressure pyrolysis conditions, the best ways of improving

external mass transfer are: increasing the diffusion coefficient by changing the carrier gas,

and minimizing the thickness of the boundary layer by either reducing the size of the

particle or increasing the velocity of the surrounding gas.[109,115]

In the case of tars, defined as volatiles that condense at ambient temperature,

evaporation is part of the external mass transfer. Therefore, using lower pressure and even

vacuum can accelerate mass transport as it has been evidenced in an increased production

of volatiles from lignite[116,117], and levoglucosan from cellulose pyrolysis in a vacuum.[42,97]

Tars and gas can also be transported through the boundary layer and into the surrounding

carrier gas by the burst of bubbles on punctual locations of the particle's surface, which has

been recently referred to as ejection of aerosols in the biomass pyrolysis literature.[111]

To verify if external mass transfer is the limiting process, a comparison should be

made between the observed reaction rate in the experiment and the theoretical reaction

rate of a mass transfer limited case. The observed rate should be much lower than the latter to discard external mass transfer limitations.[108]

<u>Extended residence times</u>

Volatiles released during pyrolysis can undergo secondary gas phase reactions to degrade into lighter gas.[73,118] In the case of cellulose pyrolysis, prolonged residence times at high temperatures promote the degradation of levoglucosan in the gas phase to produce CO, CO_2, and H_2O.[44,119] To prevent this counterproductive effect, high carrier gas velocities and short heated path lengths can be combined to minimize the residence time of volatile products.

Heat Transfer Limitations

Heat transfer limitations can interfere with accurate measurement of chemical kinetics.[3,120,121] This limitation occurs when a thermal wave penetrates the particle with a characteristic time comparable or larger than that of the reaction.[88] In general, cases with small particles made of high thermal conductivity material do not present an important thermal gradient because the overall particle closely follows the reactor's temperature. On the other hand, when heat is rapidly transferred to the surface of the particle and the particle is made of a poor thermal conductor, a large temperature gradient appears within the particle, which interferes with the pyrolysis reaction. In this case, determination of a characteristic particle temperature is difficult, and this uncertainty can modify the estimated kinetic constants. A model to predict temperature becomes necessary for this kind of experiments so that the uncertainties can be reduced; however, accurate measurement of the temperature evolution is preferred.[106]

Temperature measurement becomes challenging with small particles and high heating rates. Some researchers have overcome this challenge by using appropriate sensors. For example, Solomon et al.[118] et al. used Fourier Transform Infrared Spectroscopy (FTIR) to measure coal particle temperatures during pyrolysis in an entrained reactor.

With the aim of running an experiment with very large heating rates ($\geq$10000 $°Cs^{-1}$), laser pyrolysis has also been employed to study kinetics. [106,122] However, the creation of inevitable large temperature gradients within the pyrolyzed material complicates the interpretation of kinetic data, and the obtained apparent activation energy is low.

When measuring the temperature of the particle is not feasible, mathematical models can predict it. In the case of modeling temperature of a solid under pyrolysis in a high heating rate scenario, the influence of the particle's physical properties is large. Depending on the mechanisms of heat transfer to the pyrolyzing particle, temperature dependent changes in mass, size, density, composition, heat capacity, thermal conductivity, and optical properties can vastly modify the predicted particle temperature. Consideration of these changes should be addressed in the models to obtain better results. In the fire engineering literature, there are useful correlations for the temperature dependence of biomass and coal properties.[123] Data for biomass and its main model compounds changing during pyrolysis are still being studied in the academic community.[124–126]

To better understand the regime of pyrolysis utilized in experiments, time scale analysis is used. First, the Biot number (Bi) >0.1 indicates that the particle tends to form

temperature gradients within it, this case should be avoided. To include the rate of reaction

(k) into the time scale analysis, recently the Pyrolysis number (Py)[91] has been defined for

heat transfer effects, Equation 3 and 4. Heat transfer time scale is compared to the reaction

kinetics scale using two Py numbers:

$$Py^I = \frac{\lambda}{\rho C_P L_C^2 k} \qquad \qquad \text{Equation 9}$$

$$Py^{II} = \frac{h}{\rho C_P L_C k} \qquad \qquad \text{Equation 10}$$

These numbers include the particle's thermal conductivity (λ), density (ρ), specific

heat (C_P), characteristic length (L_C) as well as the convective heat transfer coefficient (h).

The first number (Py^I) considers intra-particle conduction heat transfer and the other one

(Py^{II}) considers convection to heat up the surface of the particle. Combined with the Biot

number, one can define the regime of pyrolysis due to heat transfer as shown in Figure 7.

Experiments to obtain valid chemical kinetics are desired to be in the regime called

kinetically-limited and isothermal, located on the upper left corner of the plot.
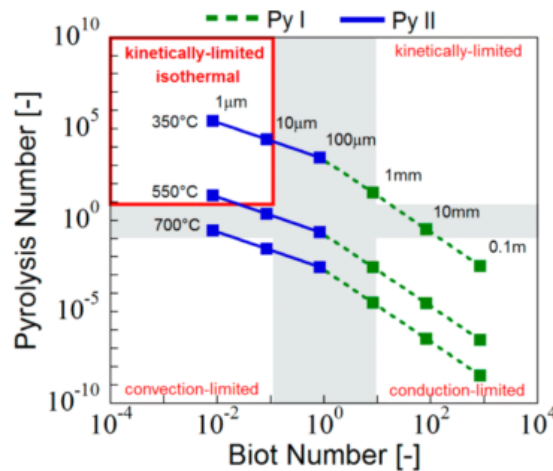
Figure 7. Reaction-heat transfer map for cellulose pyrolysis proposed by Paulsen et al. Four regimes are identified: isothermal and kinetically limited kinetically limited, conduction limited, and convection limited. Examples presented for furnace temperatures of 350, 550 and 700°C.[91]

Levenspiel and others[108] studied the effect of heat transfer in heterogeneous reactions (solid-gas) by determining the presence of thermal gradients through the thin film surrounding the particle as well as intra-particle gradients. Gradients of few degrees represent almost-isothermal experiments; however, it is common to have large gradients within the thin layer for an inert gas with low thermal conductivity. This undesired gradient of temperature can be reduced by using a gas such as helium to increase the thermal conductivity of the thin layer. Decreasing the thickness of the thin layer by reducing the particle size and/or increasing the velocity of the carrier gas to increase convection are other useful approaches.[109,115,127]

When utilizing reactors in which multiple heat transfer mechanisms participate, several factors can greatly influence the measurement and prediction of particle temperature. In reactors such as the furnace based pyrolyzer (micropyrolyzer), or the heated mesh reactor, there are factors that should be considered to identify possible strong influence on the temperature measurement. Firstly, ensure good contact between the hot heating surface and (i) reacting particle, (ii) thermocouple. Appropriate selection of heat capacity, thermal conductivity, emissivity, and size of the thermocouple bead per the same properties of the particles. Also, learn if there is an expected influence of heat on the thermocouple wires. The layer of particles covering the heating surface should be uniformly distributed, so to avoid the presence of local heavy loading of particles. Another important consideration is the impact of the heat of reaction in the local temperature of the heating element and sample.

Relevant Methods for Kinetic Studies During Pyrolysis Reactions

To study the kinetics of coal and biomass pyrolysis reactions, a variety of methods and reactors have been applied throughout the years. From the multitude of experiments, no conventional kinetic constants have been identified from a wide range of reported kinetic data; however, some values are adopted when they fit similar reacting conditions. Each experiment has its own particularities, so the real meaning of the obtained values should be considered before using the values for chemical reaction engineering calculations. Special attention should be given to the heat and mass transfer characteristics of the tests and their possible impacts on the reported results.

Another important aspect of the kinetic study is the assumption of the mechanism that represents the reaction. The use of a single step, first order reaction from the substrate to the pyrolysis products can oversimplify the mechanism; however, these can be useful to predict overall behavior of the reaction to approximate yields of tars, char, or gas.[67] In some cases, the inclusion of a step either in parallel or series increases the usability of the kinetic model without a significant increase in the complexity of the mechanism. Other studies contemplate the complexity of the pyrolysis reaction and the multitude of reactions participating at the same time and apply a distributed activation energies model. On the other hand, Burnham et al. proposed that a sigmoidal model can better explain the behavior of cellulose pyrolysis.[3]

Reactors utilized to study pyrolysis reactions kinetics include the tube reactor (drop tube, entrained flow), fixed and fluidized bed connected to mass spectrometry, heated mesh reactor, stirred reactor, shock tube, tubing bomb, as well as TGA to study the mass

evolution. TGA can also be connected to Fourier Transform – Infrared analyzer to perform

Evolved Gas Analysis (EGA).[128]

In coal and biomass pyrolysis studies, EGA of the products has been utilized to study

kinetics. EGA can be performed using Mass Spectroscopy (MS), Fourier Transform

spectroscopy (FT-IR), or Optical In-situ gas analysis.[129] An interesting configuration uses

TGA/DSC combined with MS to identify the products during their evolution; yet, this is more

valid for atomic/inorganic vapors and non-condensable gas. For organic volatiles from

pyrolysis, the interpretation of the fragments formed with MS is difficult, yet possible.[130]

Recently TGA/MS/FT-IR was applied to study pyrolysis of multiple biomass coming from

food processing wastes.[131] However, the inherent low heating rate of TGA qualifies these

studies as slow pyrolysis.

In the polymer industry, as well as in the pharmaceutical and coal pyrolysis

community, EGA performed with Fourier Transform Infrared Spectrometer (FTIR) allows

tracking absorption bands of specific gas species. Solomon et al. obtained the evolution of

H_2O, Tars, CO_2, CH_4, CO, SO_2, NH_3, C_2H_4, and COS using this type of configuration.[58,132] The

kinetics were studied using Functional group - Devolatilization, Vaporization and

Crosslinking model (FG-DVC). This model studies the decomposition and condensation of a

macromolecular network (coal) considering bond breakage and crosslinking during pyrolysis

(Stochastic approach using Monte Carlo Statistical Method).[133]

To study the kinetics of tars in the gas phase, continuous flow reactions are

useful.[134] Tube reactors and Shock tube reactors provided with MS, FTIR, or laser analyzers

can provide concentration evolution of targeted compounds. When the shock tube reactor is used, the time between the initiation of the test and the arrival of the wave to the observation point is extremely short ($\approx 10^{-8}$ s) and the sudden change in pressure heats up the gas at large heating rates. If further readings are needed, multiple observation points can be used. Nelson et al. studied the pyrolysis of tar from coal in this fashion to determine the rate of degradation of coal tars.[135]

To study liquid-phase reaction kinetics the most common approach is measurement of the concentration of a targeted compound at discrete time intervals, which in turn depends on the practical ability to either stop the reaction at a prescribed time, or to collect a sample without disturbing the reaction. Reactions of thermoplastic polymers with additives, water, and other agents have been studied measuring the concentration of carboxyl and amine end-groups from samples collected at different times.[136] Magma melt phase experiments to determine the inclusion of minerals also collect small samples to determine concentrations and determine proper kinetics.[137]

Efforts to measure kinetic parameters for pyrolysis of cellulose

Multiple authors and for a long period have devised methodologies to determine the kinetics constants for biomass and especially cellulose fast pyrolysis. Each approach had its own challenges. These efforts included multiple reaction temperatures, residence times, pressure, sample size, particle size, and material, amongst other variables applied. The variety of instruments used includes fluidized bed, TGA, electric heating elements, convective furnaces, and specialty reactors.

Many of these experiments had limitations that prevented them to qualify as fast

pyrolysis cases. A clear example is the low heating rate obtained in TGA apparatus. As early

as the 1980s, Chornet and Roy informed the lack of a conventional kinetic data set for

cellulose pyrolysis.[105,138] Multiple academic efforts took place during the upcoming years to

conciliate the widespread values for the kinetics of cellulose, and one of those studies

coordinated an international collaboration published in 1999. Eight laboratories from

Denmark, Finland, Hungary, Norway, Sweden, and USA participated using various models of

TGA instruments. The maximum heating rate applied in this study was 0.75 $°Cs^{-1}$. They all

used cellulose from the same can and nitrogen gas as the carrier gas. For low heating rates

experiments (0.1 $°Cs^{-1}$), all the results agreed well and could easily fit a single step, first

order rate equation. However, disagreement appeared when analyzing the maximum

heating rate results. Finally, the study agreed that thermal lag and large sample size were

the cause of the evidenced reduced activation energy values. This more than exemplifies

the limitations of TGA to study fast pyrolysis of cellulose.

Noteworthy, Antal et al.[39] considered these weaknesses and implemented a faster

heating rate TGA, yet the 65 $°Cs^{-1}$ upper limit was still lower than the $\geq 100 °Cs^{-1}$

characteristic of fast pyrolysis. Moreover, the activation energy obtained from experiments

conducted in this apparatus still reflected a value lower than those obtained with low

heating rates. As recent as 2015, a novel TGA approach was used by Zhou et al.[98], but the

single presence of a large metallic basket to hold the sample warns about the low heating

rates that the device could produce. Lin et al. used the same instrument with low heating

rates, but included a mathematical model to analyze the data that helped understanding the non-isothermal effect in the pyrolyzing sample.[139]

The abundance of low heating rate available kinetic studies is much greater than the minuscule number of studies done using high heating rates. Just a few of the latter are available in the literature. Some examples of these studies are the ones by Lewellen et al.[84] and Hajaligol et al.[99] These studies used electric heaters to increase the temperature of small samples of biomass. After prescribed heating time, the sample was cooled down to stop the reaction, later to collect the yields of solid residue and condensed products. The mass of the collected residue was used to infer the kinetic data. Even though the heating rates are fast, the capability to cool down and stop the reaction had its limitations because they relied on natural convection and radiation to the surroundings. The uncertain slow cooling process may have left the sample to pyrolyze longer than intended and consequently affect the kinetic constants calculation. Another aspect that may have modified the results was the procedure to recuperate and measure the vapors produced from the test, by reheating and collecting the products, after they have condensed in dedicated vessels of the apparatus.[84,99]

More recently, Zhu et al.[77] used heating pulses in microseconds time scale applied to thin film samples to study the kinetics of model compounds that represent cellulose. They called this reactor pulse-heated analysis of solid/surface reactions (PHASR). The sample's thickness used ensured it is isothermally even with large heating rates. They found two sets of kinetic constants; however, the reasoning to use the model compound, α-cyclodextrin, raises questions. There are marked differences between the levoglucosan

yields from cellulose and α-cyclodextrin (αCD) pyrolysis. Mettler et al. reported yields of 23 wt.% of levoglucosan when using the same reactor[140] meanwhile it is widely known that cellulose yields a minimum of 45 wt.% even at high furnace temperatures of 600°C.[141] Additionally, cellulose is a set of linear polymeric chains that includes reducing and non-reducing ends, meanwhile αCD is a ring that lacks ends. The kinetic data are still classified as apparent kinetic values, and further exploration is needed to clarify the picture on the energetics of cellulose pyrolysis.

Cracking and unzipping participation revealed by reaction rate curve behavior

In cellulose pyrolysis literature glycosidic bond cleavages help explaining the progression of the degradation process.[3,70,71,103,107] The cleavage of a glycosidic bond can occur at a random position. This is denominated cracking of the cellulose chain and this fragments the main chain successively, and can help explaining the rapid reduction of the degree of polymerization at early stages of cellulose pyrolysis. The cleavage selectively acting at the end of the cellulose chain is called depolymerization or unzipping and it helps explaining the release of volatile levoglucosan.[71,142]

An early hypothesis is that pyrolysis of organic materials resembles a chain reaction.[143–146] In a chain reaction, there are initiation, propagation, and termination steps. In cellulose pyrolysis, initiation can occur by random scission or unzipping.[70] Wall et al., as stated by Burnham et al.,[3,107] proposed that the behavior of the reaction rate curve can indicate the nature of the initiation of the reaction as well as the length of the unzipping steps.

Figure 8 shows theoretical curves for random and end initiation. For large unzipping lengths (large zip), the deceleration behavior is seen for both the random and end initiation. When the initiation is of random character and followed by short unzipping length (small zip), the reaction rate curve presents an acceleration portion followed by deceleration. The acceleration indicates the increase of shorter fragments that constitute reaction centers, in this case, more chain ends to be unzipped and volatilized. The following deceleration responds to a logic decrease of chain ends to be unzipped.

On the other hand, if the end initiation dominated the chain reaction with a short unzipping length (small zip), the reaction rate curve would be flat. This flat curve appears because no new chain ends would appear and the unzipping rate would be almost constant until reaching depletion of chain ends.
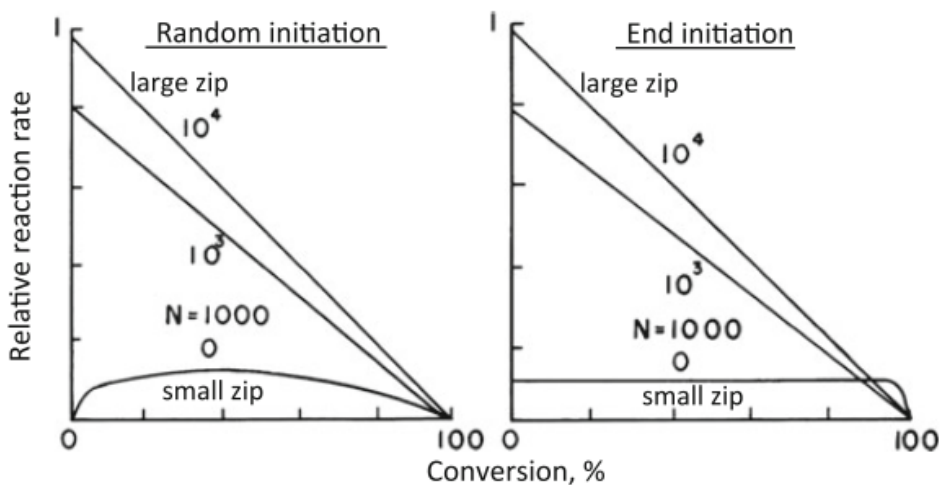
Figure 8. *Theoretical calculations of the reaction rate for the thermal degradation of an organic polymer with: (left) random initiation, and (right) end initiation.*[107,142] *In the case of Random initiation with a small unzipping length (small zip) acceleration followed by a deceleration is observed.*

The unzipping of monomers from long chains can also be affected by the molecular weight or degree of polymerization of the chain. In thermal degradation of molecules of polystyrene, unzipping produces higher yields of monomers when starting with longer chains to be pyrolyzed; however, the gain in monomeric yield was marginal after a certain DP.[147] The chain length effect was noticed by Mettler et al.[140] and Vinu et al.[71] for glucose polymers of multiple degrees of polymerization, observing important increase in the production of levoglucosan from their fast pyrolysis. Figure 9 shows the increase of yield of levoglucosan with increasing DP.
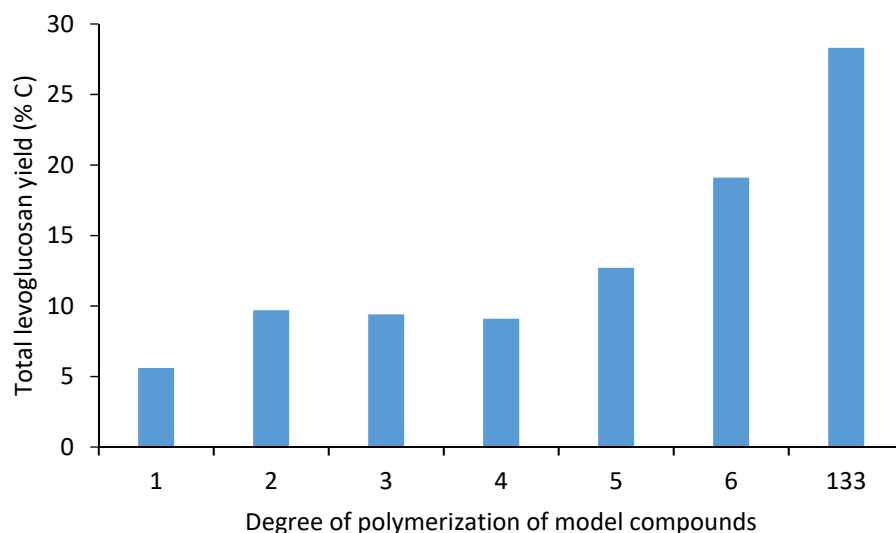
Figure 9. *Total levoglucosan carbon yield from pyrolysis of glucose polymers of varying degree of polymerization. Adapted from Mettler et al.*[140]

CHAPTER 3

METHODOLOGY

Materials

Table 1. List of materials utilized in micropyrolysis experiments during this study. Moisture content reported from thermogravimetric analysis.

Materials name	CAS	Manufacturer	Product number	Minimum purity (wt.%)	Moisture content (wt.%)
1,2-Benzanthraquinone	2498-66-0	TCI	-	95	-
Amylose	9005-82-7	Aldrich	859656-1G	90	-
Cellobiosan	35405-71-1	Alfa Aesar	J66914	98.9	
Cellobiose	528-50-7	Fluka	22150-10G	99.2	0.9
Cellopentaosan	122274-98-0	LC Scientific Inc.	AG811	98	-
Cellotetraosan	80325-59-3	LC Scientific Inc.	AG809	98	-
Cellotetraose	38819-01	Sigma	C8286-2MG	85	-
Cellotriosan	78797-67-8	LC Scientific Inc.	AG807	98	-
Cellotriose	33404-34-1	Sigma	C1167-1MG	93	-
Cellulose	9004-34-6	Sigma Aldrich	S5504-1KG	99.9	2.6
Cellulose	9004-34-6	Sigma Aldrich	310697-500G	99	
Curdlan	-	Tate and Lyle	-	-	5.5
Dextran	9004-54-0	Fluka	31394	99.9	7.2
Dextrin	9004-53-9	Acros	406281000	99.5	5.3
Fumed silica	68 611-44-9	Evonik	Aerosil R974	99.9	-
Glucose	50-99-7	Fisher	D16-500	99.9	0.9
Levoglucosan	-	Carbosynth	-	99.9	
Maltoheptaose	M-7753	Sigma	M-7753	92	-
Maltohexaose	M-7878	Sigma	M-7878	-	-
Maltose	6363-53-7	Fisher	M75-100	90	-
Maltotriose	1109-28-0	Sigma	M-8378	95	-
Microcrystalline cellulose	9004-34-6	FMC	PH-105	-	2.9
Starch		Penick & Ford	-	-	6.4
Sucrose	57-50-1	Fisher	S5-500	99.9	-
Trehalose	6138-23-4	Acros	182550250	99.5	8.9
α-cyclodextrin	10016-20-3	Sigma Aldrich	C4642-1G	98	8.3

Reactants are listed in Table 1. Reported moisture content were determined via thermogravimetric analysis, unless otherwise reported.

A digital balance (Mettler Toledo, XP6) determined the mass of the samples that are contained in cup-shaped sample holders or deposited on the surface of U-shaped wires.

Inhibition of char formation during pyrolysis was studied using physical barriers and solvents co-pyrolyzed with carbohydrates contained in a cup-like sample holder. For these cases, the sample preparation consisted in weighting the barrier material first, then adding the carbohydrate and mixing them in the cup with the use of a thin stainless steel wire. Homogeneous mixture of the co-pyrolyzing substances is very important for the success of these tests. Weighing the sample after mixing helped detect cases where mass losses of 3 μg or more would reject the sample.

Apparatus

A furnace-based micropyrolyzer (Frontier, EGA/PY-3030D) was used in this study to investigate cellulose pyrolysis. It offers favorable characteristics such as high heating rates, rapid test turnout, and compatibility with analytical instrumentation such as a gas chromatograph.[50] Figure 10 shows the schematics of the micropyrolyzer which consists of a sample dropper, a reactor tube that can be made of quartz or stainless steel, an electrical furnace, and an interface to direct the gaseous pyrolysis products to an analytical instrument. The hooked end of a stainless-steel wire is inserted into a sample cup, and the other end is gripped by the sample dropper, suspending the sample in the top of the reactor tube. Pressing a button on top of the dropper liberates the wire, and the cup lands in the

preheated reaction zone. A sudden change in the diameter of the tube provides support to the sample holder for the duration of the experiment. Helium carrier gas flows into the top of the reactor tube, entrains gasses released from the sample contained in the cup, and exits the reactor tube through the needle attached to the bottom interface.[50]

A modification to this configuration served to test for levoglucosan gas-phase degradation products. Replacing the micropyrolyzer with a tandem configuration (Frontier, Rx-3050TR), consisting of a micropyrolyzer on top of a second furnace, empty catalytic bed, allowed producing volatiles and later exposed them to a hot reacting zone for an extended period. Figure 11 shows this tandem configuration. The temperature of the top and bottom reactors and the interphase between them can be regulated independently.
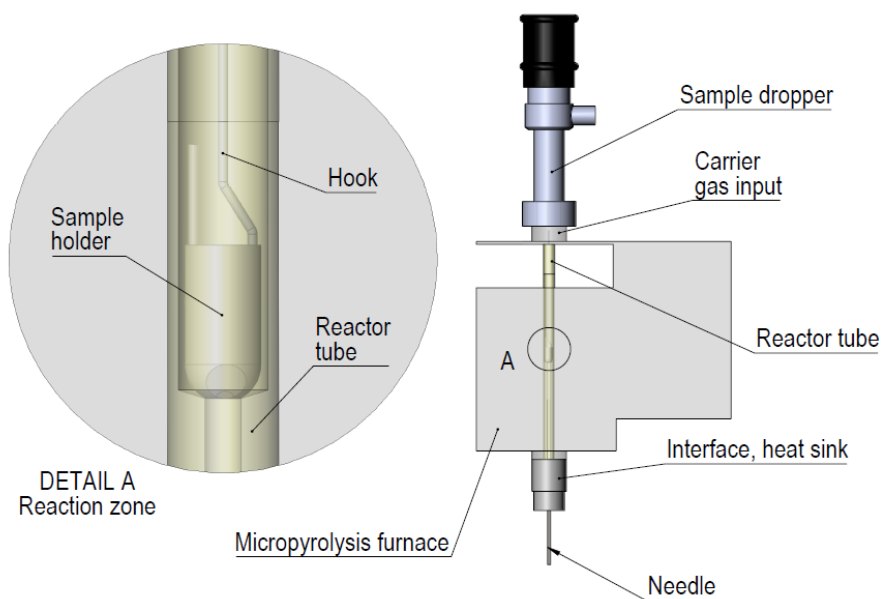
Figure 10. *Schematics of the furnace-based micropyrolyzer by Frontier Labs. Detail A shows the reaction zone where the sample holder is dropped to be heated and pyrolyzed.*[50]
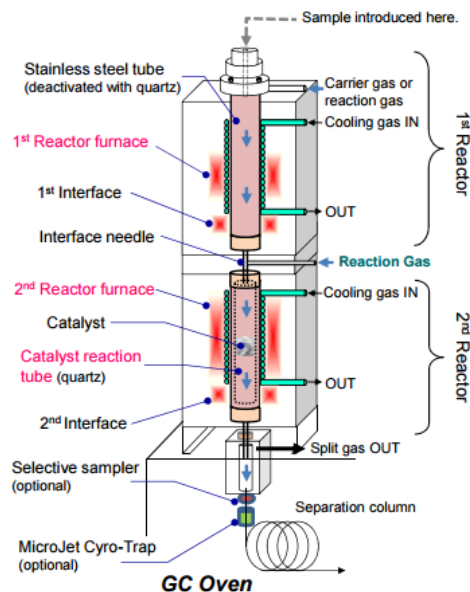
Figure 11. *Schematics of the micropyrolyzer working on top a heated catalytic bed. The catalytic bed was used to extend the residence time of vapor phase gasses coming from pyrolysis.*[148]

The Controlled Pyrolysis Duration Quench (CPD-Q) apparatus was built around a micropyrolyzer to control injection and ejection times for biomass samples, as shown in Figure 12. During operation, a mechanism lowers a sample cup suspended on a hook into the furnace zone of the reactor tube and releases the cup after a prescribed amount of time. A T-connector located underneath the furnace allows the cup to fall into a solvent vessel chilled in an ice bath, and the pyrolysis vapors exit horizontally into a stainless-steel U-tube condenser immersed in liquid nitrogen. To increase the available surface area and enhance the condensation of volatile products, the U-tube contained 3 ml of borosilicate glass beads of 1mm in diameter (Sigma Aldrich, Z273619). Both the condensed vapors and quenched residue can be recovered and analyzed via HPLC.[149] For some experiments, a paper filter separated the solid residue from the soluble products of the quenched residue.

The carrier gas was maintained by an electronic flow controller (Alicat, MC-10SCCM-D/10M).
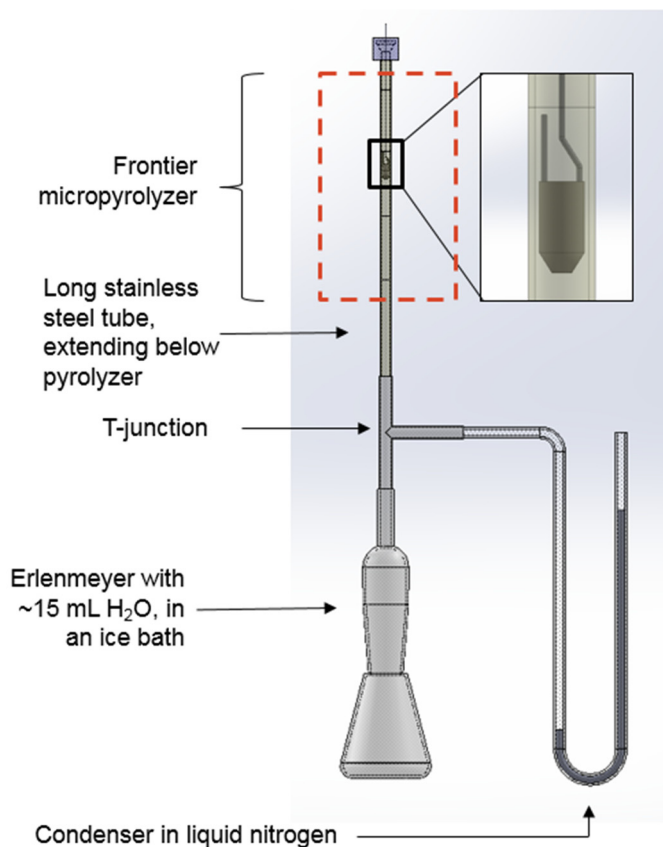
Figure 12. Schematics of the CPD-Quench Micropyrolysis System.[149]

To explore the effect of water added in the carrier gas, the gas stream bubbled though a 25-ml column of water contained in a glass impinger (Ace Glass, 7531 30ml). The water saturated the helium, at a volumetric flow rate of 100 ml min^{-1}, and the resulting stream presented a humidity ratio of 0.035 mg$_{H2O}$/mg$_{He}$. The humidity ratio was measured using an online gas detector (Gastec, Water 6AG). The collected samples were later analyzed by HPLC to quantify water soluble compounds.
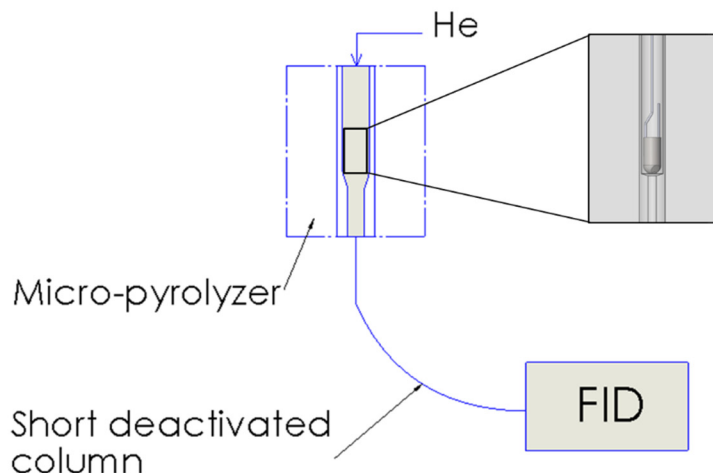
Figure 13. Schematic of the configuration to capture the evolution of volatile pyrolysis products.

Figure 13 shows the configuration utilized to obtain dynamic data of the evolution of volatiles from pyrolysis. It consisted of a micropyrolyzer (Frontier, EGA/PY-3030D) connected to a GC-FID (Varian, CP-3800 GC) via 0.5m fused silica capillary column with no stationary phase (Agilent, 160-2845-5) maintained at 400°C in the column oven to prevent vapor condensation. Cellulose, or other carbohydrates, pyrolyzed and the generated voltage signal from the FID was recorded at a frequency of 10 Hz.

Heating rates in the furnace section of the micropyrolyzer were measured by using type K, thin-wire thermocouples. In some experiments, a stainless-steel thermocouple bead of 200 mm diameter and 30 mg mass (Omega, KMQSS-010E-6) was attached to the sample hook such that the bead was suspended in the center of the curved section of the sample hook, which allowed it to be inserted easily into the center of the furnace section.

For other experiments, a pair of fine thermocouple wires (Omega, CHAL-010-BW) were spot-welded onto the floor of a deep cup to form a couple. The wires passed out through a two-bore ceramic tube, which prevented the wires from contacting one another as they passed out of the furnace. The temperatures measured from each of these thermocouple configurations were recorded by using a thermocouple meter (National Instruments, USB-TC01). The heating rate was calculated by dividing the difference between the initial temperature and 90%ofthe final temperature by the time needed to achieve the latter temperature. The characteristic time constant for heating assumed of a first-order thermal response.

Analytical Instruments

The micropyrolyzer (Frontier, EGA/PY-3030D) was connected to GC-FID (Agilent Technologies, 7890A GC System). A pair of columns conducted the pyrolysis products to (i) a mass spectrometer (Agilent Technologies, 5975C inert MSD) and (ii) a methanizer (Activated Research Company, Polyarc) and a Flame Ionization Detector. The GC–FID was calibrated with aqueous solutions of levoglucosan (Carbosynth, ML06636) for expected yields in the range of 10–100 μg. The amount of levoglucosan quantified with this experimental configuration was compared with the weight of the initial sample.

Given the high boiling point characteristic of the used aromatic compounds that may contaminate the lines and detectors, a dedicated GC-FID-MS instrument was set up for the co-pyrolysis tests. In similar configuration as mentioned in the previous paragraph, a GC with FID (Varian, CP-3800 GC) and MS (Varian, Saturn 2200) analyzed the gaseous products released from a micropyrolyzer (Frontier, EGA/PY-3030D) connected to the injector of the

GC. Between tests, a 120 minutes method was run to allow any residual aromatic compound to exit the system. The vent line of the GC was connected to a ventilation duct of the building to prevent the fumes of the aromatic compounds from contaminating the laboratory.

To analyze the products collected from the CPD-Quench tests, the products were quenched in deionized water and this solution was filtered and sent to analysis in a High-performance liquid chromatograph (HPLC) system (Dionex, Ultimate 3000 LC system). The details of this systems can be found elsewhere.[150] To detect the presence of glucose, a method prepared for quantification of this sugar after hydrolysis was utilized; however, the original mobile phase of this method, acid diluted in water, was replaced by deionized water. When glucose was not a targeted product, quantification of total water-soluble sugars was performed using a similar HPLC system.[151]

Analysis of Kinetic Data

Single step, first order approximation

To analyze the signal, the FID curve was divided into two main portions, refer to Figure 14. The rise portion starts at t= 0 s, which corresponds to the instant when the cup is dropped into the furnace. The rise portion extends up to t= t_{max}, when the maximum value of the curve appeared. The decay portion starts at t= t_{max} until the end of the recorded data.
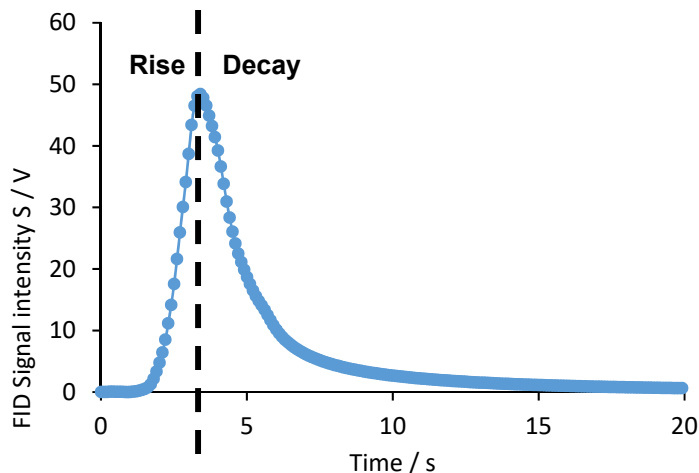
Figure 14. *Example of the FID signal from the volatilization of naphthalene from a sample cup in the micropyrolyzer. Decay and increase sections are shown divided by a vertical line coincident to the maximum signal.*[50]

The decay portion of the curve against time displayed in a semilog plot revealed a linear section from where the slope represented the negative and inverse of the characteristic time of a first order dynamic process, as shown in the example of Figure 14.
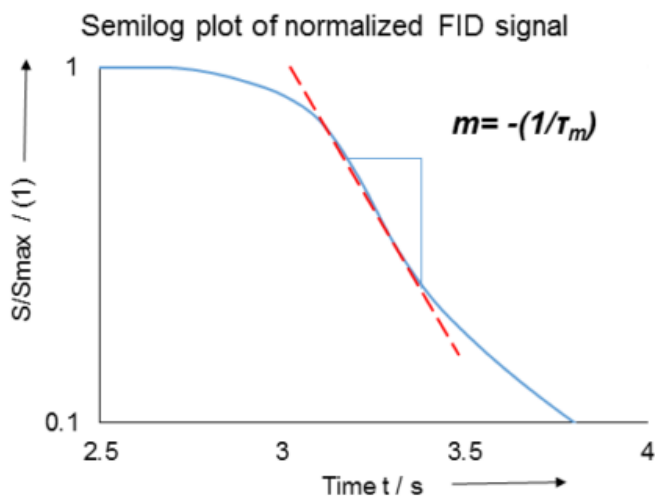
Figure 15. *Example of semi log plot of normalized FID signal vs. Time. The dotted line indicates the slope m of the linear portion that characterize the evolution of volatile gases from the micropyrolyzer.*[50]

Mathematically the linear portion of the signal was represented by Equation 13.

Where S is the voltage signal from the FID, S_{max} is the maximum value of the curve that help

normalizing S. The time is represented by t and τ_m is the characteristic time of the curve.

Rearranging the equation and using the logarithm yields Equation 14, where m represents

the slope of the curve.

$$S = S_{max}\left[1 - exp\left(\frac{t}{\tau_m}\right)\right] \qquad \text{Equation 11}$$

$$ln\left(1 - \frac{S}{S_{max}}\right) = \left(-\frac{1}{\tau_m}\right)t = mt \qquad \text{Equation 12}$$

Once the characteristic time is obtained, further analysis can help to determine the

activation energy and pre-exponential factor of the pyrolysis process. An Arrhenius plot of

multiple characteristic times for different furnace temperatures is shown in Figure 16. The

temperature is utilized assuming that the sample has reached the furnace temperate when

the linear portion of the analyzed data appears. This assumption was confirmed with the

temperature measurements.[50]
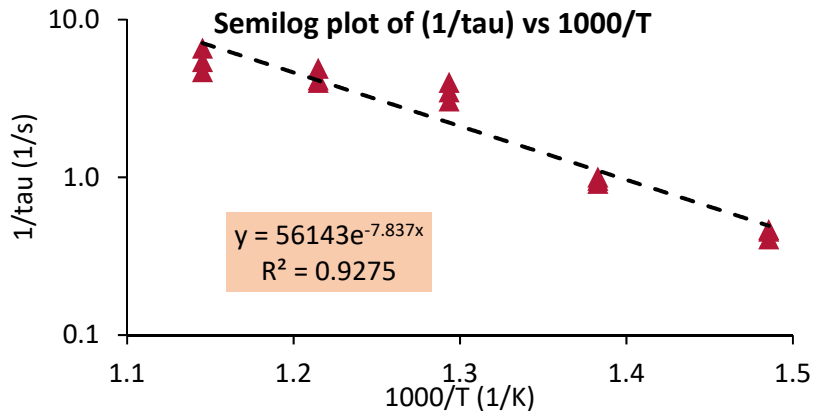
Figure 16. Example of the Analysis of activation energy for cellulose pyrolysis for furnace temperatures in the range of 400-600 °C. Arrhenius plot.

Isoconversional and model fitting methods

Derivation of condensed phase reaction kinetics is relevant to the study of cellulose

pyrolysis due to its nature to form a liquid intermediate.[21] There are two main approaches

to studying condensed phase kinetics: isoconversional and model fitting.[107]

Isoconversional methods, or Model-free kinetics, do not tie the data with any

specific phenomenological equations. These methods assume that the dependence of the

reaction rate on pressure reduces to unity. Also, the rate of reaction *dα/dt* can be expressed

as a product of the kinetic rate *k(T)* times a function of either disappearance of reactants

f(x) or appearance of volatile products (conversion) *f(α)*, this rate is expressed in Equation

15.[152]

$$\frac{d\alpha}{dt} = k(T)f(\alpha) \qquad\qquad Equation\ 13$$

$$ln\left(\frac{d\alpha}{dt}\right)_{\alpha,i} = ln[f(\alpha)A_\alpha] - \frac{E_\alpha}{RT_{\alpha,i}} \qquad Equation\ 14$$

A particular method, the Friedman method, assumes that the activation energy has

a different value for different conversion levels (α,i), regardless of the temperature history.

Equation 16 is the logarithmic form of the rate equation, useful to perform the Friedman

analysis. This method yields activation energy estimations that are in accordance with those

obtained by more advanced integral methods.[107] The Friedman method is a simple but

powerful tool to initially approach the kinetic study of condensed-phase reactions.

To perform the isoconversional method the rate of change of the produced volatiles

was plotted against the inverse temperature for specific conversion values,[107] α=0.1, 0.3,

0.5, 0.7, 0.9. Afterwards, for each conversion level using the data points a line was fitted

from which the slope and intercept determine the preexponential factor and activation

energy, per Equation 16. The Friedman plot summarizes the calculated preexponential

factors and activation energies for all the conversion levels.

The main assumption regarding the FID signal is that there is a single molar response

factor for the produced hydrocarbons along the whole signal. Since the composition of the

released volatiles is made up by levoglucosan and other molecules with 6 and 5 carbons in

its majority, this assumption is acceptable. This assumption allows elimination of the effect

of the response factor by normalizing the FID signal with respect to the maximum value.

The production of volatiles, or conversion (α), is calculated as the cumulative curve of the

FID signal and it is normalized to its maximum value.

Model fitting methods, as the name indicates, use techniques to match a set of data

with a suitable model. Linear or non-linear techniques minimize the difference between the

data and the mathematical model. Before applying this kind of method, observing the

characteristics and behavior of the data, and performing initial kinetic data estimations

guide the selection of possible candidate models. For a preliminary inspection of the data, it

is often useful to use isoconversional methods first. The model fitting initiates with the

simplest model and advances to more complex and sophisticated ones until reaching a

satisfactory fit.

Table 2 shows commonly employed mathematical models. First order models

usually suffice for global kinetic analysis; however, there are reaction features that cannot

be represented with such a simple model.[67] Sigmoidal models, such as the Avrami-Erofe'ev
and Extended Prout-Tompkins are suited for reactions where both acceleration and
deceleration of the reaction rate occur.

Table 2. Commonly employed reaction models for curve fitting in chemical kinetic studies.[107,153]

Reaction model	Differential form, $f(\alpha)$	Note
First order	$(1 - \alpha)$	-
nth order	$(1 - \alpha)^n$	-
Avrami-Efore'ev	$p(1 - \alpha)[-\ln(1 - \alpha)]^{(p-1)/p}$	Nomenclature: Ap
Extended Prout-Tomkins	$(1 - \alpha)^n[1 - q(1 - \alpha)]^m$	Nomenclature: ePT
Sestak-Berggren	$\alpha^m(1 - \alpha)^n[-\ln(1 - \alpha)]^p$	Nomenclature: S-B

A useful way to display the reaction rate is the Generalized reduced reaction rate,
Equation 17 below, that basically helps normalizing the rate curve with respect to the rate
value at 50 % conversion (α=0.5). A plot of the Generalized reduced reaction rate against
conversion is useful to compare the fit of selected models.[107,154]

$$Generalized\ Reduced\ Reaction\ Rate = \frac{(d\alpha/dt)_i}{(d\alpha/dt)_{0.5}} exp\left[\frac{E}{R}\left(\frac{1}{T_i} - \frac{1}{T_{0.5}}\right)\right] \quad Equation\ 15$$

The curve fitting toolbox available in MatLab® helped automating the process to
determine the parameters to fit the data sets. A non-linear least squares method reduced
the distance between the fitting curve and the data. The use of the Trust-Region
optimization algorithm helped to accelerate the fitting process by minimizing the distance
between the curve and the data set.[155] The metric to evaluate the fit of the curve is the
root mean squared error (RMSE) which is a measure of both the distance between the data

and the fitted model as well as the variability of this distance. A RMSE closer to zero is

preferred.[156]

Modeling Secondary Gas-Phase Reactions of Levoglucosan in Micropyrolysis Experiments

A simple system of equations evaluated the degradation of levoglucosan in the gas

phase during micropyrolysis experiments. The signal obtained from the evolution of

gaseous products detected by the FID served as the input for the instantaneous

concentration of volatiles for the equation. Equation 11 is the transient output

concentration of a fixed volume continuously stirred tank reactor (CSTR).[109]

$$C_{out}(t) = \frac{C_{in}}{1+k\tau_g}\left\{1 - exp\left[-(1 + k\tau_g)\left(\frac{t}{\tau_g}\right)\right]\right\} \qquad \textit{Equation 16}$$

$$k = A_{deg}exp\left(-\frac{E_{deg}}{RT_{deg}}\right) \qquad \textit{Equation 17}$$

Where:

C_{out} = Concentration of volatiles leaving the reactor

C_{in} = Concentration of volatiles entering the reactor

k = Kinetic rate of the thermal degradation reaction

A_{deg} = Gas phase degradation of volatiles pre-exponential factor (s^{-1})

E_{deg} = Evaporation activation energy (kJ mol^{-1})

R = Universal ideal gas constant (kJ kmol^{-1} K^{-1})

T_{deg} = Reactor temperature (K)

The reactor is assumed to be a well-mixed continuous reactor. This assumption is valid for this reactor since the motion of the helium carrier gas and its high diffusivity can create a homogeneous concentration in the reaction volume nearby the sample cup. The furnace of the reactor will keep the carrier gas in the reaction zone at a uniform temperature, so the assumption that the reactor is isothermal holds. The helium carrier gas is the main component of the mixture and is kept at a uniform pressure, so the assumption of constant density in of the fluid is also valid. The degradation of levoglucosan is assumed to be a first-order reaction.

To study the possible degradation of volatiles in the gas phase, a worst-case scenario was proposed, to expose the volatiles to a high degradation rate. This included the longest production time of volatiles, exposed to a higher furnace temperature. This case corresponds to the volatiles evolution with a furnace temperature of 400 °C and using the degradation rate for a 600 °C reacting zone. The kinetic parameters utilized for the calculations are presented in Table 3.

Table 3. *Kinetic data utilized in calculations of degradation of levoglucosan in the gas phase.*

Set	Pre-exponential factor (s^{-1})	Activation energy ($kJ\ mol^{-1}$)	Degradation rate at 600 °C (s^{-1})	Source	Note
1	4.50E+06	110.0	1.42	Font et al.[157]	Degradation of tars from biomass pyrolysis.
2	4.10E+04	102.3	0.04	Cozzani et al.	Degradation of tars from biomass pyrolysis.
3	-	-	0.45	Shin et al.[158]	Gas-phase pyrolysis of levoglucosan. Rate available for 625 °C.

Modeling Early Stages of Cellulose Pyrolysis

Cracking and unzipping initial models

Cracking (random chain scission) and unzipping models from the polymer decomposition literature served to study cellulose pyrolysis. The random characteristic of the former assumes that neither the initial chain length nor the location of the bond within it have an influence on the position of the bond scission. On the other hand, a population balance approach included unzipping into the modelling effort. Both mechanisms have individual fundamental rate constants that characterize their proliferation. Initially, the model included cracking only to later add unzipping in a combined model.

Cracking as the only depolymerization reaction

First, the model of cellulose pyrolysis assumed that only stochastic cracking occurs without including unzipping. A probabilistic approach allowed obtaining the distribution of levoglucosan (LG) and unstable monomer fragments (UM) from cellulose pyrolysis. Figure 17 shows a schematic of this model. In this simulation at each step, the cracking reaction happens at a bond chosen by a random generator based on a uniformly distributed probability. At the beginning of the simulation, a chain with an initial degree of polymerization (DP_o) will crack, forming two fragments. The two fragments, therefore, have DPs that sum to DP_o. The reaction continues to crack the polymer in this fashion until only monomers are left.

Mathematically, assuming each fragment can be given an orientation, the imposed condition specifies that for a given fragment if the bond breaking is the first one which represent a reducing end (RE), then the unit produced corresponds to levoglucosan (LG).

Likewise, if the last bond of the chain breaks which represents a non-reducing end (NR), the released part will be a monomer-size unit (UM).
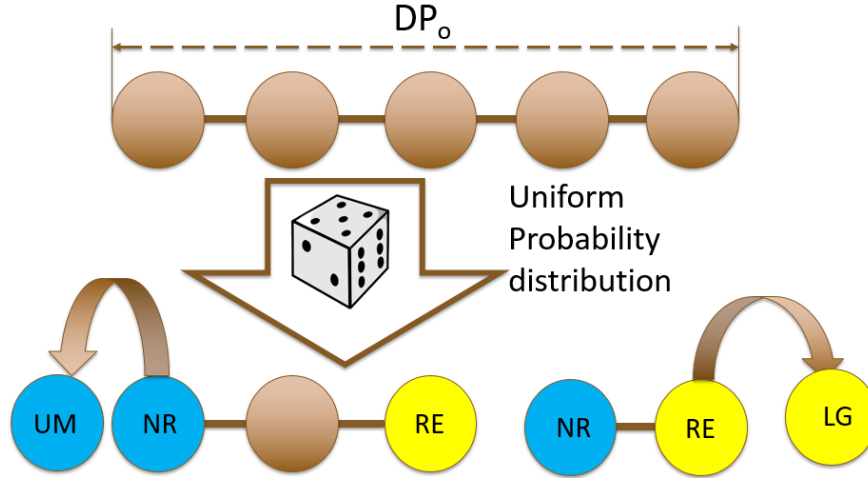
Figure 17*. Schematics of cracking reaction during early cellulose pyrolysis.*

Moreover, Khorrami et al. proposed the Random Scission Model (RSM) without the need to use a probabilistic method. The authors validated this model by comparing results with a Monte Carlo Simulation-based model.[159] The RSM assumes all the bonds of equal energy have the same probability to break under thermal decomposition. The rate equation is:

$$\frac{dC_i}{dt} = -n_i C_i k_1 + 2k_1 \sum_{n_j > n_i}^{n_z} C_j \qquad \textit{Equation 18}$$

Where:

n_i = number of main chain bonds, $n_i = DP_i - 1$

C_i, C_j = concentrations of the chain with number of bonds n_i and n_j, respectively

n_z = largest number of bonds in a chain of the decomposing substance

k_1 = fundamental kinetic rate constant for bond scission

Another considered possibility was having the bonds connecting to the non-reducing end with different activation energy than the ones of the reducing end of the cellulose chain. However, this was dismissed when the kinetic measurements of the pyrolysis of reducing and non-reducing glucose disaccharides cellobiose and trehalose respectively, gave very similar activation energies.

Cracking and unzipping model
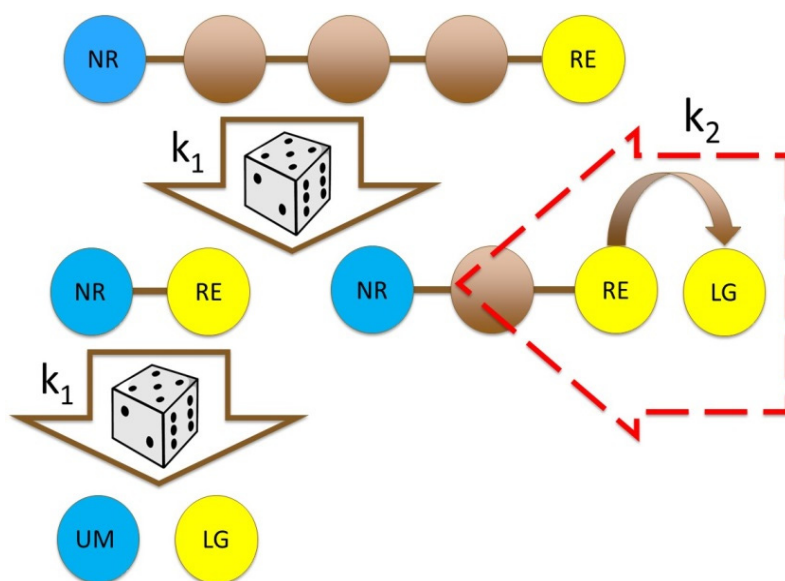
Figure 18*. Schematic of cracking and unzipping reactions during early cellulose pyrolysis.*

A population model representing the unzipping reaction was added to the random scission model to compare their relative participation. shows the schematic of this new model. Combining the two mechanisms, the new rate equation is:

For (DP$_o$-1) ≥ i ≥1:

$$\frac{dC_i}{dt} = -\left(n_i k_1 + \frac{k_2}{\Delta DP(n_i+1)}\right)C_i + \left(2k_1 + \frac{k_2}{\Delta DP(n_i+2)}\right)C_{i+1} + 2k_1 \sum_{n_j>n_{i+1}}^{n_z} C_j$$

Equation 19

For unstable monomer, UM:

$$\frac{dC_{UM}}{dt} = \left(k_1 + \frac{k_2}{2\Delta DP}\right)C_1 + k_1 \sum_{n_j>1}^{n_z} C_j \qquad \text{Equation 20}$$

For levoglucosan, LG:

$$\frac{dC_{LG}}{dt} = \left(k_1 + \frac{k_2}{2\Delta DP}\right)C_1 + \sum_{n_j>1}^{n_z}\left(k_1 + \frac{k_2}{n_j+1}\right)C_j \qquad \text{Equation 21}$$

Where:

DP_i = degree of polymerization for oligomer i

n_i = number of main chain bonds in cellulose, $n_i = DP_i - 1$

C_i, C_j = concentration of oligomers with number of bonds n_i and n_j, respectively

n_z = number of bonds in initial cellulose

k_1, k_2 = fundamental kinetic rate constants for bond scission and unzipping, respectively

Cracking and unzipping model with limited unzipping levoglucosan yields

Considering the experimental evidence gathered in this project, the combined

model needed to include an additional feature, the limited levoglucosan yields observed for

cellobiosan and larger anhydrosugars. Figure 19 shows the schematic of this model, which

includes the evidence so far experimentally supported:

- Random scission initiation complemented by unzipping depolymerize the polymer chain to produce volatile levoglucosan.

- Liquid intermediate contains HPLC detectable anhydrosugars, up to DP=7. Larger compounds are not detected due to solubility limitations in the method.

- Cellobiosan, the smallest ahydrooligosaccharide identified in the liquid intermediate, has a yield of ≈15 wt.%. There is no evidence to believe that this dimer would behave differently and yield higher levoglucosan from pyrolysis as part of cellulose pyrolysis.

- Unzipping at their reducing end or levoglucosan end of a chain yields levoglucosan amounts that depend on the length of the chain.
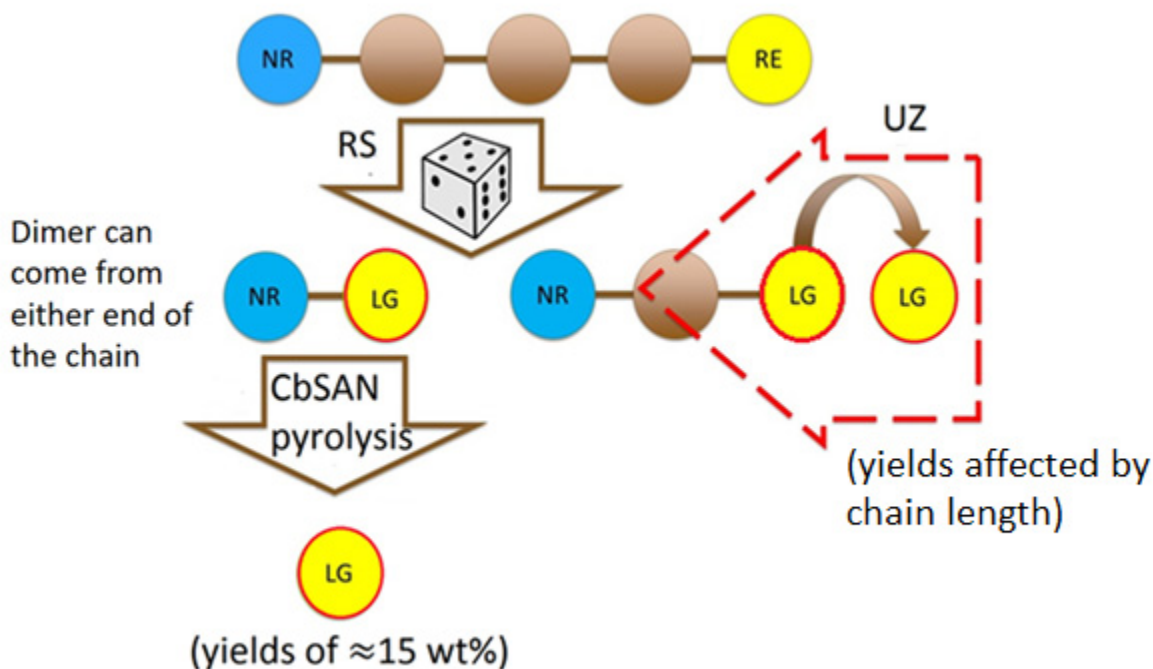
Figure 19. Schematics of the new combined model. Cellobiosan pyrolysis produces ≈15 wt.% levoglucosan, meanwhile unzipping yields of levoglucosan vary depending on the chain length. RS: Random Scission, UZ: Unzipping, RE: Reducing-end, NR: Non-reducing end, CbSAN: Cellobiosan.

The slight modification to the combined model includes the limited yields from cellobiosan. Equation 19 is maintained as presented before. Additionally, Equation 20 is lost because this model does not track production of the unstable monomer, and equation 21 is modified by adding y_f, yield factor for cellobiosan, and as presented in Equation 22.

Additionally, a logarithmic equation was selected to determine the levoglucosan yield from unzipping depending on the chain length because the LG yield increases rapidly with increasing DPs that are near to DP=2, but the gain is marginal when the DP is large (DP>200, microcrystalline cellulose).

For levoglucosan, LG:

$$\frac{dC_{LG}}{dt} = y_f \left(k_1 + \frac{k_2}{2\Delta DP} \right) C_1 + \sum_{n_j>1}^{n_z} \left\{ k_1 + \frac{k_2 [m_{uz} \ln(n_j+1) + b_{uz}]}{n_j+1} \right\} C_j \qquad \text{Equation 22}$$

Where:

DP_i = degree of polymerization for oligomer *i*

n_i = number of main chain bonds in cellulose, $n_i = DP_i - 1$

C_i, C_j = concentration of oligomers with number of bonds n_i and n_j, respectively

n_z = number of bonds in initial cellulose

k_1, k_2 = fundamental kinetic rate constants for bond scission and unzipping, respectively

m_{uz}, b_{uz} = coefficients of the equation that determines the levoglucosan yields from unzipping dependent on the degree of polymerization.

CHAPTER 4

RESULTS AND DISCUSSION

Recovery of Anhydrosugars in a Furnace-Based Micropyrolyzer

The stoichiometric yield of levoglucosan from cellulose is 100 wt.%; however,

reported yields of this anhydrosugar rarely surpass 60 wt.%.[1,21,91,97,160–162] This chapter

explores several possible explanations for the lower than stoichiometric yields observed in

practice. These include primary reactions that compete with cellulose depolymerization;

heat and mass transfer limitations during depolymerization; and secondary reactions that

degrade volatilized anhydrosugar in the gas phase. Investigations began with potential

"artifacts" of the experimental apparatus; that is, heat and mass transfer limitations and

secondary reactions before exploring potential competing primary reactions that are

inherent to cellulose pyrolysis.

Evacuation of levoglucosan from the sample holder

The first hypothesis investigated is that not all the levoglucosan devolatilizes from

sample holders during micropyrolysis experiments. Instead, some of it stays as liquid that

eventually repolymerizes and dehydrates to char and light gases.

Levoglucosan was pyrolyzed in a furnace-based micropyrolyzer using perforated

sample holders that promoted ventilation of the produced vapors. The sample mass was

within $10 - 100 \ \mu g$. Concentrated solutions of levoglucosan dissolved in deionized water (DI

Water) served as calibration standards for the gas chromatography instrument provided

with a Flame Ionization Detector (GC-FID) aided with a methanizer. The temperature of the furnace was 400 °C, which is commonly used in pyrolysis of cellulose and biomass. More importantly, tests with this temperature yields the highest amount of levoglucosan from cellulose micropyrolysis experiments.[163]
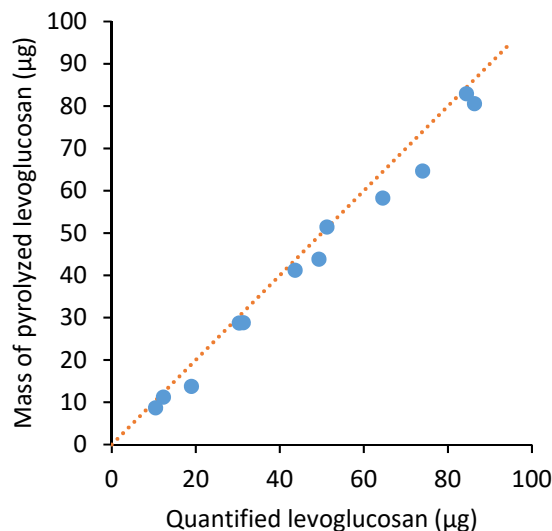
Figure 20. Comparison between pyrolyzed and quantified (recovered) levoglucosan during micropyrolysis in a furnace based reactor preheated to 400 °C.

Figure 20 evidences that the quantified levoglucosan released from a 400 °C reactor closely coincides with the input mass of the samples. The average distance to the calibration curve is 9.2 wt.% which shows the degree of compliance of the quantified yields of levoglucosan. This simple experiment does not support the hypothesis that insufficient volatility of levoglucosan is responsible for less than stoichiometric yields of this anhydrosugars from cellulose during micropyrolysis experiments.

The mathematical model presented by Bai et al.[42] predicted significant polymerization of levoglucosan under fast pyrolysis conditions. The model assumed a linear heating rate of 1000 °Cs⁻¹. The present study investigated this assumption with a thin wire thermocouple attached to a sample holder. Inserted into a 400 °C micropyrolyzer furnace, the maximum heating rate was only 140 °Cs⁻¹. Moreover, the captured temperature profile was non-linear, represented by a first order thermal dynamic system in which the temperature increases exponentially until rapidly reaching a plateau that approaches the furnace preset temperature.[164] Figure 21 shows the heating rates obtained with a micropyrolyzer for two cases: (a) Exposed bead thermocouple, which is a small metallic bead suspended by thin wires and heated by convection and radiation from the surrounding hot carrier gas and furnace wall, and (b) is the case that resembles the use of a cup-shaped sample holder which was suspended by a pair of wires welded to the interior bottom surface of the holder to form a thermocouple. Finite element analysis suggested the sample heating rate are close to those of the cup-shaped sample holder.

Imposing the non-linear heating profiles to the model proposed by Bai et al. predicted that levoglucosan would evaporate, leaving a negligible amount of char in the cup. Figure 22 illustrates the evolution of liquid levoglucosan when heated in a micropyrolyzer, predicting that the clear majority of it disappears, leaving no char behind. This result coincides with the data shown in Figure 20, which indicates complete devolatilization of levoglucosan from the cup. The time span of the process is shorter than expected, which may mean that the kinetic constants need some adjustment to be usable in the context of fast pyrolysis. These results demonstrate that, from a well-ventilated sample

holder, levoglucosan evaporates quickly enough to avoid polymerization. Consequently, the

hypothesis that polymerization of levoglucosan can explain the limitation to produce closer

to 100% theoretical yields is rejected.
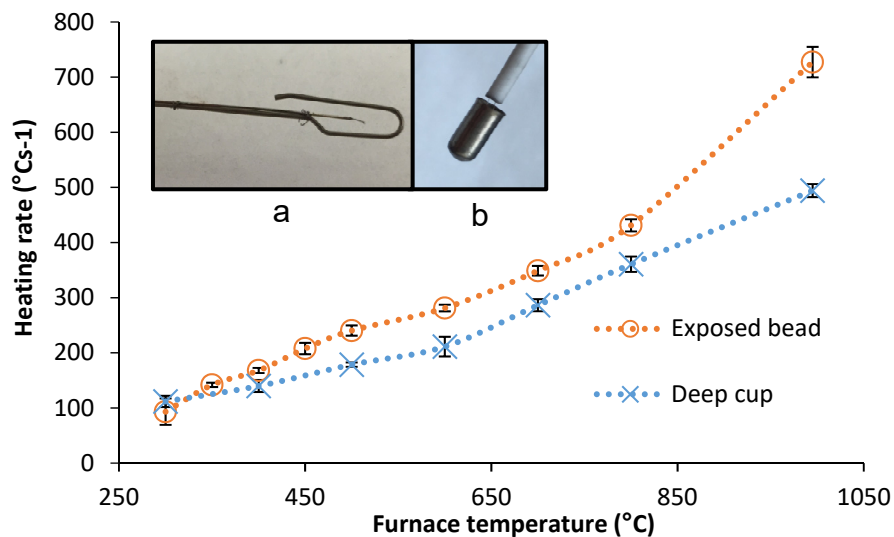
Figure 21. *Heating rates obtained in a furnace-based micropyrolyzer. (a) Exposed bead, and (b) Deep cup. When a cup was used, even for furnace temperatures as high as 995 °C, the heating rate was limited to ≈500 °Cs⁻¹.* [50]
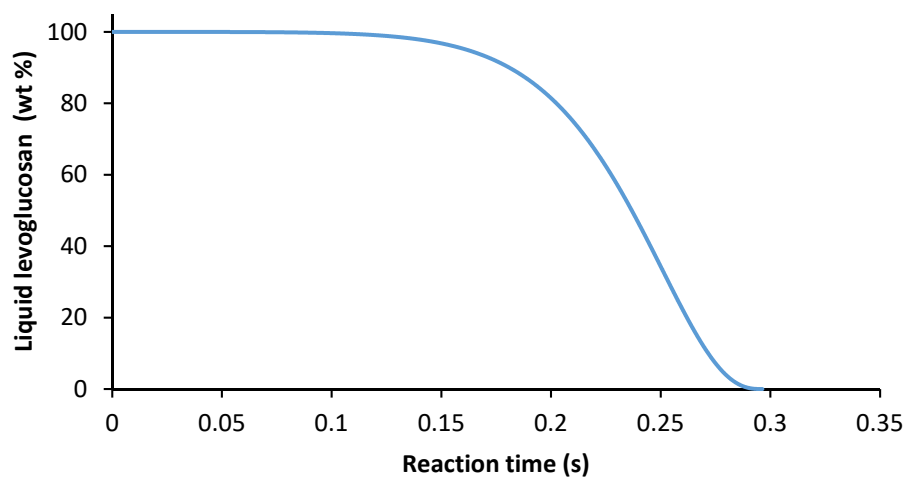
Figure 22. Evolution of levoglucosan when heated in a micropyrolyzer preheated to 400 °C. Liquid levoglucosan gets depleted, leaving virtually no char behind.

Degradation of levoglucosan in the gas phase

The second hypothesis proposes that gas-phase secondary reactions could decompose levoglucosan and reduce its yield as measured at the exit of the pyrolysis reactor. Such reduced yields are often observed for large reactors with long vapor residence times, but are not reported for micropyrolyzers, presumably because the vapor residence times are so short to preclude these secondary reactions.

An experiment considered the effect of the residence time of the pyrolysis gases by imposing a second heated zone immediately downstream of the pyrolyzer. Placing an empty catalytic bed beneath the micropyrolyzer in a tandem configuration incremented the residence time of the volatiles in a heated zone, shown in Figure 11. The vapor products leave the first reactor held at 400 °C, and the second reactor extended the residence time by ≈0.2 s with temperatures ranging between 400 − 600 °C.

For cases with lower temperatures, no significant production of non-condensable gases, such as carbon monoxide and carbon dioxide, was present in the GC-TCD chromatograms. Figure 23 clearly depicts the difference in production of degradation compounds when using commonly used pyrolysis temperatures. When the second reactor was heated to 600 °C, the production of CO and CO_2 increased significantly, orders of magnitudes higher than the signals observed at 400 and 500 °C.
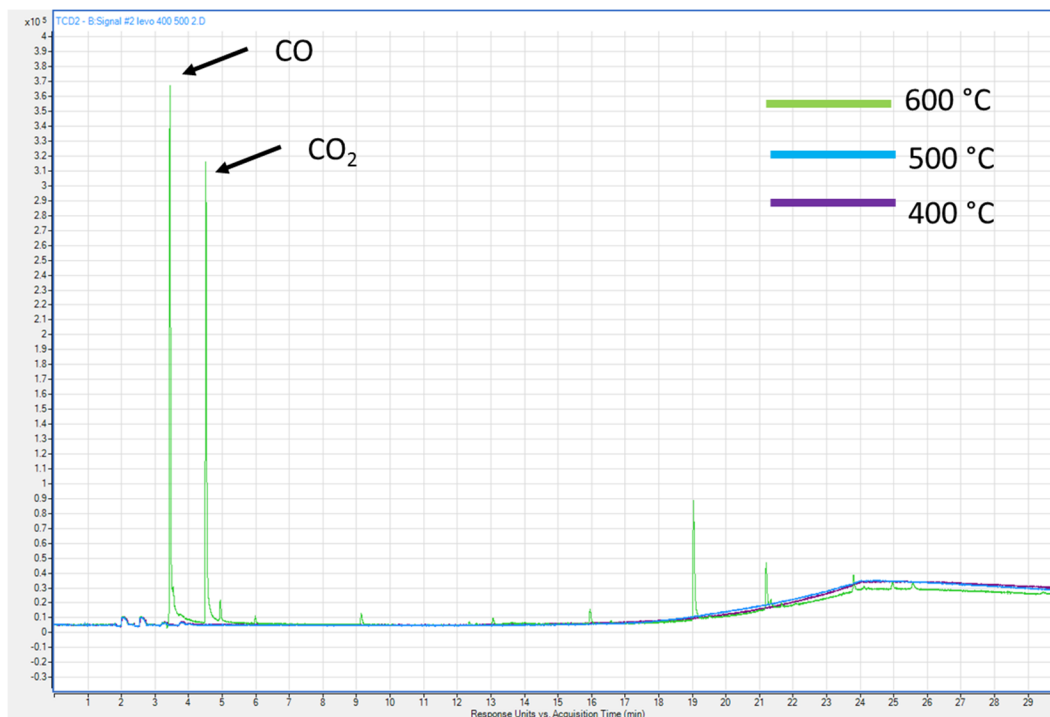
Figure 23. Overlaid TCD chromatograms from pyrolysis of levoglucosan with extended residence times. Important production of non-condensable gases is only present for the 600 °C extended reactor case.

To further explore the possibility of gas-phase degradation, the rates of secondary reactions were investigated to see if they were fast enough to occur during the relatively short transport time of vapors through the pyrolyzer. This was done by modeling the pyrolyzer as a continuously stirred tank reactor (CSTR) with the characteristic residence time of 0.2 s, and using the volatiles time evolution from cellulose pyrolysis as input to the reactor.

To determine the 0.2 s characteristic time of transport of volatiles through the micropyrolyzer, the time evolution of naphthalene vapors from the micropyrolyzer for a sample deposited on a wire hook was evaluated by connecting the furnace outlet directly to

a FID detector and later analyzed as the first order system response to an impulse input.

The same apparatus was utilized to obtain the time evolution of volatiles from cellulose

pyrolysis experiments, and some examples of this evolution are presented in Figure 24, as a

function of pyrolysis temperature.
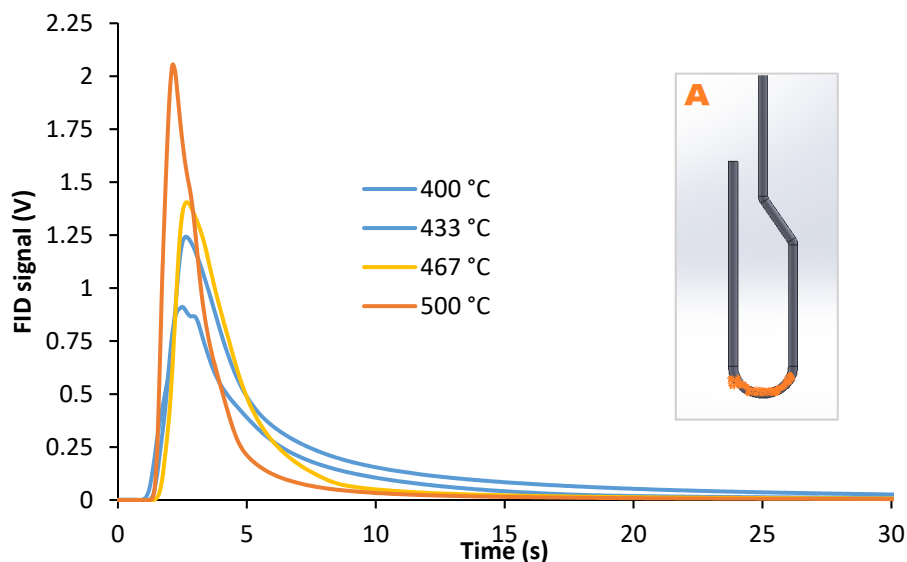
Figure 24. The FID signal indicated the time evolution of volatiles during cellulose pyrolysis in a micropyrolyzer. The image labeled A illustrates the area of the sample holder hook that was coated with a thin film of cellulose powder.

To perform the calculations, kinetic data for the gas-phase degradation of

levoglucosan was obtained from multiple sources, summarized in Table 3. Figure 25 displays

the modeled evolution of volatiles from the CSTR reactor with and without gas-phase

degradation of volatiles. Even when imposing high degradation rates, the reduction of volatile

products from cellulose is at most 13 wt.%, which rejects the hypothesis that the 60 wt.%

yield of levoglucosan is due to secondary gas phase reactions decomposing 40 wt.% of the

volatilized produced anhydrosugar.
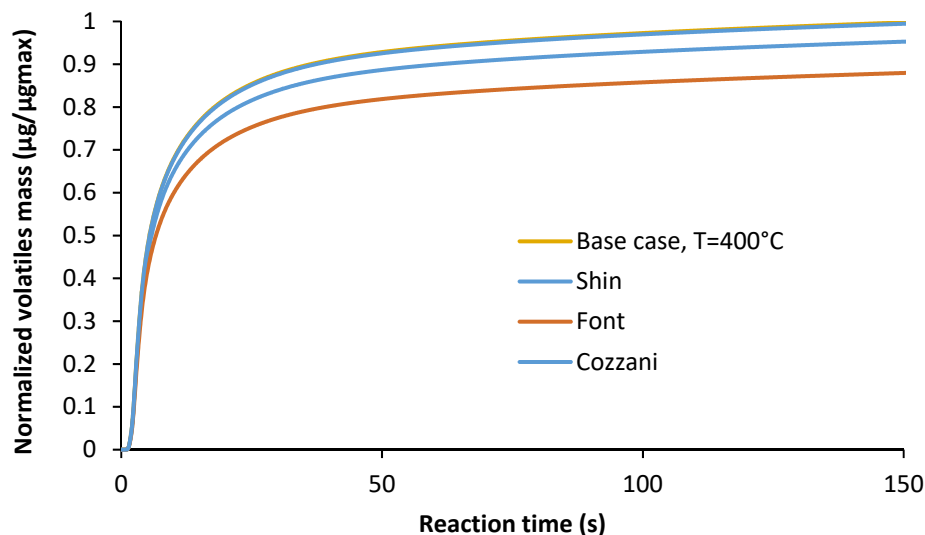
Figure 25. *Modeled evolution of volatiles, mainly levoglucosan, from cellulose pyrolysis at 400 °C. The produced levoglucosan suffered degradation rates corresponding to 600 °C to accentuate the gas-phase degradation.*

Experimental and analytical evidence does not support the hypotheses that slow devolatilization and/or gas phase degradation of levoglucosan accounts for levoglucosan yields being less than 100 % expected from stoichiometric considerations.

Repolymerization of Intermediate Products During Carbohydrate Pyrolysis

The tested hypothesis indicates that cellulose intermediate pyrolysis products repolymerize, by this means reducing the production of anhydrosugars. The studied possible products were glucose, proposed as part of the intermediate by Vinu et al.,[71] and the anhydrosugars cellobiosan, and a mixture of levoglucosan and cellobiosan, which have been identified as part of the condensed phase intermediate from cellulose pyrolysis. HPLC analysis of the condensed-phase products from the pyrolysis of model compounds allowed learning about the proposed repolymerization.

Figure 26 shows that pyrolysis of glucose at 400 °C appears to polymerize to cellobiose within 2 s. These results support the claim by Mettler et al. that indicated the pyrolysis of glucose includes a repolymerization step.[140] Additionally, xylose is not an expected product during glucose pyrolysis, so the presence of that peak should likely represent a similar product that eluted at the same time as xylose does in HPLC.
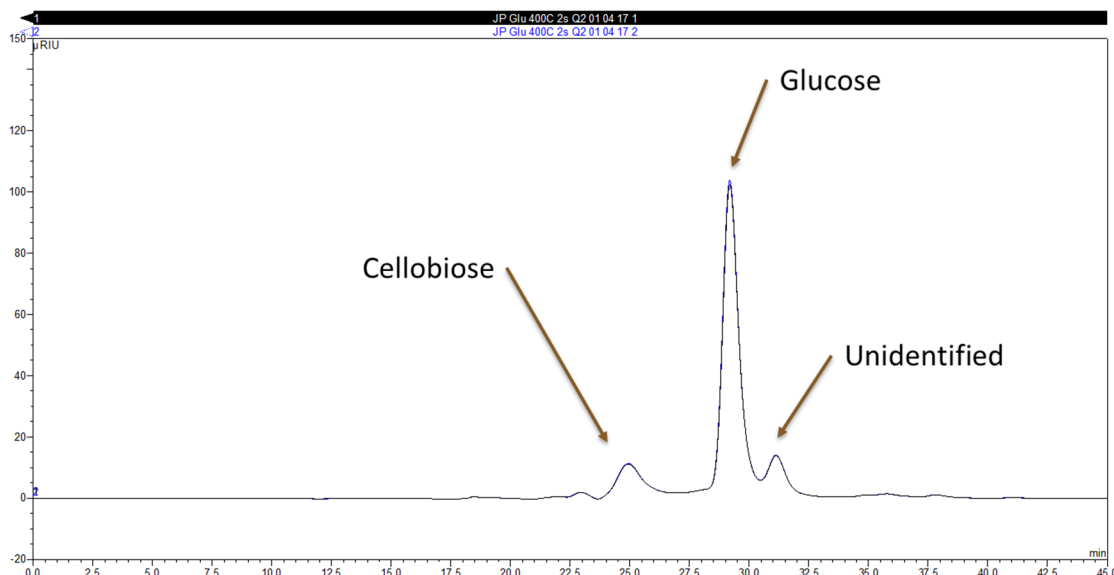
Figure 26. Condensed phase products after 2 s of glucose pyrolysis at T=400 °C. The presence of cellobiose indicates repolymerization of glucose.

In a similar situation, Figure 27 shows the water soluble cellobiosan pyrolysis products collected from the condensed phase. The plot shows no evidence of repolymerization of the anhydrodisaccharide.

Since both cellobiosan and levoglucosan are condensed-phase intermediate products of cellulose pyrolysis, the possibility that they undergo a condensation reaction was investigated. Figure 28 shows the water-soluble products from the co-pyrolysis of a 1:1

mass ratio mixture levoglucosan and cellobiosan. Only peaks of the initial materials are

visible in the plot, so their repolymerization does not appear to occur.
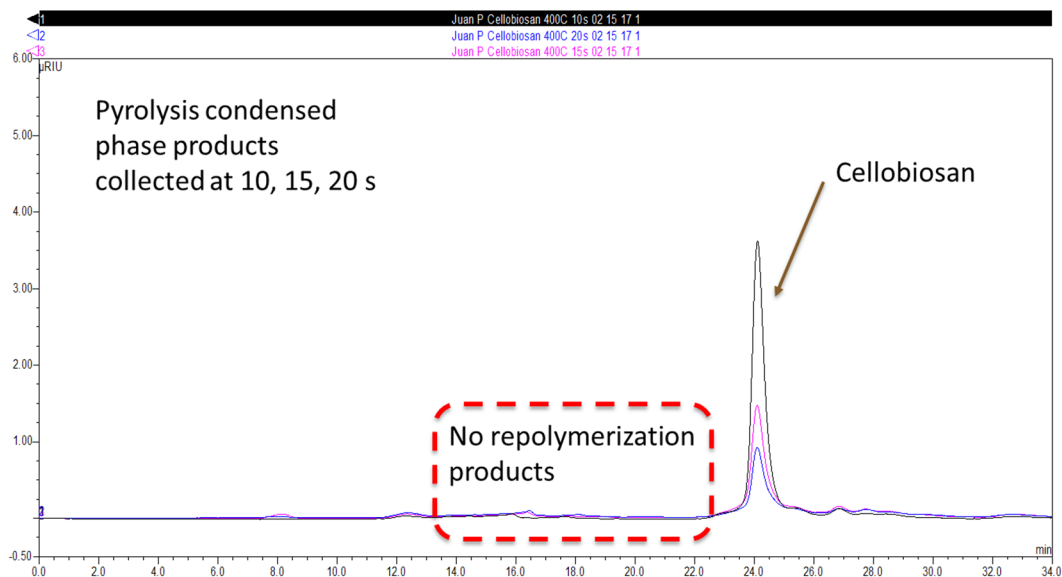
Figure 27. *Condensed phase products from sample cups during pyrolysis of cellobiosan at 10, 15 and 20 s, T=400 °C. Only peaks for the initial compound were identified, no evidence of repolymerization.*
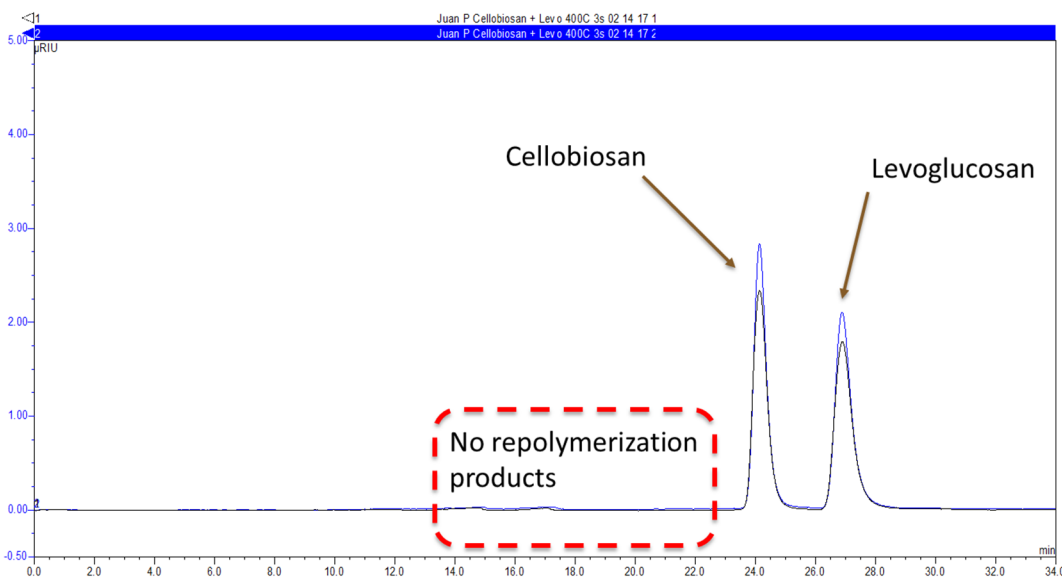
Figure 28. *Condensed phase products from sample cups during co-pyrolysis of cellobiosan and levoglucosan at 10, 20 and 30s, T=400 °C. Only peaks for the initial compounds was identified with no evidence of repolymerization.*

Continuing to explore the hypothesis that repolymerization is responsible for less than stoichiometric yields of levoglucosan, either fumed silica or a high boiling point aromatic compound was mixed with carbohydrate reactants to prevent coalescence and agglomeration during pyrolysis, potentially increasing the yield of levoglucosan. Hydrophobic fumed silica (Evonik, Aerosil R974) is an inert material commonly used as filler in paints, coatings, and adhesives.[165] The high boiling point (450 °C) aromatic compound, 1,2-benzanthoraquinone, has been shown to reduce char formation during pyrolysis of glucose.[64]
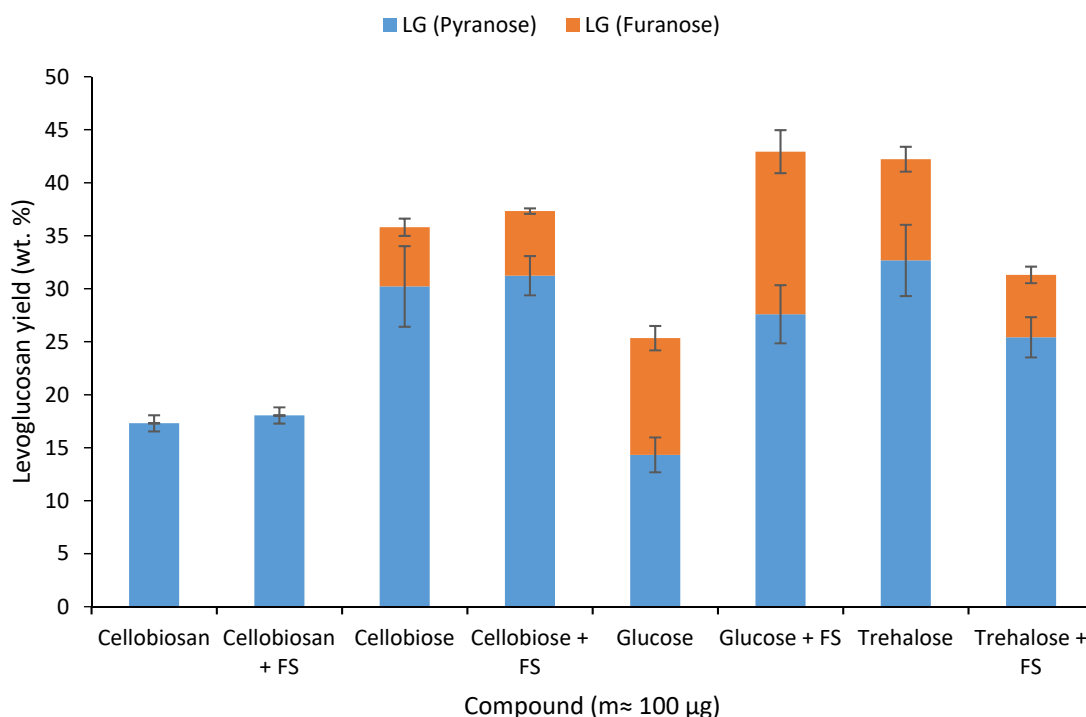
Figure 29*. Carbohydrate model compounds pyrolyzed with and without fumed silica (FS). The presence of FS increased levoglucosan yield from glucose; other model compounds either showed decreased yield of LG or little change. Error bars indicate one standard deviation in each direction from the average value.*

As presented in Figure 29, Glucose demonstrated a large and statistically significant increase in levoglucosan yield in the presence of fumed silica, which was expected since experiments confirmed there was repolymerization on the condensed phase during glucose pyrolysis. The increase in total levoglucosan was of $\approx$18 wt.%, with increasing in both the pyranose and furanose forms of levoglucosan. These results reveal a promising pathway to produce anhydrosugars from glucose in a manner that requires few extraction steps, given the low yields of other compounds such as furans.

It is interesting to observe a reduction in char from the bottom of the sample holder after the pyrolysis of the carbohydrate model compounds; however, only glucose presented an increase in levoglucosan production. Figure 30 and Figure 31 show images of the effect of fumed silica in the inhibition of char formation at the bottom surface of the sample holder for glucose and cellobiosan, respectively. Both cases show an important reduction in the formation of char, but only glucose yielded more anhydrosugars. Initial char yields from glucose pyrolysis was 4 μg and reduced to <1μg, which means that there was a small amount of char visually perceived on both the fumed silica and the surface of the cup, but the microbalance precision wouldn't allow to account for their weight.

On the other hand, the presence of cellobiosan char within the fumed silica was more noticeable, as shown in Figure 32. Since no repolymerization of cellobiosan was evidenced in the condensed phase to begin with, char inhibition was not a good candidate to increase levoglucosan yield from cellobiosan.
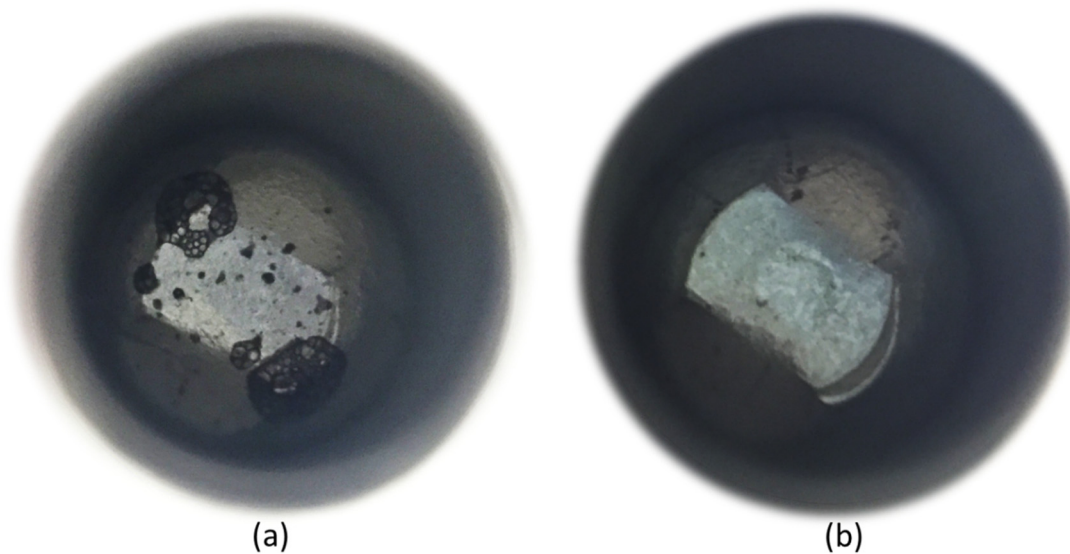
Figure 30. Solid residue at the bottom of the sample holder after pyrolysis of glucose (a) without fumed silica, and (b) with fumed silica. Char formation was clearly inhibited by the presence of fumed silica. Optical zoom 20x. The fumed silica was removed to allow visual access to the internal surface of the sample holder.
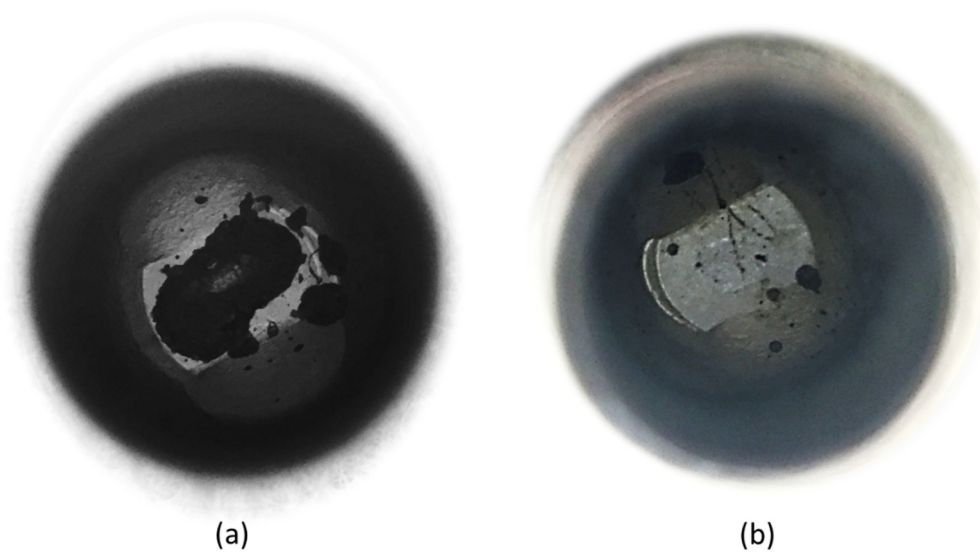
Figure 31. Solid residue at the bottom surface of the sample holder after pyrolysis of cellobiosan (a) without fumed silica, and (b) with fumed silica. Evident char formation inhibition by using fumed silica. Optical zoom 20x. The fumed silica was removed to allow visual access to the internal surface of the sample holder.
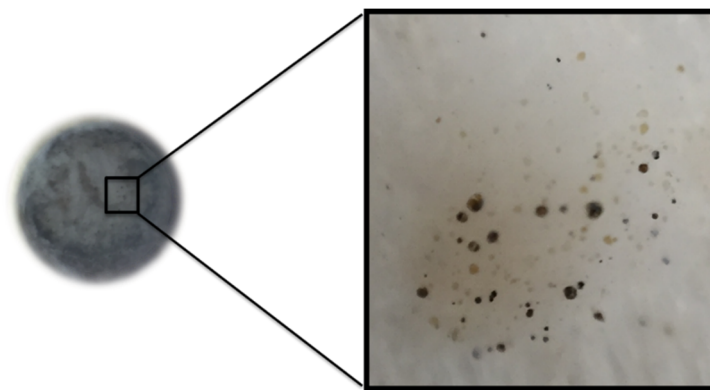
Figure 32. *Fumed silica, after cellobiosan pyrolysis. Some of the char was prevented to coat the bottom surface, but ended up distributed within the fumed silica matrix.*

In similar experiments, carbohydrate model compounds were pyrolyzed with the high boiling point 1,2-benzanthraquinone, which reportedly inhibited the production of char from cellulose pyrolysis.[64] The experimental results in the present study indicate no significant increase in the production of levoglucosan from cellulose nor cellobiosan. However, glucose presented approximately 20 wt.% increase, similarly to what happened in co-pyrolysis of glucose with fumed silica, as presented in Figure 33.
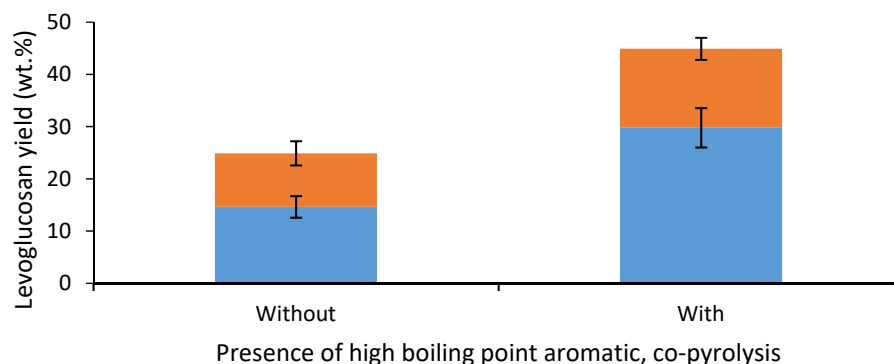
Figure 33 . *Levoglucosan yields from the co-pyrolysis of glucose with 1,2-Benzanthraquinone. Comparison with the control case reveals an approximate increase of total levoglucsaon of 20 wt.%. This result is ismilar to the one obtained from glucose co-pyrolysis with fumed silica.*

The experimental work presented no evidence of repolymerization of anhydrooligosaccharides in the condensed phase products of cellulose pyrolysis, rejecting the hypothesis that repolymerization of pyrolysis intermediates is responsible for low levoglucosan yields. On the contrary, pyrolysis of glucose production of cellobiose in the condensed phase, indicating repolymerization of glucose during pyrolysis.

On the other hand, utilizing fumed silica or 1,2-benzanthraquinone to prevent agglomeration and repolymerization of glucose increased levoglucosan yield from glucose by 18 and 20 wt.%, respectively. This suggests a potential pathway to produce anhydrosugars from glucose. However, this distinct behavior from other kinds of pyrolyzed sugars is difficult to explain.

Experimental Investigation of Thermohydrolysis During Cellulose Pyrolysis

Pyrolysis of cellulose in the presence of humidified carrier gas was performed to test the hypothesis that points to thermohydrolysis for the less than stoichiometric levoglucosan yields in this reaction. The presence of water was expected to increase thermohydrolysis to glucose. The collected condensed phase products were analyzed with HPLC looking for levoglucosan and glucose.

Figure 34 compares the concentration of levoglucosan collected at different cellulose pyrolysis duration tests $(5 - 40)$ s. The columns present cases with humidity ratio of 0 mg_{H2O}/m_{He} (no water added) and 0.035 mg_{H2O}/m_{He} (saturated carrier gas). No significant differences in any of the cases was observed. The plot presents the

concentration of levoglucosan as quantified by HPLC from the aqueous solution of

condensed phase products from cellulose pyrolysis at different times.
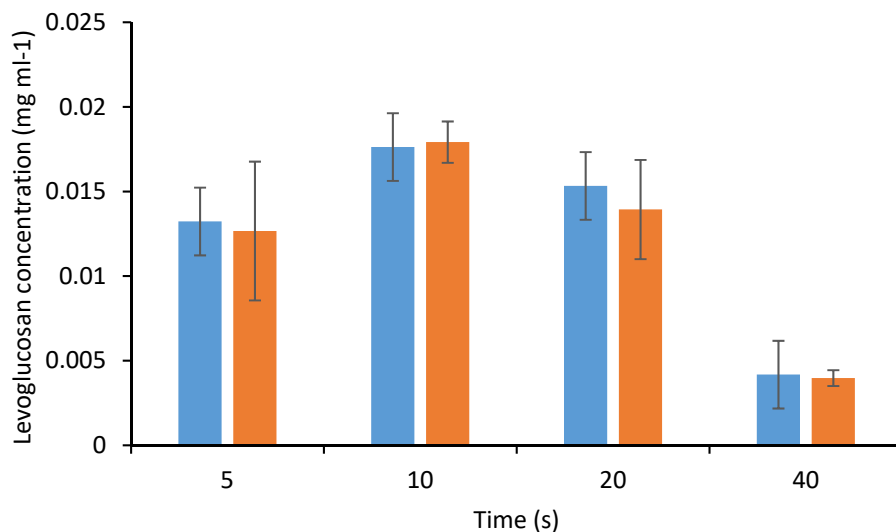
Figure 34. *Effect of added humidity to carrier gas on levoglucosan production from cellulose pyrolysis. No statistically significant difference between the levoglucosan production for any of the cases. Error bars indicate one standard deviation in each direction of the average value.*

Figure 34 shows the HPLC output signal for multiple tests, from top to bottom

duplicates at durations of pyrolysis of 5, 10, 20, and 40 s. All the cases with added humidity

to the carrier gas 0.035 mg_{H2O}/m_{He}. The lowest curve shows the output for the calibration

reading and the red box highlights the time of elution of glucose. As observed, none of the

collected condensed phase cellulose pyrolysis products presented a peak of glucose.

The results from these tests do not support the hypothesis that thermohydrolysis is

responsible for less than stoichiometric yields of levoglucosan.
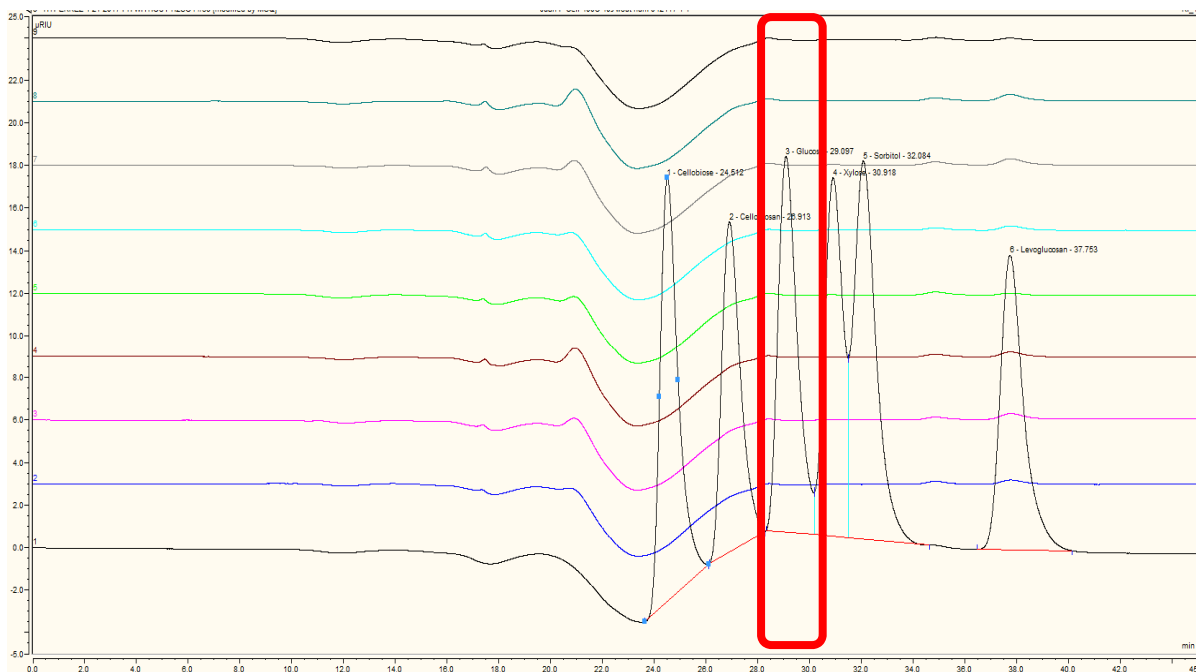
Figure 35*. Comparison between the water-soluble sugars from the condensed phase products from multiple pyrolysis experiments. From top to bottom products from tests with durations 5, 10,20, and 40 s in duplicates. For all the cases, water was added to the carrier gas to obtain 0.035 mg$_{H2O}$/m$_{He}$. The results from the calibration standard are presented reference for the positions of the peaks. None of the cases presented evidence of glucose.*

Experimental Methods to Measure Chemical Kinetic Constants

Before proceeding to measure chemical kinetic parameters for cellulose pyrolysis experiments, it was important to evaluate the possible heat and mass transfer limitations in the micropyrolysis device. The measured kinetic data is useful to model this fast pyrolysis reaction and learn some of its characteristics.

Evaluating heat and mass transfer limitations in micropyrolyzer experiments

Heat and mass transfer can limit chemical reactions and modify their apparent kinetic data. In general, it is recommended to use high carrier gas velocity, materials with high thermal conductivity, small particles/sample, and proper heating rates. This section

presents the results from the comparison of characteristic times for physical phenomena

and chemical reaction that will identify the presence or not of limitations in pyrolysis

reaction performed in the furnace-based micropyrolyzer.
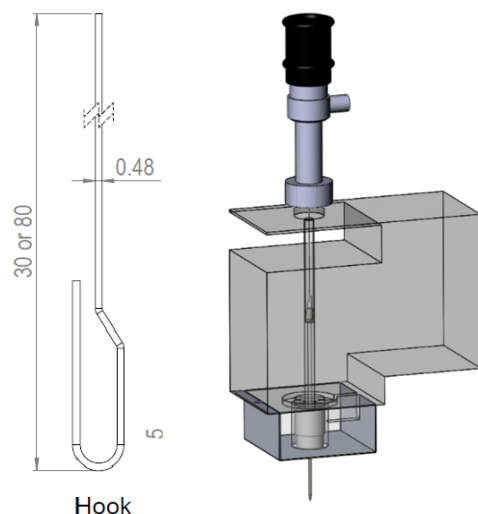
Figure 36. (Left) Hook or Simple sample holder. The thin film coats the top surface top of the U-shaped bend. (Right) Furnace-based pyrolyzer by Frontier. Sample falls into the preheated furnace to perform the experiment. Carrier gas flows from top to bottom for all the duration of the experiment.

In an effort to minimize heat transfer effects, a sample holder based on a wire hook

was employed (see Figure 36). It was possible to deposit a thin film ($\approx$4 µm) of cellulose[166]

on the U-shaped end of the hook. Experiments were performed with a furnace

temperature of 500 °C, with helium as carrier gas. Immersed in the pyrolysis furnace, the

sample is heated by convection from the carrier gas and radiation from the furnace walls.

Because the heating occurs on the outer surface of the sample, it is assumed that ejection

of aerosols from the sample does not take place, an assumption not necessarily valid when

the sample is heated from below by conduction, as occurs in the cases studied by Teixeira et

al.[111] who proposed aerosol ejection as a main mechanism of transport of products from pyrolysis.

Figure 37 summarizes the results of the analysis of heat and mass transfer limitations applied to the thin film sample used to study pyrolysis kinetics in a Frontier micropyrolyzer. Calculation of the non-dimensional Pyrolysis numbers (Py) proposed by Mettler et al.[91] indicate that heat transfer limitations are not present, neither from internal conduction (Py_I>1, Bi<0.1) nor convection to the sample (Py_{II}>1). Similarly, external mass transfer is not rate limiting because the lower value of the observed kinetic rate of produced volatiles will be the limiting factor, when compared with the mass transfer rate through the boundary layer surrounding the particle (ratio<10^{-2}). Finally, the internal mass transfer evaluated with the Wagner-Weisz-Wheeler modulus (M_W) is near the recommended value ($\approx$0.15 & <<4), as discussed in the background chapter of this document.

The use of high carrier gas flow rate is recommended to avoid mass transfer limitations, so the previous analysis is supplemented by conducting three tests with multiple flow rates to verify if the temporal responses from the gases produced during pyrolysis changes. Pyrolysis tests used thin film cellulose samples on a hook ($\approx$60 μg) in a furnace at 400 °C and with different helium flow rates (50, 100, 275 ml min^{-1}) where the flow rate recommended by Frontier is 100 ml min^{-1}. All test points were run in triplicates.

Figure 38 shows the time constant estimated for the decay portion of the FID signal from cellulose pyrolysis. For all the tested flow rates, the average constant is 3.18 s with standard deviation of 0.17 s. This indicates that the temporal response of evolution of volatiles is not affected by these changes in flow rate, reinforcing the idea of the absence of mass transfer limitations in these experiments.
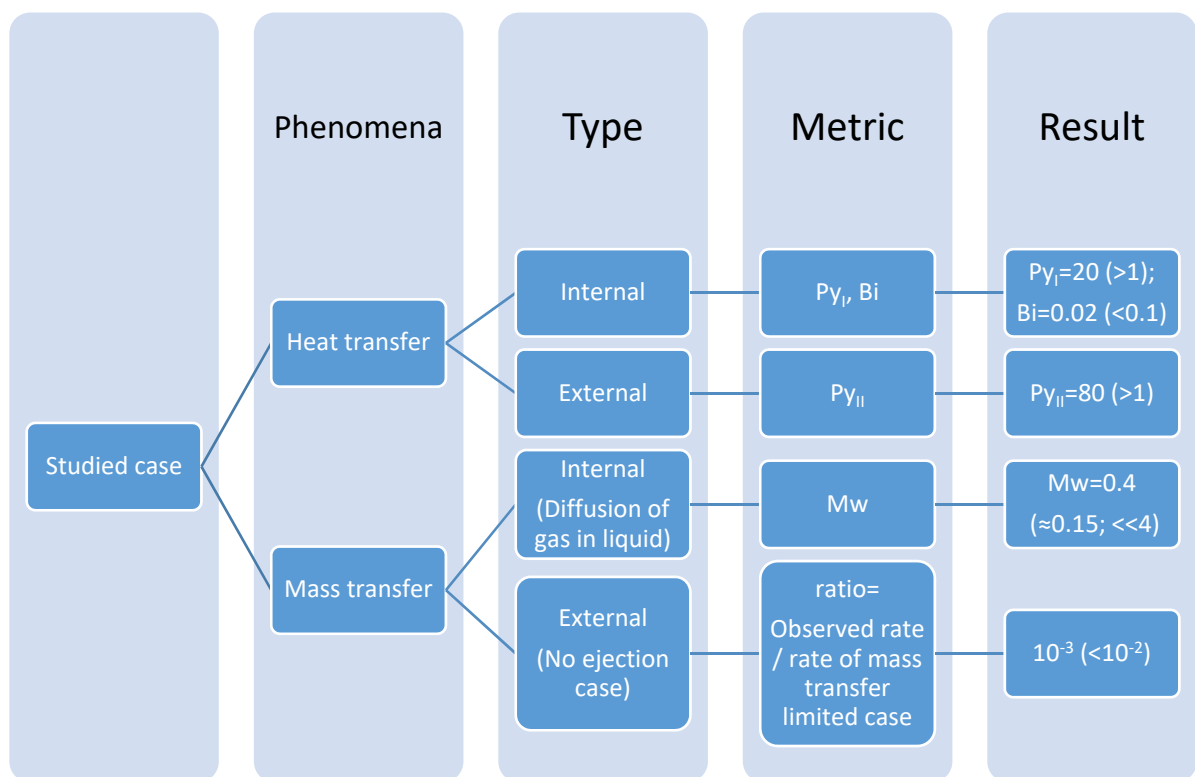
Figure 37*. Summary of heat and mass transfer considerations to implement a kinetically limited pyrolysis experiment. Diagram contains references to multiple authors.*[48,58,91,108,167]
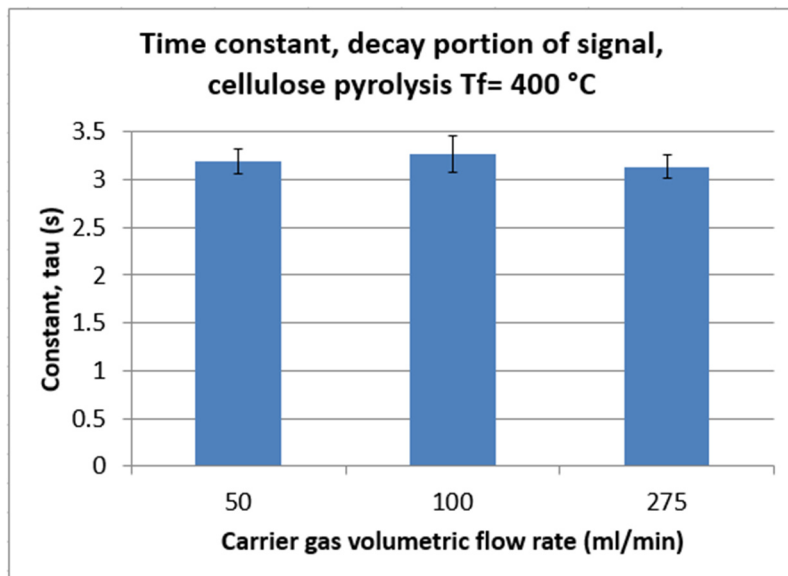
Figure 38*. Comparing the characteristic time of the time evolution of gases from pyrolysis of cellulose at multiple volumetric flow rates (50 - 275 mlmin^{-1}). No significant difference between the values.*

Global chemical kinetics of cellulose and other carbohydrates during pyrolysis

Having determined that the cellulose pyrolysis experiments conducted in the furnace based pyrolyzer are reaction kinetic limited, the data produced from this reactor can be used to determine kinetic parameters. The micropyrolyzer is assumed to be a mixed flow reactor, and the generated pyrolysis gases represent an impulse input to this reactor.[108] For all the experiments, there is a time delay from the beginning of the test, when the cup is dropped to the furnace, until the signal starts rising (y>0). This delay represents the heating time, as well as the presence of the short column connecting the pyrolyzer to the detector. This column represents plug flow where no reaction occurs [108].

Before compiling the analyzed data, it should be compared with the transport capability of the reactor to determine its usability. Figure 39 shows the FID signal of an early

set of experiments for cellulose pyrolysis. Analysis of these curves revealed the

characteristic time constants of their individual decay portions.
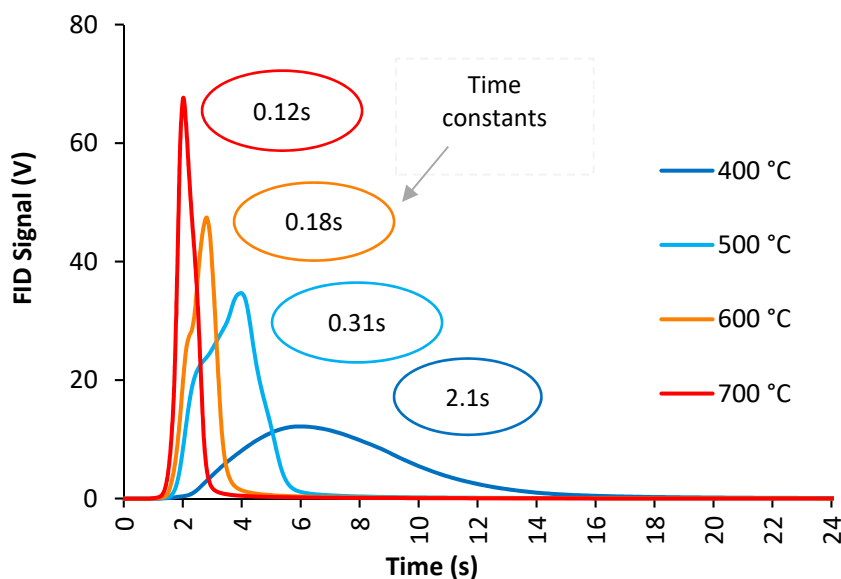
Figure 39. *The FID response during cellulose pyrolysis is highly dependent on micropyrolyzer temperature. The numbers in circles show the characteristic time for the different curves obtained at temperatures 400 – 700 °C.*

Ethanol volatilization in the reactor helped to obtain the characteristic time for the

transport of gasses out of the micropyrolyzer. The test revealed that the average transport

characteristic time is 0.15 s for temperatures between $400 - 700\ °C$, and this value became

the reference to determine the usability of the collected pyrolysis data. Figure 40

summarizes the comparison between characteristic times of the evaluated pyrolysis cases

and leads to the conclusion that only data obtained with furnace temperatures below 500

°C can be used, otherwise the data analyzed at higher temperature will provide information

of mass transfer, not from the chemical reactions.
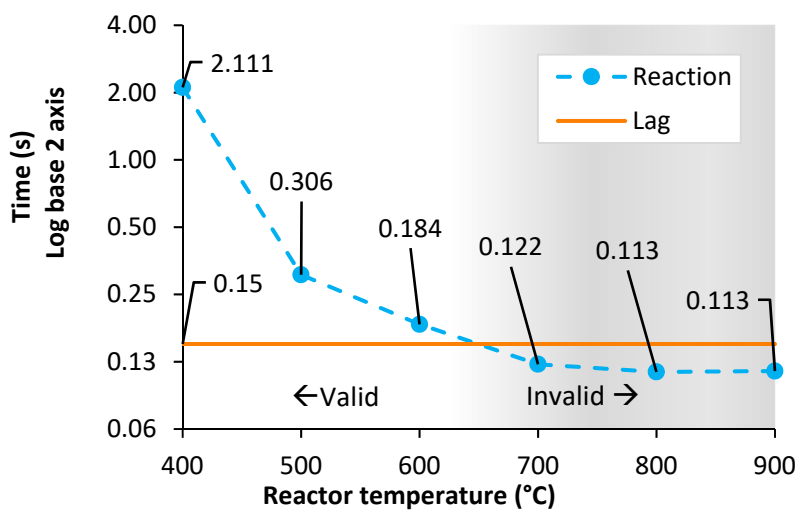
Figure 40. *Time constants below 0.15 s cannot be used to estimate kinetic parameters.*
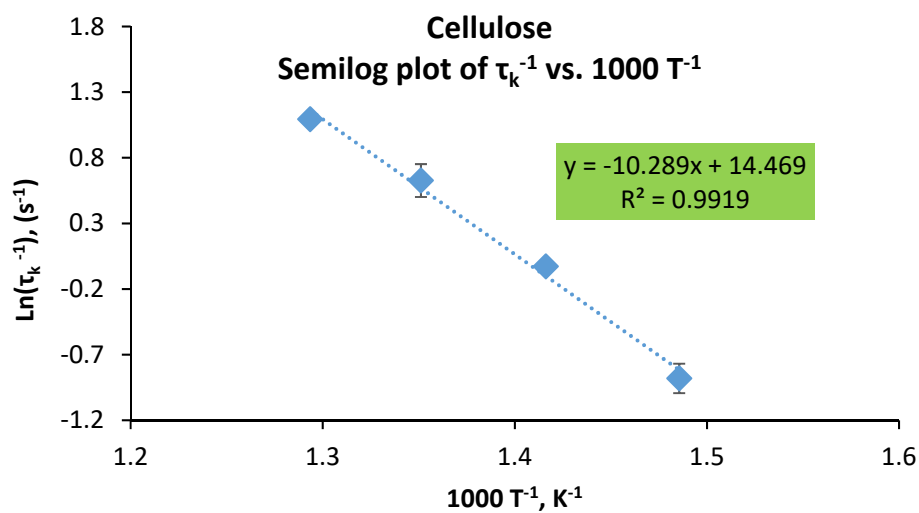
Figure 41. *Cellulose pyrolysis at furnace temperatures ranging from 400-500 °C indicates the apparent activation energy is 85 kJ/mol. Errors bar indicate the standard error in each direction, tests run in triplicates.*

Analysis of the FID signals product of the pyrolysis of cellulose and other

carbohydrates revealed interesting features of the reactions. Based on the Arrhenius

expression for activation energies, a plot of the logarithm of reciprocal kinetic time constant and reciprocal absolute temperature form a line where the slope is proportional to the activation energy. This analysis indicates an activation energy of 85 kJ mol^{-1}, which is lower than the 150 - 250 kJ mol^{-1} typically reported in the literature for cellulose pyrolysis.[38,65,70,71,78,89,168]

Pyrolysis of model compounds with different degrees of polymerization and reducing-end (RE) and non-reducing end (NR) combinations provided some interesting results. Cellulose and cellobiose contain both a RE and NR. On the contrary, trehalose and α-cyclodextrin only contain NR. Figure 42 and Figure 43 are the semi-log plots summarizing the results of the pyrolysis tests on NR containing compounds. The kinetics analysis resulted in similar values for activation energy for the model compounds, indicating that the energetic barrier to thermally decompose these compounds is not affected by the presence of the RE. Additionally, this supports the idea that cellulose and the model compound α-cyclodextrin present the same activation energy, as proposed by Zhu et al. with their PHASR reactor.[77]

Similar analysis conducted on monosaccharides such as glucose, mannose, and the disaccharide sucrose, lead to activation energies ≤40 kJ mol^{-1} which are indicative of mass transfer limitations in these tests. For all of these components the hook was covered with char-like residue that presented a macroscopic-scale structure that suggested bubble bursting and gas formation within the liquid intermediate, a case of mass transfer limitation probably due to the high boiling point of the liquid intermediate.[58,169]

α-Cyclodextrin
Semilog plot of τ_k^{-1} vs. 1000 T^{-1}

$y = -10.36x + 14.652$
$R^2 = 0.9866$
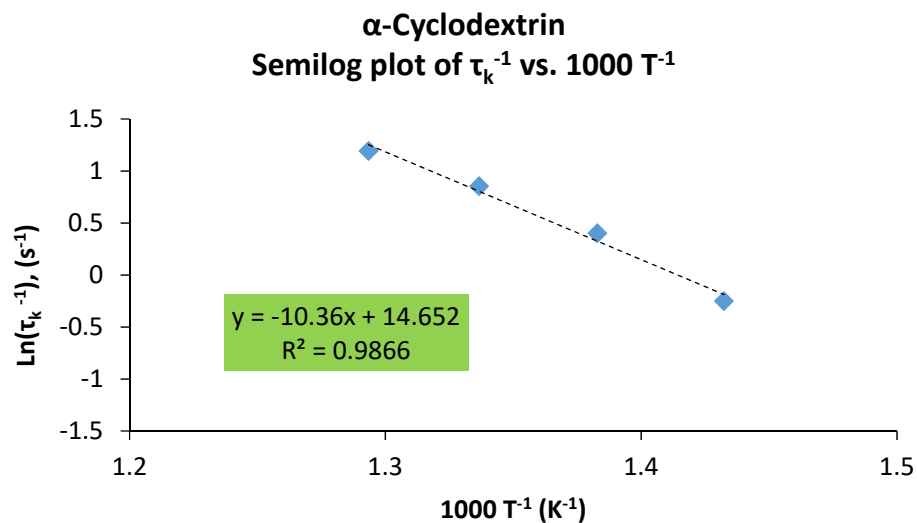
Figure 42. α-cyclodextrin pyrolysis at furnace temperatures ranging from 425-500 °C indicates the apparent activation energy is 86 kJ/mol. Error bars indicate the standard error in each direction, tests run in triplicates.

Trehalose
Semilog plot of τ_k^{-1} vs. 1000 T^{-1}

$y = -10.523x + 15.183$
$R^2 = 0.9392$
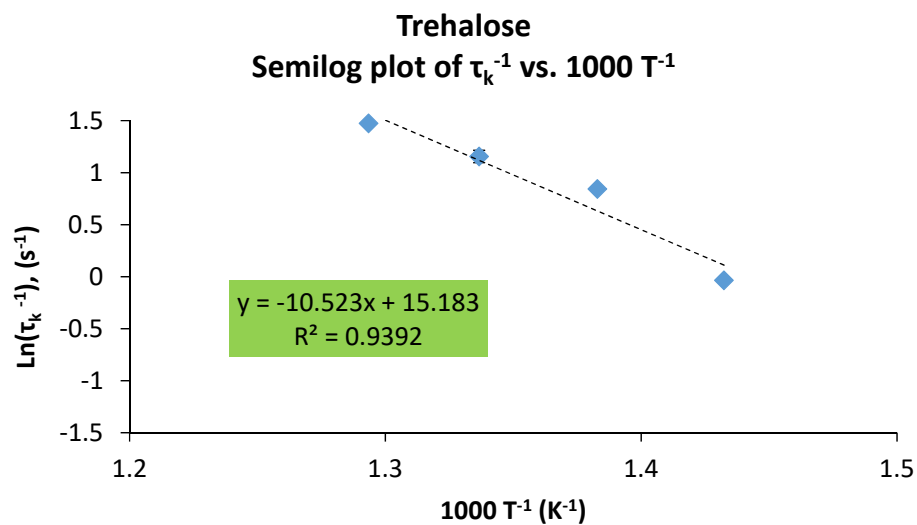
Figure 43. Trehalose pyrolysis at furnace temperatures ranging from 425-500 °C indicates the apparent activation energy is 87 kJ/mol. Errors bars indicate the standard error in each direction, tests run in triplicates

Kinetic data analysis

First-order, global kinetics as assumed for cellulose is an appropriate initial approach, however this disguises other features of the reaction. Cellulose pyrolysis is a complex combination of parallel and series competing pathways that can present different kinetic data.[107,170] Friedman analysis as well as model fitting in this section were performed on the evolution of volatiles from cellulose fast pyrolysis experiments to learn more about this complex reaction.

Fast pyrolysis of thin film of cellulose yielded the time evolution of volatiles as reported by the FID connected to a pyrolyzer through a short inert column. Friedman analysis of this dynamic data reveals a change in activation energy during the process for the tested range of temperatures (400-500 °C). It is important to notice that the FID signal utilized for these kinetic analyses comes from volatiles released during pyrolysis from which the majority is levoglucosan, but it will have other smaller molecules as well.

In complex reactions such as pyrolysis of cellulose, the presence of multiple products may be represented by multiple activation energy values.[107] In Figure 44 the variable activation energy and pre-exponential factor are shown against the conversion (α), these curves were obtained from the analysis of the evolution of volatiles curves for temperatures between 400-500 °C. Near $\alpha=0.5$, both kinetic parameters peak. The highest activation energy of 80 kJ mol^{-1} differs in about 6% from the value estimated using a first order approximation. The low values of activation energy that appear towards values of high conversion may arise from signal noise. At such high levels of conversion, no important amounts of levoglucosan are expected to be produced.
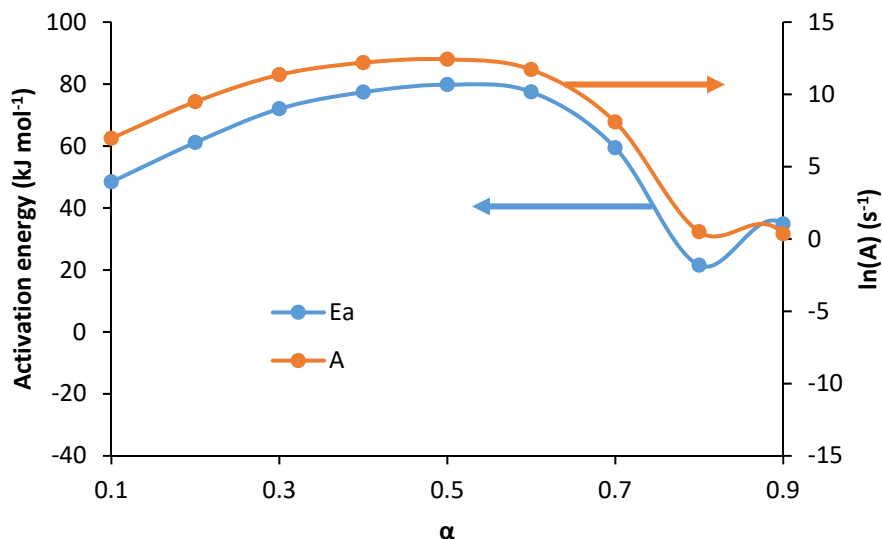
Figure 44. *Results from Friedman analysis. The plot shows the variation of activation energy and pre-exponential factor depending on the progress of volatile production, indicated by the conversion (α). Activation energy peaks at 80 kJ mol^{-1} at halfway full conversion.*

Figure 45 shows the reaction rate plotted against conversion (α) from cellulose pyrolysis experiments conducted at furnace temperatures between $400 - 500$ °C. The pyrolyzer is connected to a FID through a short inert column which allows obtaining a voltage signal that shows the time evolution of volatiles produced from cellulose. The first derivative with time of this signal represents the rate of reaction. Conversion is obtained from the same FID signal. It is interesting to observe the sigmoidal behavior of the curve, that includes accelerating and deaccelerating portions. Per Wall et al.,[107,142] this behavior is consistent with a random initiation that at first accelerates due to the increase of smaller non-volatile oligomers that will provide a high number of chain ends to be unzipped.[107] The deceleration that proceeds is due to the gradual release of volatiles that will finally consume

all the pyrolyzing material. The observed behavior indicates that the reaction initiates with the cracking reaction. The produced anhydrooligosaccharides increase the total number of chain ends that will release volatile levoglucosan via the unzipping reaction. This finding is similar to the proposed by Zhu et al.[77] of an intra-chain bond breakage that produces fragments that decompose via chain-end reaction to volatile products and char for a temperature of reaction <467 °C. Additionally, it is important to mention that other authors have observed the sigmoidal behavior of the reaction rate from slow pyrolysis gathered data,[3] meanwhile the work in this document entails fast pyrolysis experiments exhibiting the same sigmoidal behavior.
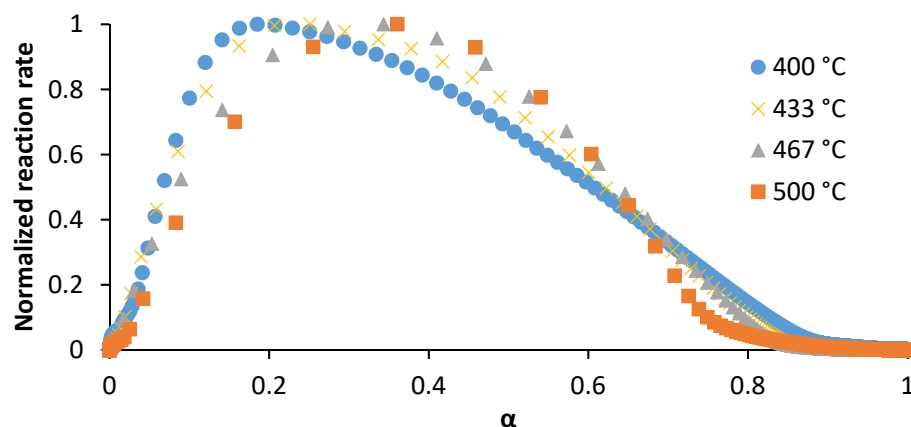
Figure 45. Reaction rate as a function of conversion (alpha) for conducted fast pyrolysis tests with furnace temperatures between 400-500 °C. The curve shows a clear initial acceleratory phase followed by a deceleration, both characteristics of a random initiation with short unzipping lengths.

The dynamic data of the evolution of volatiles from cellulose pyrolysis was analyzed using the Generalized reduced reaction rate curve plotted against conversion. This plot is used to fit the data to ever increasingly sophisticated models. Figure 46 shows multiple

models fit to the data set collected from a furnace preheated to 433 °C. The best fit corresponds to the extended Prout-Tompkins model which is of sigmoidal behavior. Between 20 and 50 % conversion there is a poor fit of the data points.

On the contrary, the more sophisticated Sestak-Berggren model closely fit the data points obtained in 500°C cellulose pyrolysis experiments, as shown in Figure 47. The Sestak-Berggren is used to represent two step reactions for polymer crystallization, where the first step is the appearance of random nucleation sites followed by the second step of crystal growth.[171] Similarly, depolymerization of cellulose can be considered of having first, the production of lower DP fragments through random scission, which corresponds to nucleation in the crystallization example, and the second step is the release of volatiles from the smaller fragments, which is equivalent to the growth of the nuclei in the crystallization example.
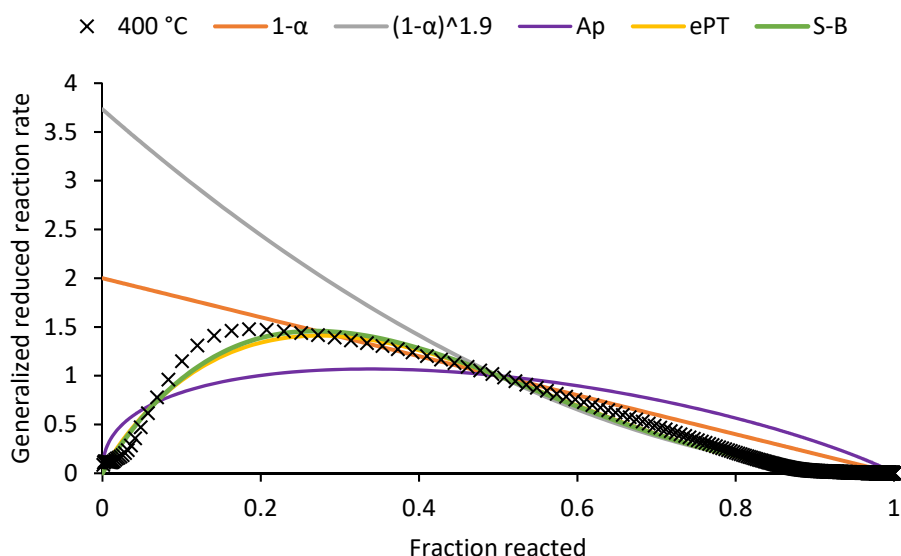
Figure 46. *Generalized reduced reaction rate as a function of conversion (α). Multiple models show different levels of fit. The extended Proust-Thomson model, ePT (m=0.9, n=2.37, q=0.999) gives the best fit for this pyrolysis test at 400 °C, with RMSE=0.020.*
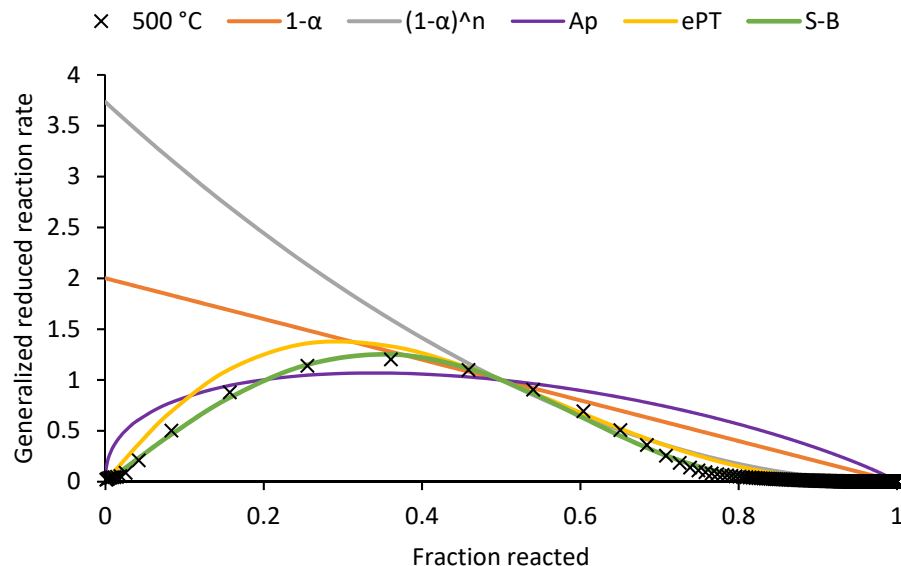
Figure 47. Generalized reduced reaction rate as a function of conversion (α). Multiple models show different levels of fit. The extended Sestak-Berggren model, S-B (m=-26.1, n=14.7, p=27.16) gives the best fit for this pyrolysis test at 500 °C, with RMSE=0.005.

The dynamics data obtained from cellulose pyrolysis was useful to obtain kinetic parameters of the reaction as well as revealing important features of the reaction. The Friedman analysis showed a varying activation energy and the model fitting efforts supported the existence of multiple steps during cellulose pyrolysis and related them with cracking and unzipping reactions proposed to explain this thermal degradation of cellulose.

Modeling Cellulose Pyrolysis

Cracking and unzipping initial models

Cracking as the only depolymerization reaction

The model could simulate the rapid decrease in the degree of polymerization of the cellulose fragments. Figure 48 summarizes the results from this simple model. Notice the

evolution of the result is presented per step. This arbitrary progression of the reaction

eliminates the need to tie the model with kinetic data. As it was expected, the results

repeatedly gave a 50/50 split between the two kinds of products, unstable monomer (UM)

and levoglucosan (LG). These results indicate the need of an additional reaction to be able

to produce more levoglucosan from cellulose pyrolysis.
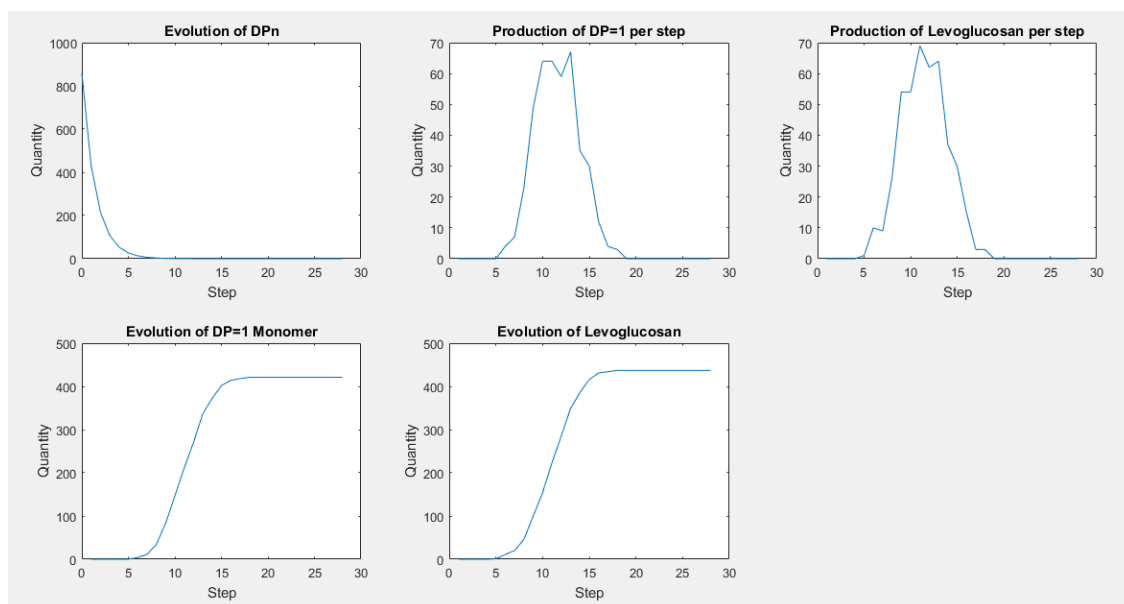
Figure 48. Results from cracking-only model for cellulose pyrolysis. T=500 °C. Lower plots show the cumulative monomer and levoglucosan evolution, resulting in a final 50/50 split.

Cracking and unzipping model

Kinetic constants were obtained from literature as well as experimentally, and are

shown in Table 4. However, the pre-exponential factor for the cracking reaction was

adjusted to $5x10^{17}$ (s^{-1}) to accommodate to the experimentally observed time scale. Mayes

et al.[70] assumed an isothermal case when they calculated the activation energy for the

cracking reaction. As previous experiments showed, there is a transient heating process at

the beginning of pyrolysis of cellulose in a micropyrolyzer.[50] A larger preexponential factor

was necessary to aid the reaction rate matching the fast pace of the cracking reaction.

Table 4. *Chemical kinetics data utilized in models*

Reaction	Activation Energy (kJ mol^{-1})	Pre-exponential factor (s^{-1})	Source
Cracking	231	4×10^{13}	Mayes et al.[70]
Unzipping	72	1×10^{5}	Own experimental data

Multiple cases were simulated to understand the participation of cracking and

unzipping during cellulose pyrolysis. In Figure 49, the relative production of levoglucosan

(LG) and unstable monomers (UM) are shown. By simulating pyrolysis of an ideal cellulose

chain at 400 °C with an initial degree of polymerization of sixty ($DP_o = 60$), a final

levoglucosan yield of 64 wt. % was approximated, similar to values obtained experimentally.

Moreover, when comparing the yields of levoglucosan produced at different temperatures,

there was good agreement between simulated and experimental results, as can be seen in

Figure 50. Even though this model matched the characteristics of the reaction, it has a

weakness, which is the use of different activation energies to break similar glycosidic bonds

by cracking and unzipping. The glycosidic bonds broken by either reaction are expected to

require similar activation energies.[172]
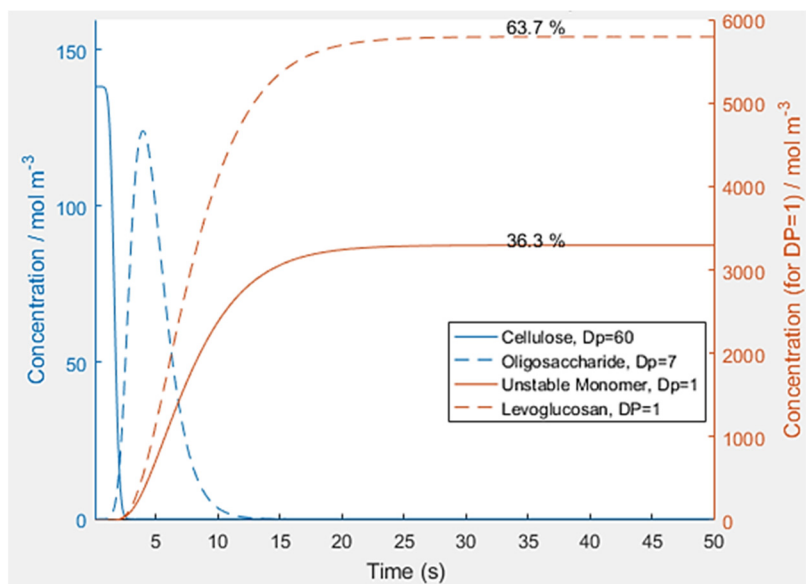
Figure 49. *Evolution of the concentration of multiple fragments during cellulose pyrolysis at 400 °C and initial DPo= 60. Fragments of size Dp=7, Dp=1, and Levoglucosan (LG) are shown.*
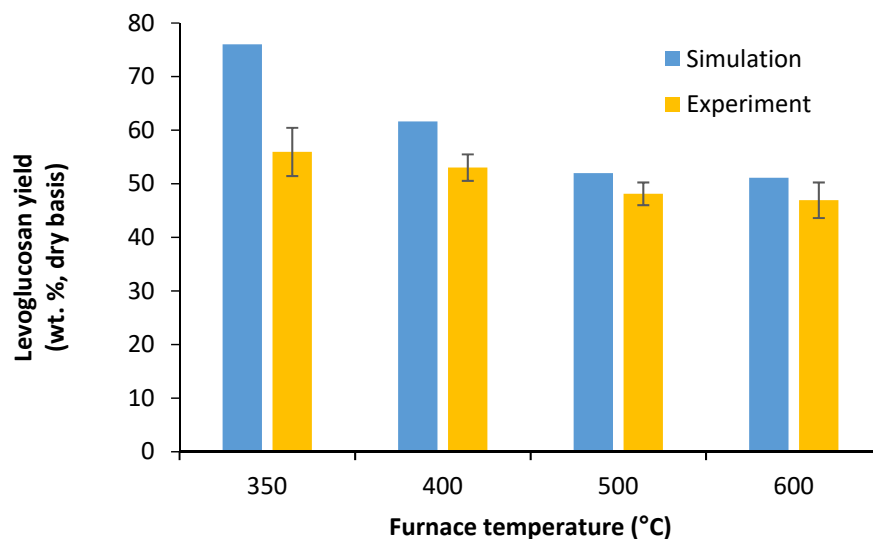
Figure 50. *Levoglucosan yield from cellulose pyrolysis at temperatures ranging 350 - 600 °C. Comparison between experimental and simulated results. Error bars show 95% confidence interval.*

<u>Cracking and unzipping model with limited unzipping levoglucosan yields</u>

The last presented model captured the behavior of the pyrolysis of cellulose by presenting a comparable time scale, as well as predicting yields of ≈ 60 wt.%, as experimentally evidenced. However, its weakness is the use of assigned kinetic data. The different activation energies assigned to cracking and unzipping go against the notion that similar bonds, glycosidic bonds for this case, should have similar activation energies for their thermal degradation.[172]

A new model was devised to overcome its predecessor's limitation. As its predecessor, this model includes thermal degradation through competing random cracking, and unzipping reactions, which produce lower DP anhydrosugars and volatile levoglucosan, respectively. Additionally, this model included the effect of the chain length in the yield of levoglucosan produced from unzipping reactions. Figure 51 shows the effect of chain length on the yield of levoglucosan from different model compounds. Pyrolysis of these model compounds was performed in a micropyrolyzer preheated to 400 °C, the sample size was 100 ± 10 μg. The trend shows an increase in levoglucosan yield with increasing degree of polymerization. Pyrolysis of other model compounds with DP 4 and 5 was performed, but the yields didn't follow the trend observed with the rest of the compounds, presenting low yields <15 wt.%. These low yields may possible be caused by large particle sizes and possible presence of inorganic impurities that can prevent the production of levoglucosan, as has been seen in the pyrolysis of cellulose and other carbohydrates.[173–176]
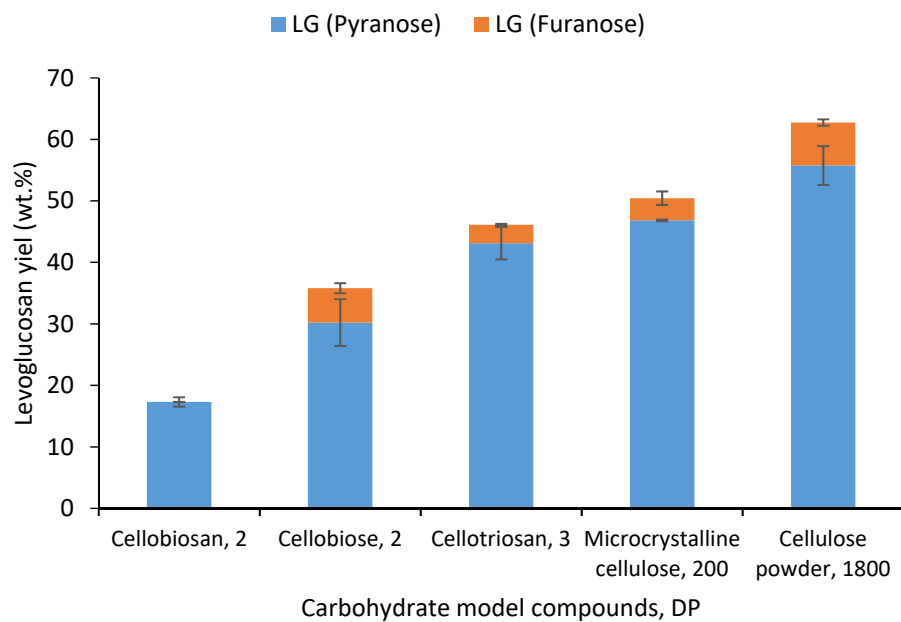
Figure 51. *Chain length effect on levoglucosan yields from the pyrolysis of increasing DP cellodextrins.*
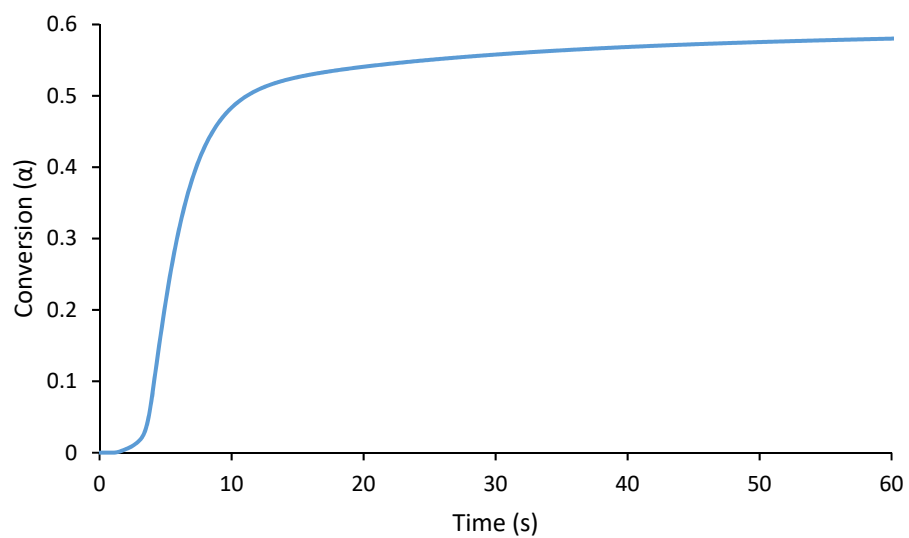
Figure 52. *Time evolution of conversion during the pyrolysis experiment on a thin film of cellulose using a furnace at 400 °C.*

Figure 53 presents the simulated results obtained with a furnace at 400 °C. The

utilized kinetic data is presented in Table 5. The time scale of the reaction and the yield of

levoglucosan are in accordance with experimental results. To aid comparison of the curve

characteristics, Figure 52 shows the evolution of volatile products during the pyrolysis of

cellulose in a test with furnace temperature at 400 °C.

Table 5. *Chemical kinetics data utilized in new combined model.*

Reaction	Activation Energy (kJ mol^{-1})	Pre-exponential factor (s^{-1})	Source
Cracking	85	1×10^5	Measured.
Unzipping	85	1×10^7	Measured; Assigned.

As displayed in Figure 53, the results obtained with the new model can reproduce

the evolution of products during cellulose pyrolysis. It is interesting to observe the evolution

of the monitored fragments with Dp=7 and Dp=2 (cellobiosan). The sharp disappearance of

the initial cellulose chain is followed by the production of DP=7, and this is followed by the

production of cellobiosan. Levoglucosan production climbs to the asymptotic value

meanwhile cellobiosan disappears. The total yield of levoglucosan in this example is

approximately 65 wt.%, close to experimental results.
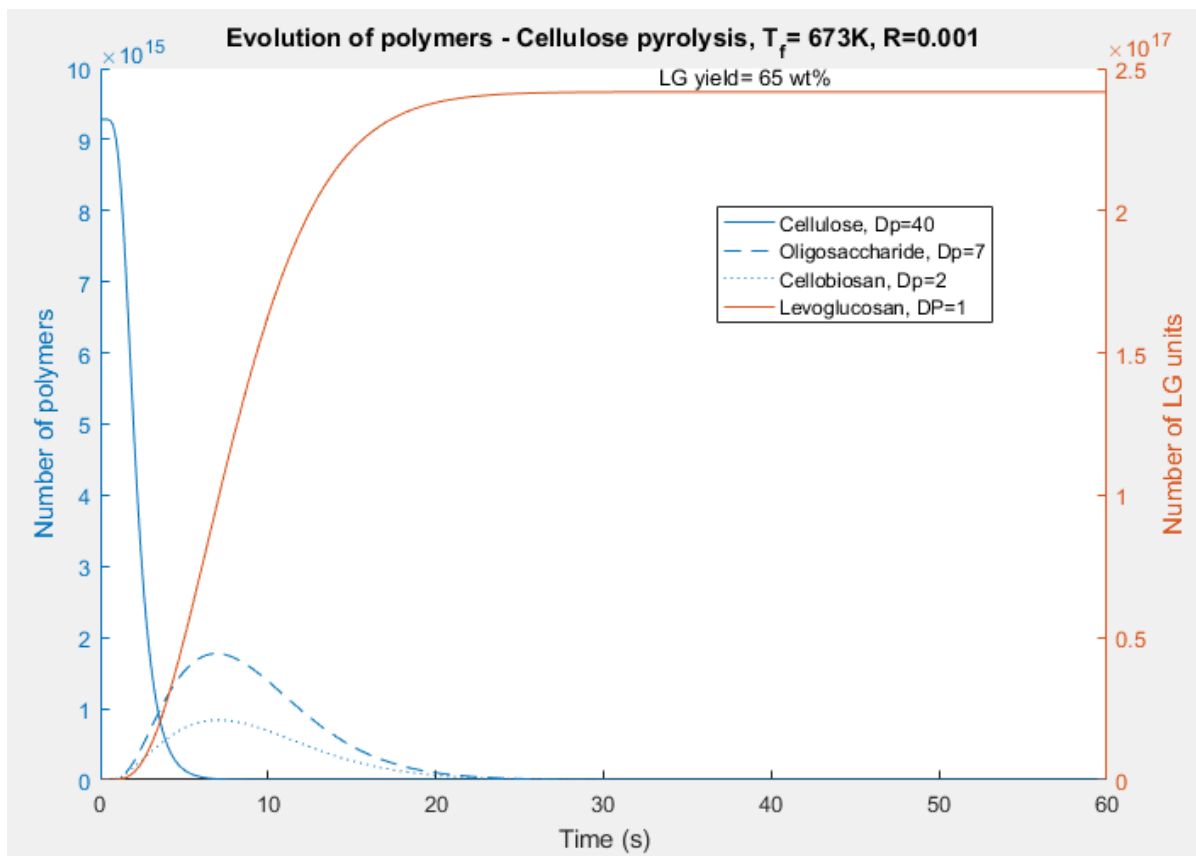
Figure 53. *Simulated evolution of products from cellulose pyrolysis, utilizing the new combined model. The model limits the production of levoglucosan to ≈60 wt.% because the chain length effect varies the yields of levoglucosan from unzipping depending on the length of the DP of the chain..*

CHAPTER 5

CONCLUSIONS AND FUTURE WORK

Conclusions

Pyrolysis of levoglucosan was conducted evidencing high recovery of this anhydrosugar. Additionally, experiments with an extended volatile products residence time did not degrade levoglucosan in the gas phase, when the reactor temperature was lower than 600 °C. Similarly, calculations predicted low level of degradation of levoglucosan leaving the furnace based reactor. The evidence does not support the hypotheses that slow devolatilization and/or gas phase degradation of levoglucosan accounts for levoglucosan yields being less than 100 % expected from stoichiometric considerations.

Pyrolysis of levoglucosan and/or cellobiosan, presented no evidence of repolymerization products present on the condensed-phase, rejecting the hypothesis that repolymerization of the ahydrooligosaccharide pyrolysis intermediates is responsible for low levoglucosan yields. Interestingly, similar experiments with glucose revealed that glucose repolymerized to form cellobiose, indicating that repolymerization takes place in pyrolysis of this monosaccharide.

Preventing the repolymerization of condensed-phase compounds during glucose pyrolysis helped increasing its anhydrosugar yields. Utilizing fumed silica or 1,2-benzanthraquinone to prevent agglomeration and repolymerization of glucose during pyrolysis increased levoglucosan yields by 18 and 20 wt.%, respectively. This suggests a

potential pathway to produce anhydrosugars from glucose. However, this distinct behavior from other kinds of pyrolyzed sugars is difficult to explain.

To enhance the proposed thermohydrolysis reaction, helium gas saturated with water was used as inert carrier in cellulose pyrolysis experiments. The results from these tests do not support the hypothesis that thermohydrolysis is responsible for less than stoichiometric yields of levoglucosan. Neither the levoglucosan contained in the condensed phase was affected by the addition of water in the carrier gas, nor glucose was found as a product in the condensed phase.

The dynamics data obtained from cellulose pyrolysis was useful to obtain kinetic parameters of the reaction as well as to reveal important features of the reaction. The Friedman analysis showed a varying activation energy, and the model fitting efforts supported the existence of multiple steps during cellulose pyrolysis and related them with cracking and unzipping reactions proposed to explain this thermal degradation of cellulose.

The modelling effort, based on population balances, indicates that cracking as the only mechanism of thermal degradation will only produce equal amounts of levoglucosan and unstable monomers, not recreating the approximately 60 wt.% to 40 wt.% observed in cellulose pyrolysis experiments. Another model which included the competition between cracking and unzipping reactions could recreate the experimental yield of levoglucosan; however, this model relied on values of activation energies that are different for each reaction, which goes against the notion that similar glycosidic bonds will require similar amounts of energy for their dissociation.

Finally, a new mathematical model included both unzipping and cracking with equal activation energies, as well as varying yields of levoglucosan from unzipping depending on the degree of polymerization of the fragment being thermally degraded. This last feature includes the chain length effect in the reaction. This model was able to reproduce levoglucosan yields similar to those observed experimentally, proposing a simple process to study cellulose pyrolysis. Based on these modeling results, it appears that levoglucosan-forming reaction rates that decrease as oligosaccharide chain length decreases is the most plausible explanation for limitations on levoglucosan yield from cellulose.

Future work

The research presented here opens new questions and ideas that will require further research. The main items to investigate in the future could include:

Comprehending the interaction between glucose and co-pyrolysis agents, fumed silica or 1,2-benzanthraquinone, which allowed at least an 18 wt.% increase on the production of levoglucosan, could open a pathway to produce anhydrosugars from glucose. Fumed silica is a good option to pursue scale up of a co-pyrolysis process to produce levoglucosan from glucose because of its low price and capability to being regenerated with heat. On the other hand, the use of the high boiling point aromatic compound, 1,2-benzanthraquinone, could be cost prohibitive, yet identifying a less expensive alternative could be a good option to explore co-pyrolysis or even solvolysis processes to produce high yields of anhydrosugars from glucose.

This work proposes that low yields of levoglucosan from the thermal degradation of short anhydrooligosaccharides contained in the condensed phase will ultimately limit the production of levoglucosan from cellulose, so the answer to achieve closer to stoichiometric levoglucosan yields from the most abundant organic polymer in the planet might rest in the pyrolysis of anhydrosugars such as cellobiosan. Considering that cellobiosan has a levoglucosan end would suggest that unzipping could separate this end to produce a levoglucosan unit, leaving the possibility of producing levoglucosan or other products from the rest of the molecule. If something like this would happen, the expected yields of levoglucosan from cellobiosan should have been at least 50 wt.%, which was not achieved experimentally. To understand these lower than expected yields, computational chemistry with the density functional theory could be used. These computational tools have already been proven powerful tools to understand the complexities of carbohydrate thermal degradation in recent years.[70,73,177] Additionally, experimentally identifying and quantifying the intermediate condensed phase products of cellobiosan, other higher degree of polymerization anhydrosugars, and cellodextrins at different pyrolysis durations could provide valuable evidence to comprehend the complex reactions occurring in pyrolysis of carbohydrates.

Moreover, cellobiosan could be a good starting point to understand the chain length effect on the production of levoglucosan from cellodextrins of varying degree of polymerization. Considering that model compounds to study this effect could be hard to come by and that the level of contaminants could negatively impact the yields of anhydrosugars from pyrolysis, working with maltodextrins could be a good option for

experimental work. Having large quantities of these materials will be useful so they can be subjected to passivation that will remove or neutralize contaminants contained within their structure. Understanding the pyrolysis product distribution from a wide range of degrees of polymerization dextrins will help understanding the chain length effect.

The simple proposed population model describing cellulose pyrolysis could be enhanced to include other primary and secondary reactions, and help explaining the overall reaction of cellulose pyrolysis and possibly be extended to other organic polymers.

Finally, experimental and/or computational studies can be conducted to obtain the energetics of the elementary step of glycosidic bond cleavage either from cracking or unzipping. This will complement the mathematical model included here, as well as providing certainty to the values for activation energy and preexponential factors proposed in the literature of thermal degradation of polymers and thermochemical processing of biomass.

REFERENCES

[1] P. R. Patwardhan, J. A. Satrio, R. C. Brown, B. H. Shanks, *J. Anal. Appl. Pyrolysis* **2009**, *86*, 323–330.

[2] X. Zhou, H. B. Mayes, L. J. Broadbelt, M. W. Nolte, B. H. Shanks, *AIChE J.* **2016**, *62*, 766–777.

[3] A. K. Burnham, X. Zhou, L. J. Broadbelt, *Energy & Fuels* **2015**, 150415093726006.

[4] K. Kamide, *Cellulose and Cellulose Derivatives*, Elsevier Science, **2005**.

[5] W. Haynes, *Cellulose, the Chemical That Grows*, Doubleday, **1953**.

[6] J. L. Wertz, O. Bédué, J. P. Mercier, *Cellulose Science and Technology*, EFPL Press, **2010**.

[7] W. C. Turner, *Energy Management Handbook, Fifth Edition*, Taylor & Francis, **2004**.

[8] R. C. Brown, *Biorenewable Resources: Engineering New Products from Agriculture*, Wiley, **2003**.

[9] L. Appels, R. Dewil, *Resour. Conserv. Recycl.* **2012**, *59*, 1–3.

[10] H. Sakuma, S. Munakata, S. Sugawara, *Agric. Biol. Chem.* **1981**, *45*, 443–451.

[11] A. V. Bridgwater, *J. Anal. Appl. Pyrolysis* **1999**, *51*, 3–22.

[12] M. Miljkovic, *Carbohydrates*, Springer New York, New York, NY, **2009**.

[13] A. Pictet, *Patent Specification for the Manufacture of Levoglucosan*, **1918**, 13530/18.

[14] V. Strezov, T. J. Evans, *Biomass Processing Technologies*, CRC Press, **2014**.

[15] J. N. Owens, H. G. Lund, *Forests And Forest Plants - Volume II: ,* **2009**.

[16] C. J. Longley, D. P. C. Fung, in (Ed.: A. V Bridgwater), Springer Netherlands, Dordrecht, **1993**, pp. 1484–1494.

[17] D. S. Layton, A. Ajjarapu, D. W. Choi, L. R. Jarboe, *Bioresour. Technol.* **2011**, *102*, 8318–8322.

[18] M. Giannoni, T. Martellini, M. Del Bubba, A. Gambaro, R. Zangrando, M. Chiari, L. Lepri, A. Cincinelli, *Environ. Pollut.* **2012**, *167*, 7–15.

[19] M. Mochida, K. Kawamura, P. Fu, T. Takemura, *Atmos. Environ.* **2010**, *44*, 3511–3518.

[20] Farbenindustrie Aktiengesellschaft, *Préparation de Lévoglucosane*, **1942**, 456.321.

[21] F. Shafizadeh, Y. L. Fu, *Carbohydr. Res.* **1973**, *29*, 113–122.

[22] G. R. Ponder, G. N. Richards, *Biomass and Bioenergy* **1994**, *7*, 1–24.

[23] J. Q. Bond, J. A. Dumesic, Y. Roma, *Role Catal. Sustain. Prod. Bio-fuels Bio-chemicals* **2013**, 261–288.

[24] A. D. Pouwels, G. B. Eijkel, J. J. Boon, *J. Anal. Appl. Pyrolysis* **1989**, *14*, 237–280.

[25] V. K. Thakur, A. S. Singha, B. N. Misra, *J. Appl. Polym. Sci.* **2011**, *122*, 532–544.

[26] E. Kontturi, email conversation, **2017**.

[27] M. Van de Velden, J. Baeyens, A. Brems, B. Janssens, R. Dewil, *Renew. Energy* **2010**, *35*, 232–242.

[28] H. Kawamoto, W. Hatanaka, S. Saka, *J. Anal. Appl. Pyrolysis* **2003**, *70*, 303–313.

[29] W. Schnabel, *Polymer Degradation: Principles and Practical Applications*, Hanser International, **1981**.

[30] D. E. Levy, P. Fügedi, *The Organic Chemistry of Sugars*, CRC Press, **2005**.

[31] E. B. Sanders, A. I. Goldsmith, J. I. Seeman, *J. Anal. Appl. Pyrolysis* **2003**, *66*, 29–50.

[32] G. R. Ponder, G. N. Richards, *Carbohydr. Res.* **1993**, *244*, 341–359.

[33] B. Zhang, E. Leng, P. Wang, X. Gong, J. Zhang, Y. Zhang, M. Xu, *J. Anal. Appl. Pyrolysis* **2015**, *114*, 119–126.

[34] S. Matsuoka, H. Kawamoto, S. Saka, *Carbohydr. Res.* **2011**, *346*, 272–279.

[35] S. Matsuoka, H. Kawamoto, S. Saka, *Polym. Degrad. Stab.* **2011**, *96*, 1242–1247.

[36] H. B. Mayes, M. W. Nolte, G. T. Beckham, B. H. Shanks, L. J. Broadbelt, *ACS Sustain. Chem. Eng.* **2014**, *2*, 1461–1473.

[37] M. Ohara, A. Takagaki, S. Nishimura, K. Ebitani, *Appl. Catal. A Gen.* **2010**, *383*, 149–155.

[38] A. G. W. Bradbury, Y. Sakai, F. Shafizadeh, *J. Appl. Polym. Sci.* **1979**, *23*, 3271–3280.

[39] M. J. Antal, G. Varhegyi, E. Jakab, *Ind. Eng. Chem. Res.* **1998**, *37*, 1267–1275.

[40] T. Shoji, H. Kawamoto, S. Saka, *J. Anal. Appl. Pyrolysis* **2014**, *109*, 185–195.

[41] T. Hosoya, H. Kawamoto, S. Saka, *Carbohydr. Res.* **2006**, *341*, 2293–2297.

[42] X. Bai, R. C. Brown, *J. Anal. Appl. Pyrolysis* **2014**, *105*, 363–368.

[43] F. Shafizadeh, in *Symp. Math. Model. Biomass Pyrolysis Phenom.*, ACS Division Of Fuel Chemistry, Preprints, Washington DC, **1983**, pp. 285–290.

[44] T. Hosoya, H. Kawamoto, S. Saka, *J. Anal. Appl. Pyrolysis* **2008**, *83*, 64–70.

[45] X. Gong, Y. Yu, X. Gao, Y. Qiao, M. Xu, H. Wu, *Energy and Fuels* **2014**, *28*, DOI 10.1021/ef501112q.

[46] J. Piskorz, P. Majerski, D. Radlein, A. Vladars-Usas, D. . Scott, *J. Anal. Appl. Pyrolysis* **2000**, *56*, 145–166.

[47] D. S. T. a. G. Radlein, A. Grinshpun, J. Piskorz, D. S. Scott, *J. Anal. Appl. Pyrolysis* **1987**, *12*, 39–49.

[48] X. Bai, P. Johnston, R. C. Brown, *J. Anal. Appl. Pyrolysis* **2013**, *99*, 130–136.

[49] R. Perry, D. Green, J. Maloney, *Perry's Chemical Engineers' Handbook*, **1997**.

[50] J. Proano-Aviles, J. K. Lindstrom, P. A. Johnston, R. C. Brown, *Energy Technol.* **2017**, *5*, 189–195.

[51] G. Ellis, *Control System Design Guide: Using Your Computer to Understand and Diagnose Feedback Controllers*, Elsevier Science, **2012**.

[52] F. Shafizadeh, Y. Z. Lai, *J. Org. Chem.* **1972**, *37*, 278–284.

[53] M. R. Nimlos, R. J. Evans, *Fuel Chem. Div. Prepr.* **2002**, *47*, 393.

[54] L. Abella, S. Nanbu, K. Fukuda, R. May, *Mem. Fac. Eng. Kyushu Univ.* **2007**, *67*, 67–74.

[55] I. M. Rocha, T. L. P. Galvão, E. Sapei, M. D. M. C. Ribeiro Da Silva, M. A. V Ribeiro Da Silva, *J. Chem. Eng. Data* **2013**, *58*, 1813–1821.

[56] H. Kawamoto, M. Murayama, S. Saka, *J. Wood Sci.* **2003**, *49*, 469–473.

[57] P. A. Johnston, J. Lindstrom, J. Proano-Aviles, P. Gable, R. C. Brown, in *Tcbiomass 2015 - Int. Conf. Thermochem. Convers. Sci.*, Bioeconomy Institute - ISU, Chicago, **2015**, p. 1.

[58] R. H. Schlosberg, *Chemistry of Coal Conversion*, Springer US, Boston, MA, **1985**.

[59] G. Gavalas, *Coal Science and Technology 4: Coal Pyrolysis*, Elsevier B.V., **1982**.

[60] S. Zhou, R. C. Brown, X. Bai, *Green Chem.* **2015**, *17*, 4748–4759.

[61] D. J. Nowakowski, A. V. Bridgwater, D. C. Elliott, D. Meier, P. de Wild, *J. Anal. Appl. Pyrolysis* **2010**, *88*, 53–72.

[62] T. Hosoya, H. Kawamoto, S. Saka, *J. Anal. Appl. Pyrolysis* **2009**, *85*, 237–246.

[63] T. Hosoya, H. Kawamoto, S. Saka, *J. Anal. Appl. Pyrolysis* **2007**, *80*, 118–125.

[64] T. Shoji, H. Kawamoto, S. Saka, *J. Anal. Appl. Pyrolysis* **2016**, DOI 10.1016/j.jaap.2016.12.026.

[65] R. Ball, a. C. McIntosh, J. Brindley, *Phys. Chem. Chem. Phys.* **1999**, *1*, 5035–5043.

[66] G. Varhegyi, E. Jakab, M. J. Antal, *Fuel Energy Abstr.* **1995**, *36*, 119.

[67] C. Di Blasi, *Fuel* **1996**, *75*, 58–66.

[68] S. Matsuoka, H. Kawamoto, S. Saka, *J. Anal. Appl. Pyrolysis* **2014**, *106*, 138–146.

[69] S. Matsuoka, H. Kawamoto, S. Saka, *Carbohydr. Res.* **2016**, *420*, 46–50.

[70] H. B. Mayes, L. J. Broadbelt, *J. Phys. Chem. A* **2012**, *116*, 7098–106.

[71] R. Vinu, L. J. Broadbelt, *Energy Environ. Sci.* **2012**, *5*, 9808.

[72] J. K. Lindstrom, P. Gable, R. C. Brown, **2016**, 1630404.

[73] X. Zhang, W. Yang, W. Blasiak, *Fuel* **2012**, *96*, 383–391.

[74] J. L. Banyasz, S. Li, J. Lyons-Hart, K. H. Shafer, *Fuel* **2001**, *80*, 1757–1763.

[75] J. L. Banyasz, S. Li, J. L. Lyons-Hart, K. H. Shafer, *J. Anal. Appl. Pyrolysis* **2001**, *57*, 223–248.

[76] R. Ball, A. C. Mcintosh, J. Brindley, *Combust. Theory Model.* **2004**, *8*, 281–291.

[77] C. Zhu, C. Krumm, G. G. Facas, M. Neurock, P. J. Dauenhauer, *React. Chem. Eng.* **2017**, *2*, 201–214.

[78] Y. C. Lin, J. Cho, G. a. Tompsett, P. R. Westmoreland, G. W. Huber, *J. Phys. Chem. C* **2009**, *113*, 20097–20107.

[79] J. Lédé, *J. Anal. Appl. Pyrolysis* **2012**, *94*, 17–32.

[80] A. Gonzalez-Quiroga, K. M. Van Geem, G. B. Marin, *Biomass Convers. Biorefinery* **2017**, DOI 10.1007/s13399-017-0251-0.

[81] M. J. J. Antal, G. Varhegyi, *Ind. Eng. Chem. Res.* **1995**, *34*, 703–717.

[82] I. Milosavljevic, E. M. Suuberg, Suuberg, in *207th Am. Chem. Soc. Natl. Meet.*, American Chemical Society, Washington, DC (United States), Washington DC, **1994**, pp. 860–864.

[83] J. A. Conesa, J. A. Caballero, A. Marcilla, R. Font, *Thermochim. Acta* **1995**, *254*, 175–192.

[84] P. C. Lewellen, W. A. Peters, J. B. Howard, *Symp. Combust.* **1977**, *16*, 1471–1480.

[85] J. Lédé, F. Blanchard, O. Boutin, *Fuel* **2002**, *81*, 1269–1279.

[86] A. Tabatabaie-Raissi, W. S. L. Mok, M. J. Antal, *Ind. Eng. Chem. Res.* **1989**, *28*, 856–865.

[87] A. L. Brown, D. C. Dayton, M. R. Nimlos, J. W. Daily, P. Adisak, J.-L. Aider, N. Sommier, T. Raafat, J.-P. Hulin, M. F. Ashby, et al., *Bioresour. Technol.* **2011**, *102*, 863–871.

[88] T. Reed, C. Cowdery, *ACS Annu. Meet. 1987* **1987**, 68–81.

[89] E. Ranzi, a Cuoci, T. Faravelli, a Frassoldati, G. Migliavacca, S. Pierucci, S. Sommariva, *Energy and Fuels* **2008**, *22*, 4292–4300.

[90] A. L. Brown, D. C. Dayton, J. W. Daily, *Energy & Fuels* **2001**, *15*, 1286–1294.

[91] A. D. Paulsen, M. S. Mettler, P. J. Dauenhauer, *Energy and Fuels* **2013**, *27*, 2126–2134.

[92] Unspecified, *Mettler Toledo Flash DSC* **2016**.

[93] V. Mathot, M. Pyda, T. Pijpers, G. Vanden Poel, E. van de Kerkhof, S. van Herwaarden, F. van Herwaarden, A. Leenaers, *Thermochim. Acta* **2011**, *522*, 36–45.

[94] B. Weddle, email conversation, **2015**.

[95] E. J. Murphy, *Trans. Electrochem. Soc.* **1943**, *83*, 161.

[96] I. Milosavljevic, E. M. Suuberg, *Prepr. Pap.Am. Chem. Soc., Div. Fuel Chem.* **1992**, *37*, 1567–1574.

[97] S. L. Madorsky, V. E. Hart, S. Straus, *J. Res. Natl. Bur. Stand. (1934).* **1956**, *56*, 343.

[98] H. Zhou, Y. Long, A. Meng, S. Chen, Q. Li, Y. Zhang, *RSC Adv.* **2015**, *5*, 26509–26516.

[99] M. R. Hajaligol, J. B. Howard, J. P. Longwell, W. a Peters, *Ind. Eng. Chem. Process Des. Dev.* **1982**, *21*, 457–465.

[100] W. K. Tang, W. K. Neill, *J. Polym. Sci. Part C Polym. Symp.* **1964**, *6*, 65–81.

[101] A. E. Lipska, W. J. Parker, *JOUliNAL Appl. POLYMEH Sci.* **1966**, *10*, 1439–1453.

[102] A. M. Kanury, *Combust. Flame* **1972**, *18*, 75–83.

[103] R. R. Baker, *J. Therm. Anal.* **1975**, *8*, 163–173.

[104] G. Varhegyi, M. J. Antal, E. Jakab, P. Szabó, *J. Anal. Appl. Pyrolysis* **1997**, *42*, 73–87.

[105] M. Grønli, M. J. Antal, G. Várhegyi, *Ind. Eng. Chem. Res.* **1999**, *38*, 2238–2244.

[106] P. R. Solomon, M. A. Serio, E. M. Suuberg, *Prog. Energy Combust. Sci.* **1992**, *18*, 133–220.

[107] A. K. Burnham, *Global Chemical Kinetics of Fossil Fuels*, Springer International Publishing, Cham, **2017**.

[108] O. Levenspiel, *Chemical Reaction Engineering*, John Wiley & Sons, **1999**.

[109] H. S. Fogler, *Elements of Chemical Reaction Engineering*, Pearson Education, **2016**.

[110] L. P. Yarin, G. Hetsroni, A. Mosyak, *Combustion of Two-Phase Reactive Media*, Springer Science & Business Media, **2013**.

[111] A. R. Teixeira, K. G. Mooney, J. S. Kruger, C. L. Williams, W. J. Suszynski, L. D. Schmidt, D. P. Schmidt, P. J. Dauenhauer, *Energy Environ. Sci.* **2011**, *4*, 4306.

[112] Q. Liu, S. Wang, K. Wang, X. Guo, Z. Luo, K. Cen, *Acta Physico-Chimica Sin.* **2008**, *24*, 1957–1963.

[113] S. Zhou, B. Pecha, M. van Kuppevelt, A. G. McDonald, M. Garcia-Perez, *Biomass and Bioenergy* **2014**, *66*, 398–409.

[114] P. R. Solomon, D. G. Hamblen, in *Chem. Coal Convers.*, Springer US, Boston, MA, **1985**, pp. 121–251.

[115] T. L. Bergman, A. S. Lavigne, F. P. Incropera, D. P. Dewitt, *Fundamentals of Heat and Mass Transfer*, **2011**.

[116] E. M. Suuberg, W. a Peters, J. B. Howard, *Ind Eng Chem Process Des Dev* **1978**, *17*, 37–46.

[117] E. Suuberg, V. Oja, *J. Chem. Thermodyn.* **1997**, *12*, 243–248.

[118] P. R. Solomon, M. A. Serio, R. M. Carangelo, J. R. Markham, *Fuel* **1986**, *65*, 182–194.

[119] H. Kawamoto, H. Morisaki, S. Saka, *J. Anal. Appl. Pyrolysis* **2009**, *85*, 247–251.

[120] S. Vyazovkin, A. K. Burnham, J. M. Criado, L. A. Pérez-Maqueda, C. Popescu, N. Sbirrazzuoli, *Thermochim. Acta* **2011**, *520*, 1–19.

[121] S. Barrel, E. Per-, T. Unstable, M. Using, D. Scanning, D. T. Ana-, S. Calorimeters, **2008**, *i*, 1–11.

[122] N. Gat, *Effect of Rapid Heating Rate on Coal Nitrogen and Sulfur Release. Quarterly Technical Progress Report No. 3, March 19-June 19, 1982*, Redondo Beach, CA (USA), **1982**.

[123] G. H. Yeoh, K. K. Yuen, *Computational Fluid Dynamics in Fire Engineering: Theory, Modelling and Practice*, Elsevier Science, **2009**.

[124] P. N. Ciesielski, M. F. Crowley, M. R. Nimlos, A. W. Sanders, G. M. Wiggins, D. Robichaud, B. S. Donohoe, T. D. Foust, *Energy & Fuels* **2015**, *29*, 242–254.

[125] V. Hankalin, T. Ahonen, R. Raiko, *Process Eng.* **2009**, 1–20.

[126] T. Gaur, S., Reed, *An Atlas of Thermal Data for Biomass and Other Fuels*, National Renewable Energy Laboratory, **1995**.

[127] Y. a. Cengel, S. Klein, W. Beckman, **2002**, 896.

[128] S. Li, J. Lyons-Hart, J. Banyasz, K. Shafer, *Fuel* **2001**, *80*, 1809–1817.

[129] W. W. Wendlandt, *Thermal Methods of Analysis*, Wiley-Interscience. New York, **1974**.

[130] M. S. Lee, *Mass Spectrometry Handbook*, Wiley, **2012**.

[131] G. Özsin, A. E. Pütün, *Waste Manag.* **2017**, DOI 10.1016/j.wasman.2017.03.020.

[132] P. R. Solomon, M. A. Serio, R. M. Carangelo, R. Bassilakis, Z. Z. Yu, S. Charpenay, J. Whelan, *J. Anal. Appl. Pyrolysis* **1991**, *19*, 1–14.

[133] M. A. Serio, P. R. Solomon, Z. Z. Yu, S. Charpenay, *ACS Div. Fuel Chem. Prepr.* **1990**, *35*, 479–488.

[134] M. R. Wright, *Introduction to Chemical Kinetics*, John Wiley & Sons, **2005**.

[135] P. F. Nelson, I. W. Smith, R. J. Tyler, *ACS Div. Fuel Chem. Prepr.* **1987**, *32*, 142–147.

[136] W. Zheng, K. B. Mcauley, E. K. Marchildon, K. Z. Yao, **2007**, *85*, 180–187.

[137] A. Dosseto, S. Turner, J. Van-Orman, *Timescales of Magmatic Processes*, John Wiley & Sons, **2011**.

[138] E. Chornet, C. Roy, *Thermochim. Acta* **1980**, *35*, 389–393.

[139] Y. Lin, J. Cho, J. M. Davis, G. W. Huber, *Chem. Eng. Sci.* **2012**, *74*, 160–171.

[140] M. S. Mettler, A. D. Paulsen, D. G. Vlachos, P. J. Dauenhauer, *Green Chem.* **2012**, *14*, 1284.

[141] P. R. Patwardhan, *Chem. Eng.* **2010**, *Ph. D.*, 162.

[142] R. Simha, L. A. Wall, *J. Phys. Chem.* **1952**, *56*, 707–715.

[143] F. O. Rice, *J. Am. Chem. Soc.* **1931**, *53*, 1959–1972.

[144] F. O. Rice, W. R. Johnston, B. L. Evering, *J. Am. Chem. Soc.* **1932**, *54*, 3529–3543.

[145] F. O. Rice, W. R. Johnston, *J. Am. Chem. Soc.* **1934**, *56*, 214–219.

[146] F. O. Rice, K. F. Herzfeld, *J. Am. Chem. Soc.* **1934**, *56*, 284–289.

[147] T. Faravelli, M. Pinciroli, F. Pisano, G. Bozzano, M. Dente, E. Ranzi, *J. Anal. Appl. Pyrolysis* **2001**, *60*, 103–121.

[148] Frontier Laboratories Ltd., *Multi-Shot Pyrolyzer EGA/PY-3030D, Operation Manual*, Frontier Laboratories Ltd., **n.d.**

[149] J. Proano-Aviles, J. K. Lindstrom, P. A. Johnston, R. C. Brown, in *Tcbiomass2015 - 4th Int. Conf. Thermochem. Biomass Convers. Sci.*, Chicago, **2015**, p. 1.

[150] P. A. Johnston, R. C. Brown, *J. Agric. Food Chem.* **2014**, *62*, 8129–8133.

[151] M. R. Rover, P. a. Johnston, B. P. Lamsal, R. C. Brown, *J. Anal. Appl. Pyrolysis* **2013**, *104*, 194–201.

[152] P. Šimon, *J. Therm. Anal. Calorim.* **2004**, *76*, 123–132.

[153] S. Vyazovkin, C. a. Wight, *Int. Rev. Phys. Chem.* **1998**, *17*, 407–433.

[154] F. J. Gotor, J. M. Criado, J. Malek, N. Koga, *J. Phys. Chem. A* **2000**, *104*, 10777–10782.

[155] Unspecified, *MatLab Curve Fitting Toolbox ™ User ’ s Guid.* **2016**.

[156] K. W. Smith, F. W. Cain, G. Talbot, *J. Agric. Food Chem.* **2005**, *53*, 3031–3040.

[157] R. Font, A. Marcilla, J. Devesa, E. Verdú, *J. Anal. Appl. Pyrolysis* **1993**, *27*, 245–273.

[158] E.-J. Shin, M. R. Nimlos, R. J. Evans, *Fuel* **2001**, *80*, 1697–1709.

[159] P. Khorrami, C. J. Radke, *SPE Reserv. Eng.* **1988**, *3*, 349–352.

[160] G. J. Kwon, D. Y. Kim, S. Kimura, S. Kuga, *J. Anal. Appl. Pyrolysis* **2007**, *80*, 1–5.

[161] P. R. Patwardhan, D. L. Dalluge, B. H. Shanks, R. C. Brown, *Bioresour. Technol.* **2011**, *102*, 5265–9.

[162] X. Zhou, M. W. Nolte, B. H. Shanks, L. J. Broadbelt, *Ind. Eng. Chem. Res.* **2014**, *53*, 13290–13301.

[163] X. Zhou, M. W. Nolte, H. B. Mayes, B. H. Shanks, L. J. Broadbelt, *Ind. Eng. Chem. Res.* **2014**, *53*, 13274–13289.

[164] C. M. Close, D. K. Frederick, J. C. Newell, *Modeling and Analysis of Dynamic Systems*, John Wiley, **2003**.

[165] Unspecified, *AEROSIL ® R 974 Prod. Inf.* **2016**, 1–2.

[166] J. Zhang, M. W. Nolte, B. H. Shanks, *ACS Sustain. Chem. Eng.* **2014**, *2*, 2820–2830.

[167] M. R. Hajaligol, W. A. Peters, J. B. Howard, *Energy & Fuels* **1988**, *2*, 430–437.

[168] I. Milosavljevic, E. M. Suuberg, **n.d.**, 860–864.

[169] T. Yoshida, *Mater. Trans.* **2003**, *44*, 2489–2493.

[170] A. Khawam, D. R. Flanagan, *J. Phys. Chem. B* **2006**, *110*, 17315–17328.

[171] J. a Foreman, R. L. Blaine, *Test* **n.d.**

[172] X. Zhang, **2017**.

[173] P. R. Patwardhan, R. C. Brown, B. H. Shanks, *ChemSusChem* **2011**, *4*, 636–643.

[174] N. Kuzhiyil, D. Dalluge, X. Bai, K. H. Kim, R. C. Brown, *ChemSusChem* **2012**, *5*, 2228–2236.

[175] N. Shimada, H. Kawamoto, S. Saka, *J. Anal. Appl. Pyrolysis* **2008**, *81*, 80–87.

[176] P. R. Patwardhan, J. A. Satrio, R. C. Brown, B. H. Shanks, *Bioresour. Technol.* **2010**, *101*, 4646–4655.

[177] X. Zhang, W. Yang, W. Blasiak, *Fuel* **2013**, *109*, 476–483.